

Submitted for

National Plan for Science, Technology and Innovation

King Saud University

**Geothermal and Volcanic Evaluation of Harrat
Rahat, Northwestern Arabian Peninsula**

Project No. : 11 – SPA 2208 - 02

Prof. Abdullah M. Al-Amri (PI)

Dr. Robert Mellors (CO - I)

Dr. David Harris (CO - I)

Prof. Kamal A. El- Sayed (CO – I)

November 9, 2016

Abstract

This is the final report of the project **11 – SPA 2208 – 02** entitled " Geothermal and Volcanic Evaluation of Harrat Rahat, Northwestern Arabian Peninsula " sponsored by National Plan for Science, Technology and Innovation, King Abdulaziz City for Science & Technology (**NPST**).

Saudi Arabia offers a strong potential for geothermal energy, but only a limited amount of exploration efforts have taken place. We conducted a preliminary, low-cost, reconnaissance level evaluation of the western volcanic areas (harrats) based on mapped geology and existing seismic data. The emphasis is on the Harrat Rahat volcanic area in western Saudi Arabia although a survey of other major harrats is conducted using geologic data. The goal is to test the procedure and identify areas for future, more intensive study.

The geologic survey of the harrats focused on evaluating potential sources of subsurface heat and groundwater. Subsurface heat is based on age of erupted volcanics and expected volume of subsurface magma chambers. An analogy with an existing geothermal field in a similar setting in Mexico suggests that the faults and coincident seismicity may be associated with higher permeability. We have processed data from four seismic stations within the Harrat Rahat for detection of microseismic events and processed ambient noise for construction of a velocity model. Low velocities are observed within Harrat Rahat and two areas with coincident basements faults and possible enhanced subsurface temperatures are identified. The harrats are ranked in terms of geothermal potential, with Harrat Rahat, Lunayir, and Khaybar selected as highest potential. During the course of this work, two extended abstracts and presentations were made at the 2015 and 2016 Geothermal Resources Council annual meeting and this provided useful input.

Acknowledgments

This Project was funded by the National Plan for Science, Technology and Innovation (**MAARIFAH**), King Abdulaziz City for Science and Technology, Kingdom of Saudi Arabia, Award Number (**11 – SPA 2208 - 02**). The authors would like to express their thanks and gratitude to Dr. D. Dodge for his contribution in data analysis, to Saudi Geological Survey for providing seismic data and to Musaed Al-Harbi and Saeed Shaltoni for supervising construction of seismic stations and data collection.

Table of Contents

List of Figures	4
List of Tables	4
1.0 Introduction	5
1.1 Objectives.....	8
2.0 Methods & Materials	10
2.1 Geologic & Geophysical Maps	10
2.2 Conceptual Model Development	10
2.3 Passive Seismic Data	12
3.0 Results & Data Analysis.....	17
3.1 Geological Constraints.....	17
3.2 Event Detection Processing	45
3.3 Ambient noise analysis.....	52
3.4 Earthquakes, faults, and permeability	59
4.0 Discussion & Interpretation	61
5.0 Conclusions	63
6.0 Publications resulting from this work	66
7.0 References.....	66
Appendices.....	76

List of Figures

Figure 1. Regional map of tectonic, lithostratigraphic, and magmatic features of western Saudi Arabia. ..	7
Figure 2. Analog field at Las Tres Virgines, MX.	12
Figure 3. Map of seismic stations	14
Figure 4. Simplified block diagram of detection framework	15
Figure 5. Moho depth distribution and depth	22
Figure 6. Index map showing harrat study.	25
Figure 7. Geologic map of Harrat Lunayyir.....	27
Figure 8. Eight-kilometer fracture in northern Harrat Lunayyir	28
Figure 9. The high central vent system of Harrat Khaybar	30
Figure 10. Steam fumarole on Harrat Khaybar	32
Figure 11. Lava flows and vents of Harrat Ithnayn.....	33
Figure 12. Lava flows, pyroclastic deposits, and vent types of Harrat Hutaymah.....	35
Figure 13. Geologic map of northern Harrat Rahat,	37
Figure 14. Distribution of non-eroded lava flows of upper Madinah basalt	39
Figure 15. Vertical cross-sections of P-wave tomography.	41
Figure 16. Fault trends on northern Harrat Rahat and in the surrounding Precambrian basement.	42
Figure 17. Ground fissures in northern Harrat Rahat,.....	44
Figure 18. Local earthquakes	46
Figure 19. Vertical-component waveforms.....	47
Figure 20. Detection statistic.....	48
Figure 21. Event waveforms	50
Figure 22. Event maps	52
Figure 23. Raypaths covered by the ambient noise correlation	52
Figure 24. Example of Green's functions	53
Figure 25. Green's function displayed as a function of distance.	54
Figure 26. Comparison of paths inside the volcanic region with shield paths.	55
Figure 27. All velocity profiles generated from the Green's functions.	56
Figure 28. Comparison of velocities for shield and volcanic.....	57
Figure 29. Map of raypaths.....	58
Figure 30. Map of seismic stations and earthquakes from available data.....	59
Figure 31. Example of local earthquake showing clear signal-to-noise.....	60
Figure 32. Earthquakes plotted on fault map and volcanics	61
Figure 33. Possible areas for further investigation (in yellow).....	65

List of tables

Table 1. Historical eruptions of some Harrats in Western Arabia.....	8
Table 2. Framework detectors.....	45
Table 3. Summary of results.	64

1.0 Introduction

Initial studies and investigations [Al-Dayel, 1988; Roobol, 2007; Rehman, 2005; 2010; Lashin et al., 2014; 2015] suggested several major potential areas for geothermal production in Saudi Arabia: hot springs in the southwestern region (Jizan and Al-Lith), volcanic areas (harrats), granites in the northwest may be potentially productive as a site for Enhanced Geothermal Systems and deep aquifers in eastern Saudi Arabia [Lashin et al., 2015]. While the Kingdom of Saudi Arabia (KSA) possesses abundant hydrocarbon energy resources, an understanding of the potential of renewable energy sources such as geothermal power is a topic of interest [Hashem, 2012; Lashin et al., 2015]. Possible uses are for power production or direct use.

However, despite the potential of significant high-temperature resources, little work has been conducted for geothermal exploration in the volcanic areas. In this work we propose a low-cost exploration strategy that relies on available geological and geophysical data to conduct a first-order reconnaissance survey to identify geothermal prospects within a harrat. The exploration will combine passive seismic data with regional and local geologic maps to detect and characterize anomalous zones in the shallow upper crust.

The western third of the Arabian Peninsula is composed of the Precambrian Arabian Shield, overlain to the east by younger Phanerozoic rocks of the Arabian Platform (Figure 1). The Arabian Shield is composed of at least five geologically distinct terranes that were sutured together 715-630 million years ago and created the Najd fault zone, a major, 2000-km-long, left-lateral wrench fault that displaced the northern part of the craton ~250 km to the northwest [Stern, 1985, Stoesser and Camp, 1985]. Much later, about 30 million years ago, the Red Sea rift began to form [Pallister, 1987; Bohannon et al., 1989]. About 12 million years ago, period of continental basalt magmatism began and produced the harrat volcanic fields of western Saudi Arabia [Camp and Roobol, 1992]. Surprisingly, this volcanism is offset and appears distinct from the Red Sea rift zone. The volcanic activity is centered along the Makkah-Madinah-Nafud volcanic line, which is defined by a north-trending series of en echelon vent systems forming the central axes of Harrats Rahat, Khaybar, and Ithnayn [Camp and Roobol, 1992]. This volcanism continues to the present data, with historical eruptions every few hundred years, with vents in Harrats Rahat, Khaybar, and Ithnayn [Coleman et al., 1983; Camp et al., 1987; Camp et al.,

1991](Table 1). However, very young basaltic volcanism occurs in other harrats to the east and west of the Makkah-Madinah-Nafud volcanic line. One of these harrats, Lunayyir, was the site of intensive seismic activity and geodetic deformation in 2009, which was interpreted as injection of a 0-km-long dike into a shallow fault zone [*Pallister et al.*, 2010].

This study will focus primarily on Harrat Rahat, which covers almost 20,000 km³ and extends over 300 km. Two eruptions are known from historical records, most notably one in 1256 AD that erupted about 0.5 km³ from a vent located approximately 22 km from the city of Madinah. The Precambrian basement beneath northern Harrat Rahat is distinguished by containing large left-lateral wrench faults associated with the northwest-trending Najd fault system. These extensive wrench faults are linear weak zones that could provide ideal conduits for rising magma and/or ascending hydrothermal fluids.

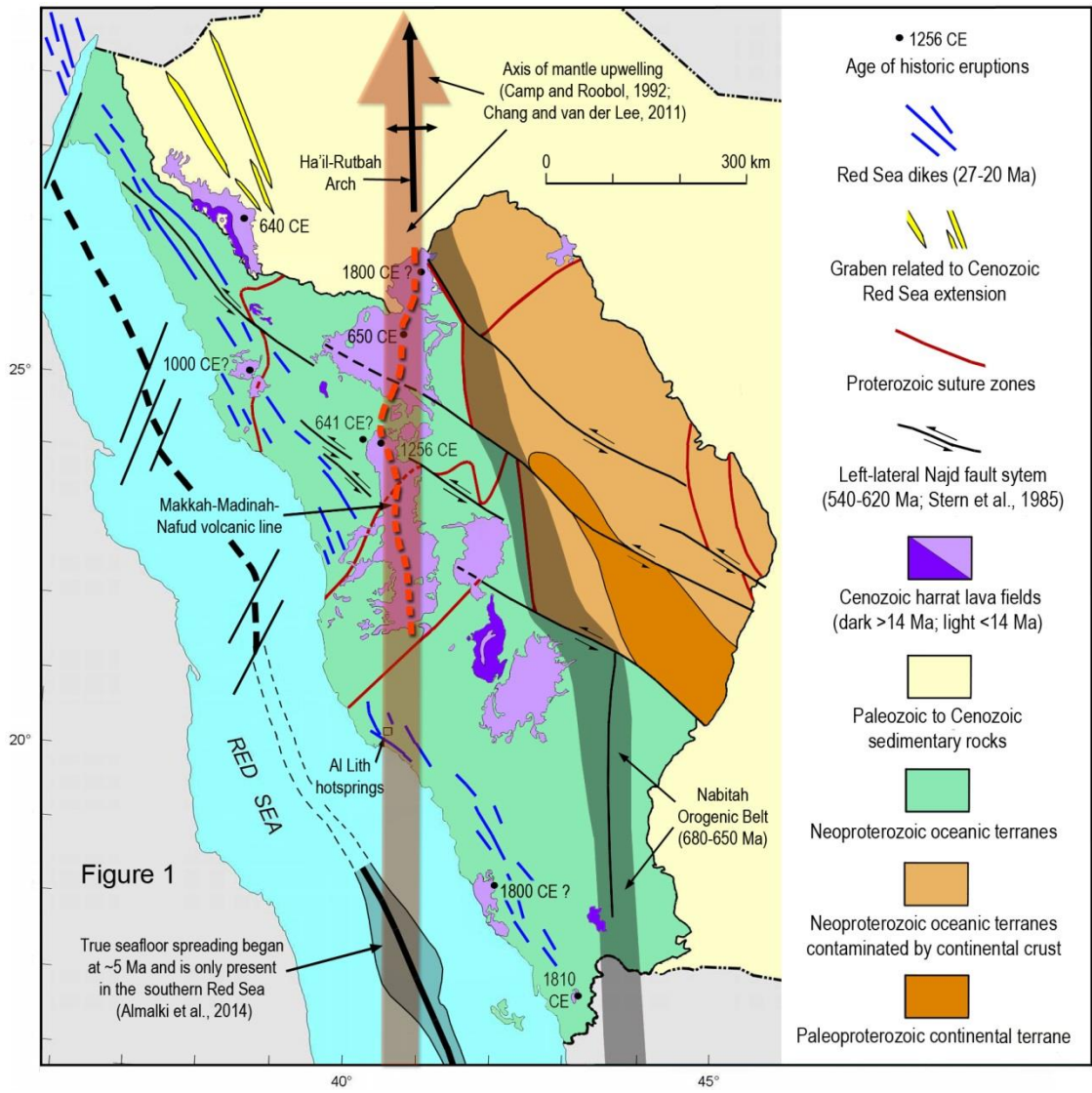


Figure 1. Regional map of tectonic, lithostratigraphic, and magmatic features of western Saudi Arabia. Several tectonic and structural trends underlie the Cenozoic Harrat lava fields. The most prominent of these include (1) prevalent NE-trending folds, faults, and suture zones reflecting the Neoproterozoic collision of ensimatic island arcs of the western Arabian Shield (Camp, 1984; Stoeser and Camp 1985; Pallister et al., 1987), (2) NNW-trending normal faults, graben, and dikes associated with Cenozoic extension of the Red Sea basin (e.g., Bosworth et al., 2005), (3) major NW-trending, left-lateral wrench faults of the Najd fault system, active from 620-540 Ma (e.g., Stern, 1985), and (4) the northerly trending Nabitah orogenic belt, generated from 680-650 Ma during collision of the western shield arc terranes with terranes to the east having older Proterozoic to Archean, continental affinity (Stoeser and Camp, 1985; Stoeser and Stacey, 1988; Robinson et al., 2014). The north-trending Nabitah orogenic belt forms the eastern boundary of the harrat province and may well reflect a major lithospheric boundary where thicker continental lithosphere provides a barrier to sublithospheric mantle flow, allowing basaltic lavas to rise into thinner, denser lithosphere of the western arc terranes. The main zone of mantle upwelling beneath the harrats is the 600-km-long Makkah-Madinah-Nafud (MMN) volcanic line marking the main eruption sites for Harrats Rahat, Khaybar and Ithnayn.

Table 1. Historical eruptions of some Harrats in Western Arabia

Harrat	Recent eruptions	Sub-surface water	Proximity to cities
Lunayyir	2009* AD	?	50-100 km
Khaybar	Holocene	Yes	50-100 km
Hutaymah	Holocene	Yes	50-100 km
Ithnayn	Holocene	?	100-150 km
Rahat	641, 1256 AD	?	Close

1.1 Objectives

The objectives of this project are to define areas of potential geothermal resources in the western Arabian Peninsula with an emphasis on the Harrat Rahat area by using new technology applied to the existing data. Specifically, we intend to 1) combine seismic and geologic data to define areas of high geothermal potential (districts) in the western Arabian Peninsula and 2) use innovative and state-of-the-art seismic data analysis combined with in-depth geologic knowledge to infer crustal parameters such as temperature, fault and fracture concentration, and potentially fluid flow, which will be crucial for defining geothermal prospects and understanding the possible geologic risks of their development.

Geologic data will be utilized to identify areas of young volcanism, which are often associated with shallow intrusions and related high heat flow. Geologic data are also useful in recognizing faults that may serve as conduits for fluid flow. Moreover, seismic data will be used to infer regional heat flow by defining areas of high attenuation and brittle-ductile transition zones. Furthermore, local seismicity occurs in high-strain regions and may be a proxy for permeability. The combination of geologic and seismic data will provide a high-resolution model for resource evaluation.

The benefits and results of this work will include the following:

- Development of regional maps of geothermal potential centered around volcanic areas (harrats) based on integrated seismic and geologic data, including the development of a conceptual model of geothermal prospects in the context of their geologic settings.

Comparisons to similar areas with successful geothermal production elsewhere in the world will also be made.

- Completion of a prospect-level evaluation focused on the Harrat Rahat region based on advanced seismic analysis that includes ambient noise cross-correlation for tomography and state-of-the-art detection analysis. The purpose of this case study is to use the seismic data to define likely prospects within the Harrat Rahat region and understand the underlying volcanic structure, which is essential for geothermal exploitation.

OBJECTIVES	PHASES	TASKS
1. Overview; geothermal and volcanic potential of the region	Geothermal and volcanic characterization	<ul style="list-style-type: none"> • <i>Study regional geology - tectonics, structure and surface indications (e.g., hot springs, fumaroles).</i> • <i>Study regional geophysics - crustal and mantle velocities and attenuation, depth of seismicity, heat flow.</i> • <i>Develop conceptual models and identify potential analog prospects.</i>
2. Detect and collect seismic data	Seismic waveform collection and detection	<ul style="list-style-type: none"> • <i>Collect existing waveform data from networks (Madinah and other relevant stations). Perform waveform correlation and/or matched field detection.</i>
3. Conduct a detailed examination of Harrat Rahat	Seismic and volcanic data analysis	<ul style="list-style-type: none"> • <i>Map microseismicity and sources, conduct ambient noise tomography (interferometry) and characterize the geology of Harrat Rahat.</i>

All objectives have been reached and tasks addressed. We begin with identification of an analog geothermal field (Tres Virgines) and then attempt to match characteristics by using a blend of geological mapping and seismic data. Regional geological data is first used to identify likely Harrats and based on that data and proximity to a major city (i.e. potential customers for geothermal electricity), we focus on Harrat Rahat. Seismic data from a network around Harrat Rahat is used in two ways: first, to identify micro-seismicity that might define faulting and areas

of potential high permeability and second, to use interferometry (ambient noise) to define areas of low velocities and possibly shallow high temperatures. Finally, all results are blended to create a ranked list of prospective harrats.

2.0 Methods & Materials

We will conduct a two-part strategy: first, identify geologic regions with high geothermal potential, and second, use low-cost regional geophysical exploration to attempt to refine the mapping and develop maps. This type of evaluation is important in evaluating ‘district’ level prospects, such as Harrat Rahat, especially where surface expression of geothermal energy is limited. Traditional geothermal exploration often uses intensive focus on specific areas using heat flow measurements and techniques such as MT to identify high-conductivity zones typical of geothermal prospects. This type of exploration is useful, but impractical on a large-scale without extensive time and resources. Therefore, we begin with low-cost exploration using existing available data sets: geologic mapping and seismic data. Sites of known geothermal significance, such as fumaroles, will also be included in the analysis.

2.1 Geologic & Geophysical Maps

The first dataset consists of detailed geological maps of Harrat Rahat and other Harrats compiled by Camp [e.g. *Camp et al.*, 1987; *Camp and Roobol*, 1991]. These maps show the vents and distinct basaltic flows as well as structural features. By using these maps we will identify the most recent vents and areas of possible fracturing for enhanced permeability.

Standard digital elevation data is used as a reference for the maps of the seismic stations. Some features such as the outline of major volcanic flows and the location of Holocene cinder cones are based on the geologic maps and plotted on the geophysical maps. Locations of the seismic stations are taken from metadata provided along with the seismic data.

2.2 Conceptual Model Development

We will base our conceptual model on an analog geothermal field based on geologic setting. A close analog of possible geothermal prospects of the western Saudi harrats is the geothermal

plant at Las Tres Virgenes in Baja California, which produces about 10 Mw from granitic fractured rocks below volcanic cover [*Hernandez et al.*, 1995]. The tectonic setting is very similar, as both Las Tres Virgenes and the Saudi Harrats lie on the edges of an extension rift system. For Las Tres Virgenes, it is the Gulf of California rift, which is roughly analogous to the Red Sea rift. Tres Virgenes is a Holocene set of volcanoes that occur at the intersection of faults in a granitic basement.

The heat source for Tres Virgenes is likely derived from a magma chamber. The surface expression was primarily fumeroles but the location was the site of micro-seismicity prior to geothermal development and showed anomalies in attenuation and V_p/V_s ratio [*Wong et al.*, 2001; *Wong and Munguia*, 2007]. Permeability appears related to the intersection of faults in the basement and characterized by active seismicity, even prior to the installation of the geothermal plant. Also, like western Saudi Arabia, Baja California is arid, with low rainfall. Therefore, for the potential Saudi resource we seek a shallow magma chamber that is near mapped faults and with active micro-seismicity (Figure 2).

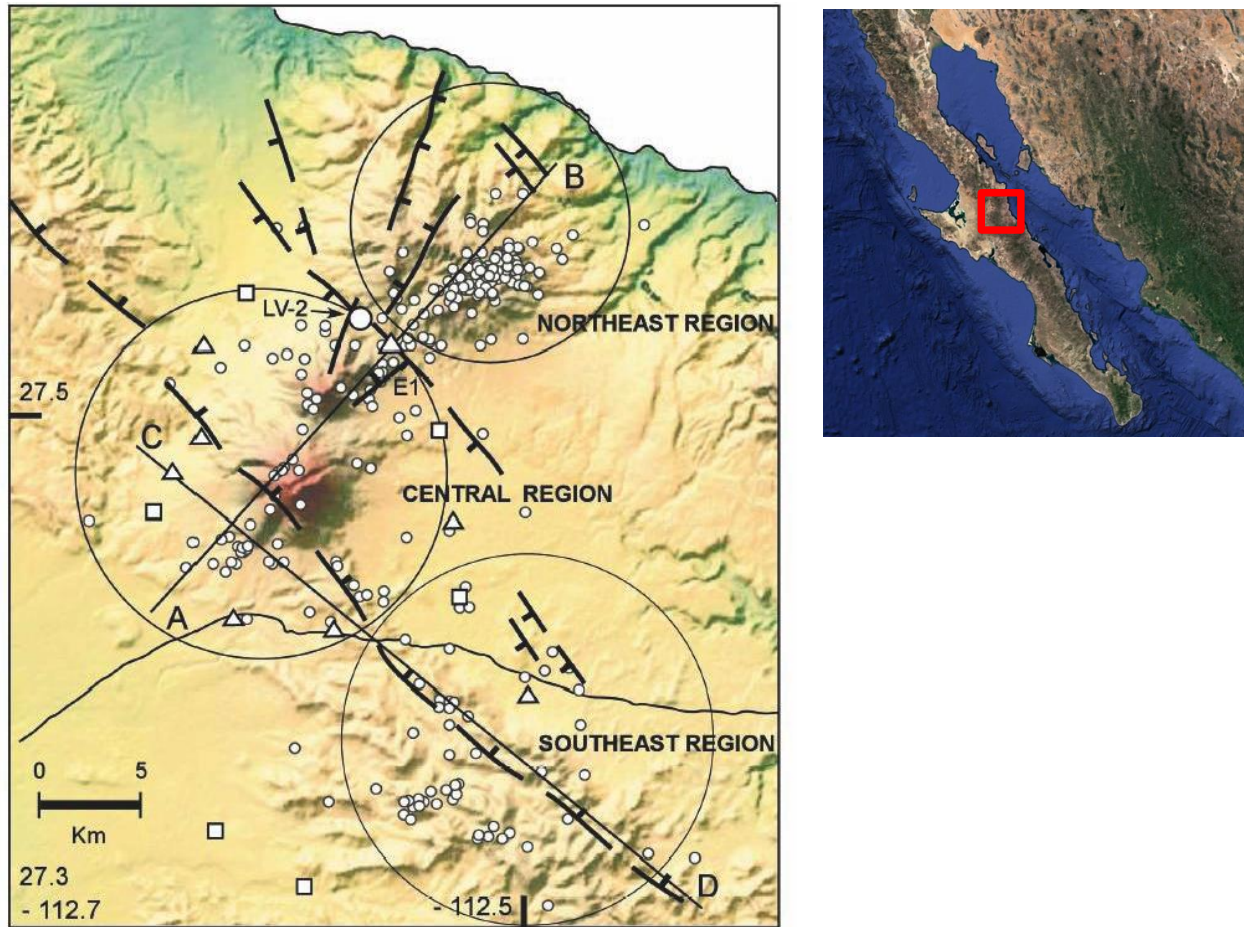


Figure 2. Analog field at Las Tres Virgenes, MX. Note seismicity associated with the faulting.

The geothermal plant itself consists of two 5 Mw flash units and power is supplied to nearby cities. For Harrat Rahat, potential use is in the nearby cities of Medina (to the north) and Mecca and Taif (to the south). This reduces the need for extensive power lines. The major uncertainty is the availability of sufficient water. However, it might be possible to use recycled water from the cities as injection water, as it done at the Geysers geothermal field in California using recycled water from the city of Santa Rosa, which is sent to the Geysers field via a 50 km long pipeline.

2.3 Passive Seismic Data

The second dataset is passive seismic data collected by local and regional seismic networks. Previously, passive seismic data has been used to identify geothermal resources [e.g. *Foulger, 1982*]. Several geothermal areas have been characterized using this method. *Wilson and Jones*

[2003; 2004] used passive seismic data to identify magma chambers under the Coso geothermal field in California, USA. *Zucca et al.*, 1994 used attenuation to examine the Geysers field, also in California. *Wong et al.*, [2001; 2006] also used attenuation at the Tres Virgenes Volcanic Area, which, as mentioned previously, is a volcanic area that is similar in setting to the harrats and which now has a 10 MW geothermal plant. More recent studies use novel techniques such as ambient noise tomography to map the Lake Toba magma chamber in Indonesia [*Stankiewicz et al.*, 2010] and *Muksin et al.*, [2013], also in Indonesia, identified variations in V_p/V_s using local earthquakes associated with a geothermal field. Similar investigations [*Koulakov et al.*, 2015; *Hansen et al.*, 2013] in Saudi Arabia have identified anomalies associated with possible magma chambers at Harrat Lunnayir, although not for the purpose of finding geothermal energy.

While passive seismic data can be used to infer velocity or attenuation structures through tomography with seismic event travel-time or phase amplitude measurements or ambient noise correlation measurements, it also can be used to search for microseismicity possibly associated with fluid motion in volcanic centers. We have begun our exploration of the data obtained from the Saudi Geologic Survey network surrounding the Harrat Rahat with a search for microseismicity. Our working assumption is that microseismicity associated with a volcanic field will be repetitive, possibly being driven by fluid flow within a relatively static system of conduits. Consequently, we use an autonomous correlation detection framework [*Harris and Dodge*, 2011; *Dodge and Harris*, 2015] designed to discover the occurrence of repetitive transients in a continuous data stream from a network of stations.

We performed an initial search of one year of data (July 2013 – July 2014) at the four central stations of the network (RHT14, RHT01, RHT15, RHT04; Figure 3) in a fairly low frequency band (2-10 Hz) intending to detect somewhat larger events over the whole study region. This step results in a number (around 20) of groups of related events in the study region. We attempt to screen out groups of explosions, which are common in this region, to focus on natural seismicity.

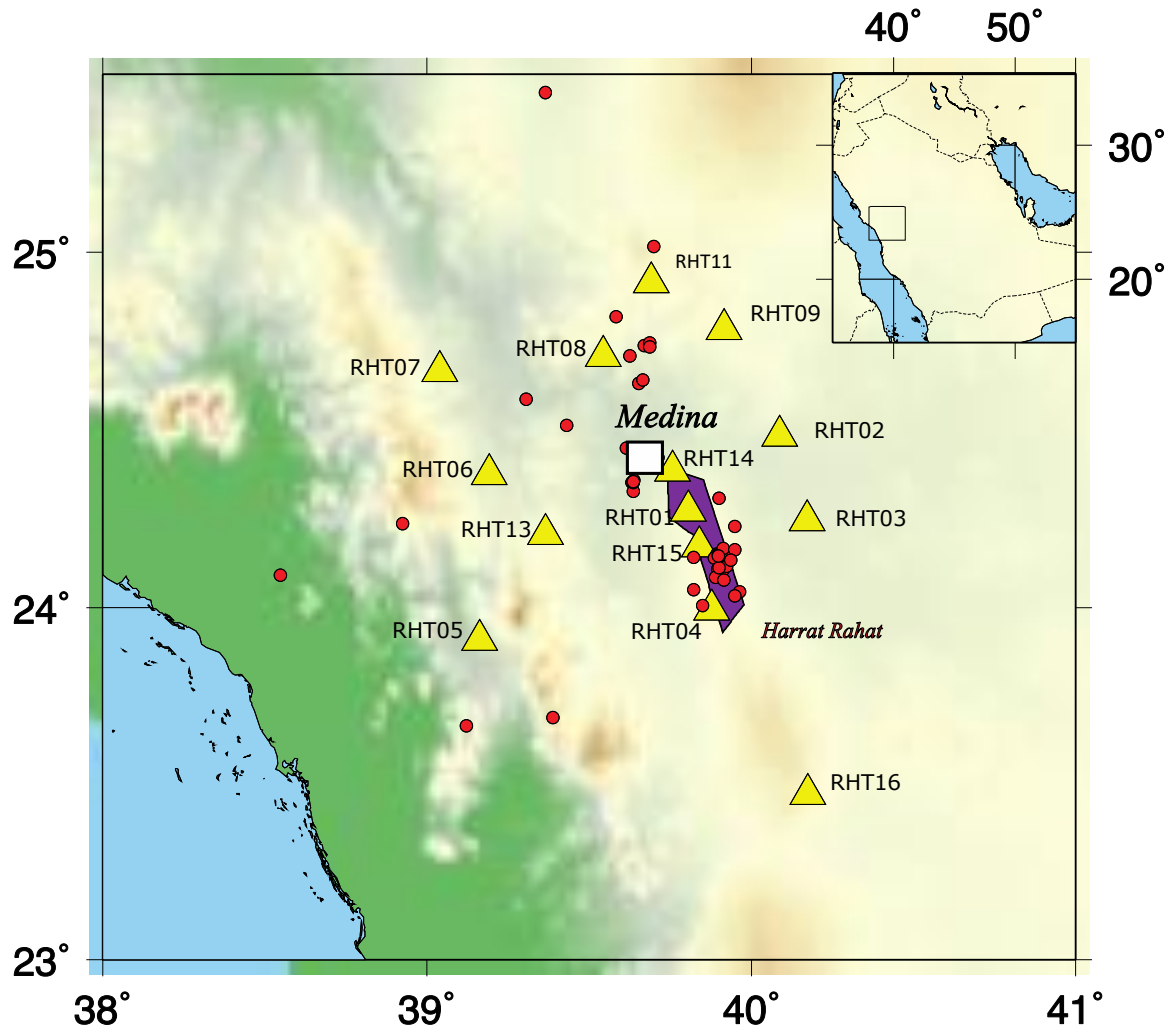


Figure 3. Map of seismic stations (yellow triangles), earthquakes from the period 2004-2005 (red circles), the central area of Harrat Rahat deemed most prospective (purple), and the city of Medina.

For those event groups that appear to arise from natural sources, we perform a second correlation detection step, processing the data at the best-observing station in a higher frequency band (4-20 Hz). The objective of this step is to reduce the detection threshold to find a larger number of repetitive natural events.

2.4 Detection Framework

A simplified diagram of the autonomous system is shown in Figure 4.

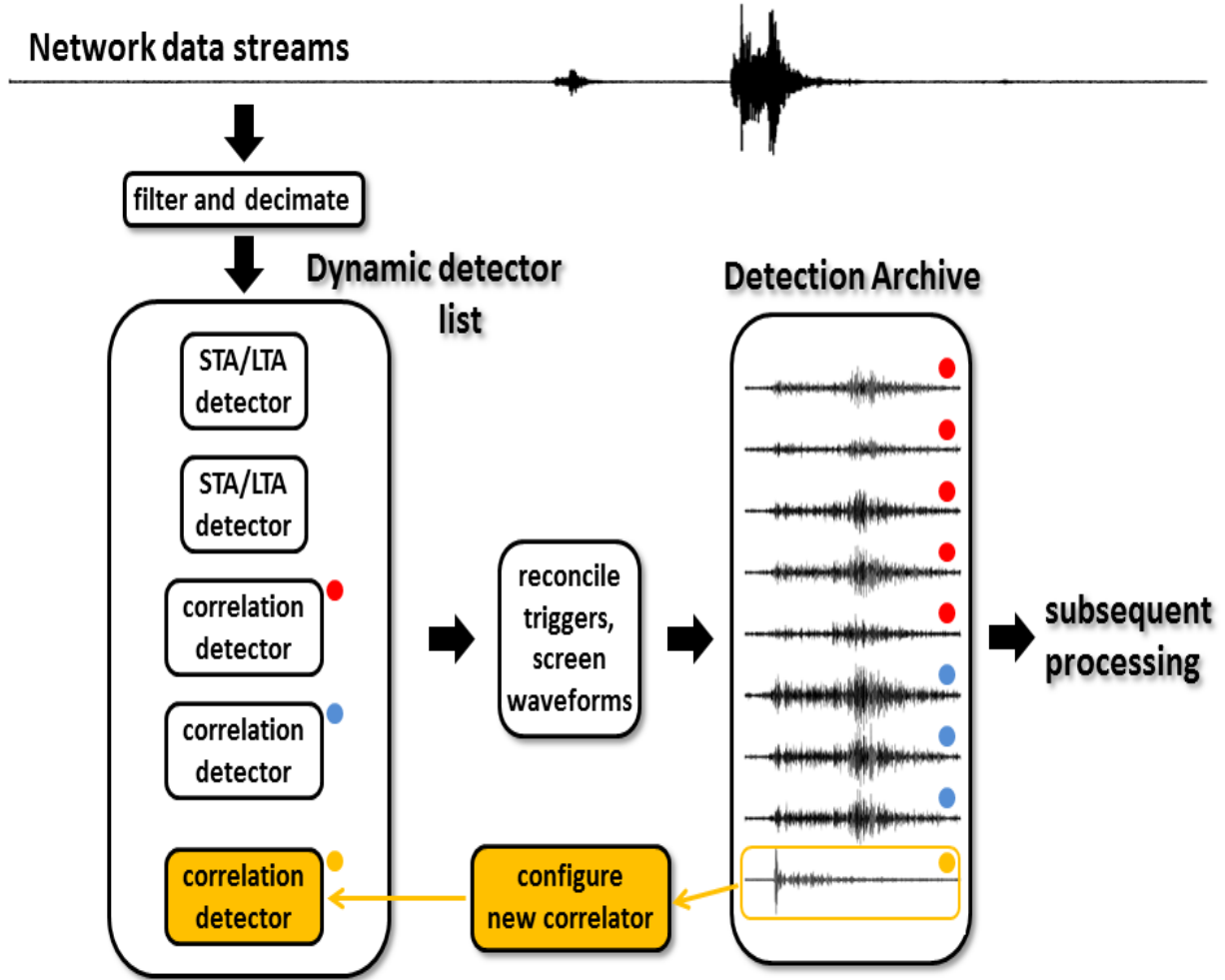


Figure 4. Simplified block diagram of autonomous correlation detection framework used to process the RHT data.

Since this system includes both power detectors and empirical detectors, it largely obviates the disadvantage of systems using empirical detectors alone, i.e. it can discover signals representative of new waveform patterns associated with sources not previously observed.

The system operates by maintaining a dynamic list of detectors, which process network stream data in consecutive, contiguous blocks. For each block, each detector in the list calculates a detection statistic, which is scanned for excursions above a pre-set threshold. Upon initiation of a run, the detector list is populated just by one or several power detectors. As the system processes the data, the power detectors trigger on waveforms which are screened by a set of measurements and rules intended to cast out triggers on noise bursts, dropouts and spikes. Waveforms which pass these tests are used as templates for correlation detectors. The correlation detectors are created and added to the detector list, then immediately begin detection operations along with the power detectors.

When several detectors trigger simultaneously on the same signal, as often happens, a set of rules determines which trigger will be considered to be the system-wide detection. The rules are simple: correlation detector triggers always take precedence over power detector triggers, and for triggers on two or more detectors of the same type, the detector with the largest detection statistic takes precedence over the other detectors. Detections are logged to an archive, retaining information on the originating detector, the value of the detection statistic, the detection time, and measurements of waveform characteristics. The system naturally sorts events into groups determined by a common correlation detector. It is for this reason that the autonomous detection framework is ideally suited to search for repetitive events in swarms associated with volcanic sources.

3.0 Results & Data Analysis

Examination and preparation of geologic maps have been completed. The preferred area is in the center of the Northern Harrat Rahat as based on recent volcanic activity, faults, and microseismicity. Seismic data has been prepared and initial processing for microseismic detection and cross-correlation has been performed. The approach that we have adopted to find clusters of microseismicity has yielded a small swarm of 13 events just outside (north) of the Harrat Rahat study region.

3.1 Geological Constraints

Geologic Setting

The western third of the Arabian Peninsula is composed of the Precambrian Arabian Shield, overlain to the east by younger Phanerozoic rocks of the Arabian Platform (Figure 1). The Arabian Shield is composed of at least five geologically distinct terranes separated by ophiolite-bearing suture zones. These five terranes were sutured together by terrane accretion in a series of collisional events occurring 715-630 million years ago to form the Arabian craton (Stoeser and Camp, 1985). Collision-related deformation continued from ~630 to 550 million years ago to produce the Najd fault zone, a major, 2000-km-long, left-lateral wrench fault system composed of several northwest-trending faults that together displaced the northern part of the craton ~250 km to the northwest (Stern, 1985).

After a long period of tectonic quiescence, continental extension and dike intrusion began in western Arabia about 30 million years ago as the Red Sea rift began to form (*Pallister, 1987; Bohannon et al., 1989; Bosworth et al., 2005*), although true seafloor spreading did not begin until ~5 million years ago where it is restricted to the southern half of the rift zone (*Cochran, 1983; Cochran et al., 1991*). Fission-track data on crustal apatites show that an accelerated rate of crustal uplift began in western Saudi Arabia about 14 million years ago (Bohannon et al., 1989). This is consistent with the widespread deposition of mid-Miocene boulder conglomerates adjacent to the Red Sea escarpment and massive, coeval evaporite deposits in the deeper parts of the Red sea graben (*Schmidt and Hadley, 1984, Bayer et al., 1988*). Uplift appears to have continued into Holocene times to produce a broad topographic feature known as the West

Arabian Swell [Almond, 1986]. Importantly, this period of late Cenozoic uplift is also contemporaneous with a period of continental basalt magmatism that began about 12 million years ago to produce the harrat volcanic fields of western Saudi Arabia (Camp and Roobol, 1992). This period of thermal uplift and magmatism appears to be related to the late Cenozoic emplacement of hot mantle asthenosphere beneath western Arabia (Camp and Roobol, 1992; Chang *et al.*, 2011).

Harrat Volcanic Province

The Cenozoic Harrat Province is one of the largest areas of alkali olivine basalt eruption on Earth, covering about 180,000 km² of an area that extends from Yemen in the south to Syria in the north. In Saudi Arabia, the province is composed of 12 separate basalt fields covering about 90,000 km² (Figure 1), with total eruptive volume estimated to be 10³ to 10⁵ km³ (Coleman *et al.*, 1983). Several individual harrats have been mapped in detail and described in the scientific literature; these include Harrats Kishb (Roobol and Camp, 1991a; Camp *et al.*, 1992), Rahat (Camp and Roobol, 1989, 1991), Khaybar-Kura-Ithnayn (Camp, 1991; Roobol and Camp, 1991b), Hutaymah (Pallister, 1984; Thornber, 1990), and Lunayyir (Al-Amri *et al.*, 2012).

Compositionally, many harrats are dominated by olivine transitional basalt, alkali-olivine basalt and hawaiiite, with subordinate amounts of more evolved rock types that vary from mugearite to benmoreiite, trachyte and comendite. Some of the more silica-undersaturated harrats, however, contain significant volumes of basanite and phonotephrite, as well as subordinate amounts of phonolite. Ultramafic xenoliths can be found entrained in several of the nepheline-normative basanites, alkali basalts and hawaiiites, particularly common on Harrats Kishb, Al-Birk, Ithnayn, Uwayrid and Hutaymah (Kuo and Essene, 1986; McGuire, 1988a, b; Henjes-Kunst *et al.*, 1990; Thornber, 1990; Camp *et al.*, 1992; Blusztajn *et al.*, 1995).

The style of harrat eruption was just as variable its lava composition, with most of the volcanic products derived from Strombolian-type eruptions fed by dike intrusion delineated by contemporaneous scoria cones arranged along linear trends. The aggregate of numerous eruptions along these aligned cones generated extensive linear vent systems that form the main eruption site at the geographic center of each harrat. Scoria-cone eruptions typically generated small-volume, channel-filling basaltic lavas that vary in surface character from a'a to pāhoehoe.

More extensive pāhoehoe sheetflows and aggregate flow fields of shelly pāhoehoe were derived from Hawaiian-type eruptions associated with shield volcanoes. These are typically more common in the older stratigraphy of each harrat. The more felsic rock types are less extensive and typically associated with trachytic to comenditic or phonolitic domes and associated pyroclastic rocks that vary from air fall accumulations to pyroclastic flows and surge deposits.

Of particular interest to geothermal prospecting is the relatively common occurrence of post-Neolithic (<6000 yrs. B.P.; e.g., McClure [1978]) and historic eruptions. At least 21 eruptions on the Arabian Peninsula have been recorded in the past 1500 years, with the most recent occurring at Dhamar in northern Yemen in 1937 (*Van Padang*, 1963; *Siebert et al.*, 2010). Smithsonian's Global Volcanism Program recognizes credible evidence of nine historic eruptions in Saudi Arabia (*Simkin et al.*, 1984; *Seibert et al.*, 2010) that took place on Harrat Ithnayn (age unknown), Harrat Kishb (age unknown), Harrat al Birk (age unknown), Harrat Lunayyir (1000 CE), Harrat ar Rahah (500-650 CE), Harrat Khaybar (650 CE), Harrat Uwayrid (640 CE), Harrat Rahat (641 and 1256 CE), and Jabal Yar (1810 CE). Many historic eruptions have probably gone unrecorded. Several flows on the Arabian harrats lack erosion and wind-blown dust which generally ponds on older flows, whereas other flows disrupt Neolithic monuments built on older harrat lava. The surface of several non-eroded flows are barren of Neolithic monuments although surrounded by them on older flow surfaces.

The most intensely studied historic eruption occurred on northern Harrat Rahat near the holy city of Madinah, Saudi Arabia, in 1256 CE (654 AH). The eruption took place along six scoria cones aligned along a NNW trend to produce a 23-km-long lava flow that approached the ancient city within 8 km. *Camp et al.* (1987) used whole-rock and mineral chemistry data combined with petrographic analysis of disequibrated mineral assemblages to demonstrate that the eruption generated two chemical types representing distinctly different ranges in PTX environment: a low-K, olivine transitional basalt and a high-K, alkali olivine basalt, together with a subordinate hybrid type from the mixing of these two basalt types. This multiple-vent eruption also generated a compound tephra blanket surrounding the vents. Statistical analysis from *Kawabata et al.* (2015) suggest that most tephra was produced during variable wind conditions from high Hawaiian fountains of at least 500 m and perhaps as high as 1000 m from the northern three vents.

The most recent activity on the Arabian plate occurred between April and June 2009 when a magma-induced swarm of more than 30,000 earthquakes struck Harrat Lunayyir, forcing the evacuation of 40,000 people from the region. The earthquake swarm resulted in the development of a northwest-trending surface rupture 8 km long. It seems clear from geologic, geodetic and seismic data that the earthquakes and surface rupture resulted from magmatic dike intrusion with the tip of the dike rising to a depth less than 2 km from the surface (*Pallister et al.*, 2010; Baer and Hamiel, 2010; *Hanson et al.*, 2013; *Koulakov et al.*, 2014, 2015). This near eruption, together with documented historic eruptions and young lava and tephra deposits are reminders that the harrats are still underlain by active magmatic systems capable of producing volcanic hazards, but also with the potential reward of geothermal energy.

Tectonics, Structure, and the Makkah-Madinah-Nafud Volcanic Line

Miocene extension of the Red Sea graben is recorded in numerous northwest-trending faults, dikes, intrusive complexes and basaltic vent systems along the entire eastern margin of the Red Sea. Radiometric ages on these volcanic rocks and shallow intrusions vary from 30-20 Ma, with a peak between 24 and 21 Ma (*Sebai et al.*, 1991; *Camp and Roobol*, 1992). Most of the linear vent systems that fed the Arabian harrats, however, are younger (<12 Ma) and emplaced along northerly trends that diverge from the Red Sea trend by about 25°. It is therefore unlikely that harrat volcanism can be attributed to the same tectonic environment associated with rifting and magmatism in the Red Sea Basin.

Harrat volcanism followed the initiation of significant uplift at ~14 Ma to form the West Arabian Swell (*Almond*, 1986; *Bohannon et al.*, 1989). Uplift of the swell is asymmetric across the Red Sea Basin, with the Arabian side at a consistently higher elevation than the Nubian side. Volcanism is also asymmetric with the Arabian side containing numerous harrat lava fields, but the Nubian side showing no evidence of Quaternary volcanism. It is difficult to connect the origin of this topographic and volcanic asymmetry to a genesis related to Red Sea extension. Several workers instead have attributed it to a north-trending zone of mantle upwelling emplaced beneath western Arabia since ~14 Ma (*Camp and Roobol*, 1992; *Park et al.*, 2007; *Chang and van der Lee*, 2011; *Chang et al.*, 2011; *Hanson et al.*, 2006, 2012).

The topographic crest of the west Arabian swell corresponds with the Makkah-Madinah-Nafud (MMN) volcanic line, a volcanic alignment that extends for a north-south distance of over 600 km

(*Camp and Roobol, 1992*). It is delineated by slightly *en echelon*, north-trending linear vent systems that form the high topographic spine of Harrats Rahat, Khaybar, and Ithnayn, an axis that has been the major site of volcanism in Saudi Arabia over the past 10 million years. *Camp and Roobol (1992)* demonstrate that basaltic volcanism along the MMN volcanic line generated mildly alkaline eruptions, in contrast to all other harrats lying on opposing sides of the MMN line where strongly alkaline basaltic rocks were generated with greater incompatible-element enrichment. This overall difference in composition led *Camp and Roobol (1992)* to propose that the lavas along the MMN line were derived by greater degrees of partial melting at shallower depths of melting than those harrat lavas that erupted to the west and east. This would be consistent with a crest of mantle upwelling lying beneath the MMN volcanic line. More recent seismic data appears to be consistent with this interpretation (*Park et al., 2007; Chang and van der Lee, 2011; Chang et al., 2011, Hanson et al., 2006, 2012*).

A northward propagation of upwelling mantle beneath the volcanic line is also suggested by the respective age of its volcanic products. This is reflected in (1) a northward decrease in the age of the oldest basalts in each province, from 10 Ma for Harrat Rahat, to 5 Ma for Harrat Khaybar, to 3 Ma for Harrat Ithnayn, and (2) the lack of young volcanism in the southern half of the volcanic line together with a progressively greater volume of young lavas to the north. *Camp and Roobol (1992)* proposed two potential models for Harrat volcanism and its northward propagation along the MMN volcanic line: (1) the northward advance of mantle upwelling emanating from the Ethiopian mantle plume, or (2) a separate plume beneath the western Arabian Plate. More recently, the three dimensional S-velocity model of *Chang and Van der Lee (2011)* together with the shear-wave splitting experiments of *Hansen et al. (2006)* appear to confirm northward horizontal flow beneath western Arabia through a low-velocity channel emanating from the Afar/Ethiopian plume (Figure 5).

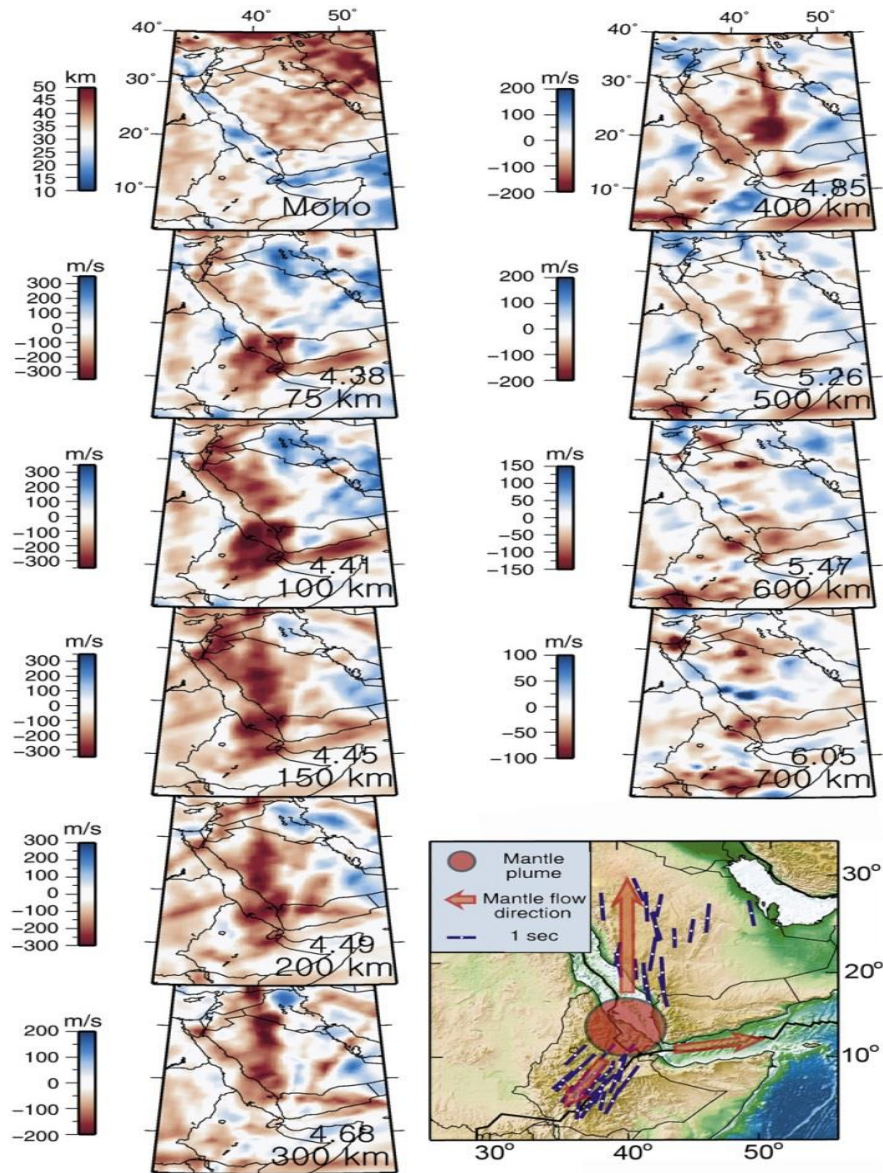


Figure 5. Moho depth distribution and depth slices at 75, 100, 200, 300, 500, 600, and 700 km, modified from the joint inversion model of Chang and Van der Lee (2011). Velocity perturbations are relative to the reference model “MEAN” (Marone et al., 2004), and the reference S velocity at each depth is written on the right side in km/s scale. Inset lower right is a schematic map showing the location of the Afar plume and mantle flow directions along with fast axes of shear-wave splitting from Hansen et al. (2006).

Whereas mantle control for the source of basalt volcanism is evident in the chemical and seismic data, it is more difficult to place development of north-trending linear vent systems in a tectonic context. The apparent E-W extensional strain implied by this trend lies oblique to the Red Sea trend where the maximum extensional stress orientation is to the NE-SW. One possibility

conforms with the model of *Sengor and Burke* (1978) who suggested that N-S fissures began to develop in the northern Arabian plate after about 12-15 Ma in response to collision of the Arabian and Eurasian plates along the Bitlis suture of southern Turkey. This explanation, however, seems an unlikely mechanism to explain E-W extension in southern Saudi Arabia more than 1500 km to the south. Further, there is a distinct lack of late-Miocene to recent rifting or normal faulting along north-south trends in Saudi Arabia and no apparent tectonic explanation for the north-south dikes underlying the linear vents.

An argument can be made that the north-south vent systems are not the product of extension at all, but rather the result of magma overpressure and forceful dike injection, with an orientation inherited from a deeper process in the sublithospheric mantle. Such a model is consistent with the north-south orientation of upwelling mantle (Figure 1) evident in the shear-wave splitting experiments of *Hansen et al.* (2006). An additional control on dike orientation and the geographic location of harrat volcanism is the north-trending Nabitah orogenic belt forming the eastern boundary of the harrat province. This belt appears to be a major lithospheric boundary where thicker and older continental lithosphere to the east provides a barrier to sublithospheric mantle flow, allowing basaltic lavas to rise into thinner, denser lithosphere of the western oceanic arc terranes.

Thermal Energy Source

The relatively high elevation of western Saudi Arabia is consistent with a thermally buoyant lithosphere. *Voggenreiter et al.* (1988) note that there is an asymmetry in the Bouguer gravity field across the Red Sea Basin, with the Arabian side having values of -110 mGal and the Egyptian side having values of -80 mGal, despite the fact that both regions are underlain by Precambrian crust of similar composition. They interpret these data as evidence that the lithosphere beneath Saudi Arabia is on average less dense and hotter. Xenolith data also confirms elevated upper mantle temperatures beneath several harrats (*Thornber and Pallister*, 1985; *Kuo and Essene*, 1986; *McGuire*, 1988a,b; *Henjes-Kunst et al.*, 1990; *Nasir*, 1992; *Kaliwoda et al.*, 2007). This appears to be supported by a seismic velocity model beneath the southern MMN line at Taif, Saudi Arabia indicating high upper mantle temperatures (*Julia et al.*, 2003).

Camp and Roobol (1992) used Rayleigh law calculations on the degree of partial melting to predict high mantle melting temperatures that vary between 1354°C for basanite compositions beneath Harrat Kishb to 1436°C for olivine transitional basalt beneath the MMN volcanic line. These data are consistent with *Park et al.* (2007) who identified a low-velocity structure beneath the MMN line that they attributed to a mantle thermal anomaly responsible for uplift and volcanism on the Arabian plate. They calculated that a temperature perturbation to about 1300°C is necessary to explain the low-velocity anomaly. On the other hand, heat-flow measurements from the Saudi Arabian shield rocks in this region (*Gettings*, 1982) are similar to the global average for Precambrian terrains (*Artemieva and Mooney*, 2001). This indicates that the thermal anomaly in the upper mantle has not yet equilibrated to the surface, except perhaps in those areas that may be underlain by shallow magma chambers.

Although geothermal prospects require heat at relatively shallow levels in the crust, conduction of thermal energy from mantle to shallow crust is a slow and inefficient process. The transference of thermal energy from the mantle, over short time spans, therefore requires more localized advection of heat associated with the rapid, adiabatic rise of a fluid phase. A contemporary environment of such a process is evident in harrat lava fields containing late Pleistocene to recent volcanism (i.e., < 1.0 Ma). As a first-order test of such regions, we examine here the geologic constraints for geothermal resource potential in four young magmatic systems. These include the central vent systems for Harrats Lunayyir, Khaybar, Ithnayn, and Hutaymah (Figure 6). We follow this with a more in-depth study that includes both geological and geophysical data using advanced capabilities to detect and characterize anomalous zones of high enthalpy in the shallow upper crust beneath northern Harrat Rahat.

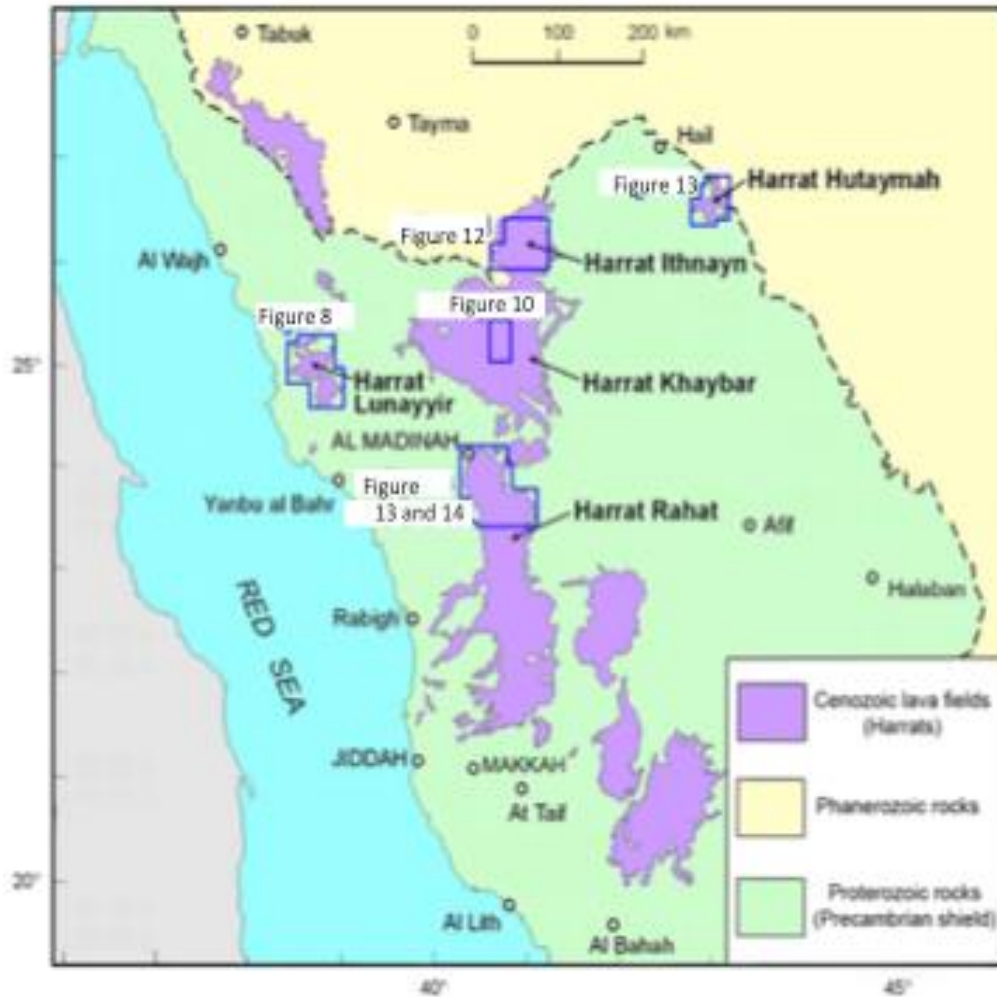


Figure 6. Index map showing harrat study areas that have geothermal potential, and the location of detailed plates 1-6, which are map compilations at 1:200,000 scale of volcanic features associated with their central vent systems.

Geothermal Potential of Harrats Lunayyir, Khaybar, Ithnayn and Hutaymah Based on Reconnaissance Mapping and Geological Constraints

To help assess the geothermal potential of Harrats Lunayyir, Khaybar, Ithnayn and Hutaymah, we have reproduced colored plates of the central vent systems of each harrat at 1:200,000-scale (Plates 1-4; digital appendix 1), modified after *Pallister (1984)*, *Thornber (1990)*, *Camp and Roobol (1991)*, *Roobol and Camp (1991b)*, and *Al-Amri et al. (2012)*. The designation of stratigraphic units for each harrat is largely based on diagnostic erosional patterns, including lateritic disconformities for some of the older units with progressively decreasing degrees of

erosion for younger units separated by diagnostic patterns of drainage and incision. The youngest units (typically < 500 ka) lack erosion but vary in weathered surface character and are progressively covered by surface dust ponds with increasing age. Post-Neolithic (<6000 yrs. B.P.) and historic lavas are denoted by their lack of burial mounds, erosion and ponded dust. Their fresh nonweathered surface allows them to be discriminated successfully on both aerial photographs and satellite imagery. This methodology in developing a coherent stratigraphy was used consistently for each harrat. An exception, however, is Harrat Hutaymah which is characterized only by young, noneroded flows that cannot be readily differentiated into separate stratigraphic units.

Harrat Lunayyir

Harrat Lunayyir is a small harrat covering about 3575 km² on the western edge of the Red Sea escarpment (Figure 7). Although the harrats lying along the MMN volcanic line are dominated by tholeiitic olivine basalt and subordinate alkali olivine basalt, Harrat Lunayyir is more undersaturated and more alkalic, with lavas that vary in composition from basanite to alkali olivine basalt and trachybasalt (Duncan and Al-Amri, (2013). Until recently, there were no age determinations for Harrat Lunayyir. Estimated ages were therefore based solely on comparing erosion surfaces to those of other harrats where radiometric ages are available. Jarad basalt, the oldest unit on the harrat, is deeply eroded with individual flows no longer distinct. Its erosional characteristics are consistent with a late Neogene in age of about 3 Ma. The remaining Quaternary units were originally thought to be less than about 1.7 Ma, also based on erosional characteristics.

Twenty-four new ⁴⁰Ar/³⁹Ar age determinations have recently been reported from the harrat, six from Al-Amri et al. (2012), and remaining eighteen from Duncan and Al-Amri (2013). The location of the Al-Amri et al. (2012) samples are shown in Figure 4, but the location of specific sample numbers from Duncan and Al-Amri (2013) are unavailable. Based on these new ages, all Quaternary volcanic activity on Harrat Lunayyir appears to be less than 600,000 years ago, which suggests a significant time break between the Tertiary Jared basalt (Tj) and all younger units. The youngest stratigraphic unit (Qm5) contains four eruption sites of black cones and lava flows with surrounding mantles of black airfall ash that still cover adjacent steep slopes. One of these may have erupted in the 10th century, about 1000 years ago (Richard et al., 1957).

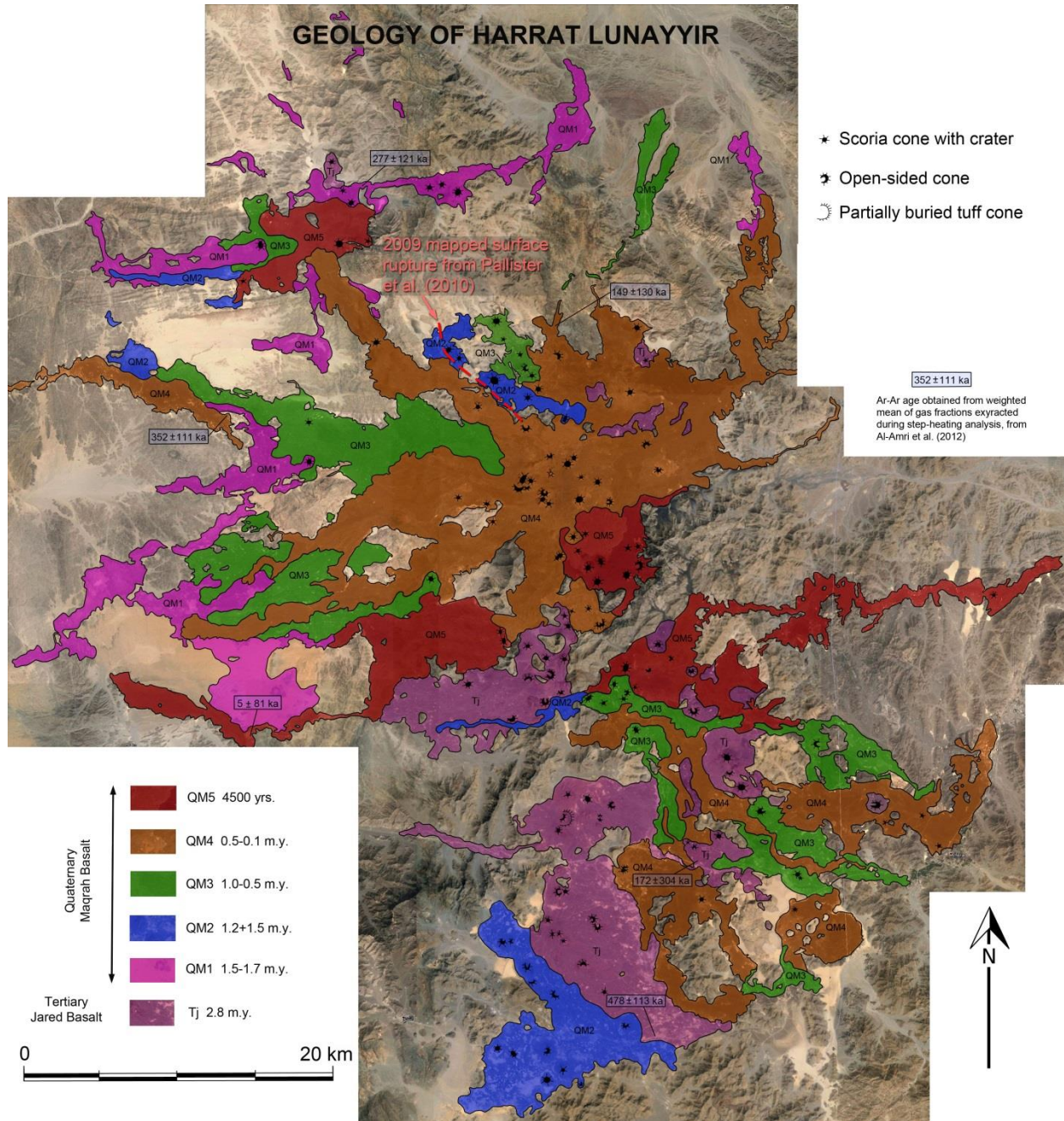


Figure 7. Geologic map of Harrat Lunayyir, (map data modified from Al-Amri et al, 2012).

Harrat Lunayyir contains about a fairly broad vent system of about 50 cones lying along a N-S trend. The most recent activity in 2009 began with about 30,000 earthquakes with epicenters lying along this same trend, but changing to a NW-SE Red Sea trend at the northern limit the vent system. *Pallister et al.* (2010) noted that this event was contemporaneous with the

generation of an 8-km long surface rupture that resulted from intrusion of a northwest-trending shallow dike about 10 km long (Figures 8A and B).



Figure 8. Eight-kilometer fracture in northern Harrat Lunayyir generated as the result of dike intrusion in 2009.

By every measure, Harrat Lunayyir appears to be an active magmatic system with moderate geothermal potential. In addition to young flows and historic activity, the area also displays geothermal features such as moderately elevated groundwater temperatures and fumarole emissions (Al-Dayel, 1988; Roobol et al., 2007). In 2007, well-water measurements attained temperatures up to 32°C (Al-Amri et al., 2012). Reports of steam observed in many places on the harrat during cold winter mornings were first noted by the Saudi Geological Survey in 2011. The geographical fingerprint of a geothermal source is likely to be small and localized, however. Although shallow crustal magma chambers are the most ideal source for significant heat exchange, tomographic models do not recognize a shallow chamber beneath the Harrat Lunayyir (Hanson et al., 2013). The lack of a shallow crustal reservoir is consistent with high concentration of primitive lavas and the general lack of fractionated lavas in the surface stratigraphy. The small amount of fractionation that did take place is likely to have occurred in

deeper reservoirs near the crust-mantle boundary or in the lower crust (Camp and Roobol, 1992). Sporadic dike intrusion in the absence of a shallow magma chamber is more likely to generate only small and localized regions of geothermal potential.

However, Harrat Lunayir is located relatively close to the normal faults bounding the Red Sea rift, which makes it very analogous to the Tres Virgines geothermal site, which is also located near extension rifting. This, as well as the seismicity, suggests that it may host areas of high permeability favorable for geothermal exploitation.

Harrat Khaybar

The lavas of Harrat Khaybar (5 Ma to present) cover a total area of about 14,00 km² which is the largest component of three coalesced harrats that also includes Harrat Kura to the west (11.5 to 5.5 Ma; 2500 km²) and Harrat Ithnayn to the north (3 Ma to present; 4000 km²). Typical of the MMN volcanic line, Harrat Khaybar is dominated by olivine transitional basalt with alkali olivine basalt becoming more common up section. Thirty-three K-Ar ages for Harrat Khaybar range from 4.33 to 0.14 Ma (Roobol and Camp, 1991b). Abyad Basalt, the youngest unit (1.0 Ma to present), has the greatest compositional range of any stratigraphic unit in the Arabian harrats, with primitive to highly evolved compositions varying from basanite to olivine transitional basalt, alkali olivine basalt, hawaiite, mugearite, benmoreiite, trachyte, and comendite (Roobol and Camp, 1991b; Camp et al., 1991).

The seven subunits of Abyad Basalt are best developed in the elevated central area of Harrat Khaybar, which contains a broad north-south central vent system 50 km long and 20 km wide (Figure 9). Here, young volcanism is evident in the recognition of eight post-Neolithic scoria cones and lava flows (Qb6) and nine historic flows and vents (Qb7). Some of the historic lavas overlie Neolithic walls associated with kite-shaped animal traps, and all are probably younger than about 2000 years B.P. (Roobol and Camp, 1991b). The most distinct of the historic vents is the Jabal Qidr stratovolcano, the only known stratovolcano in the Arabian harrats. It is unknown which of these historic products is the 650 CE. eruption recognized by the Smithsonian Global Volcanism Program (Seibert et al., 2010). Fairer (1986) suggested that an eruption occurred on Harrat Ithnayn in about 1800 CE (referred to in Simkin et al., 1984), but this is improbable because there are no Qb7 deposits on Ithnayn; instead, it is more likely that such activity was at the Jabal Qidr stratovolcano on Harrat Khaybar (Roobol and Camp, 1991b).

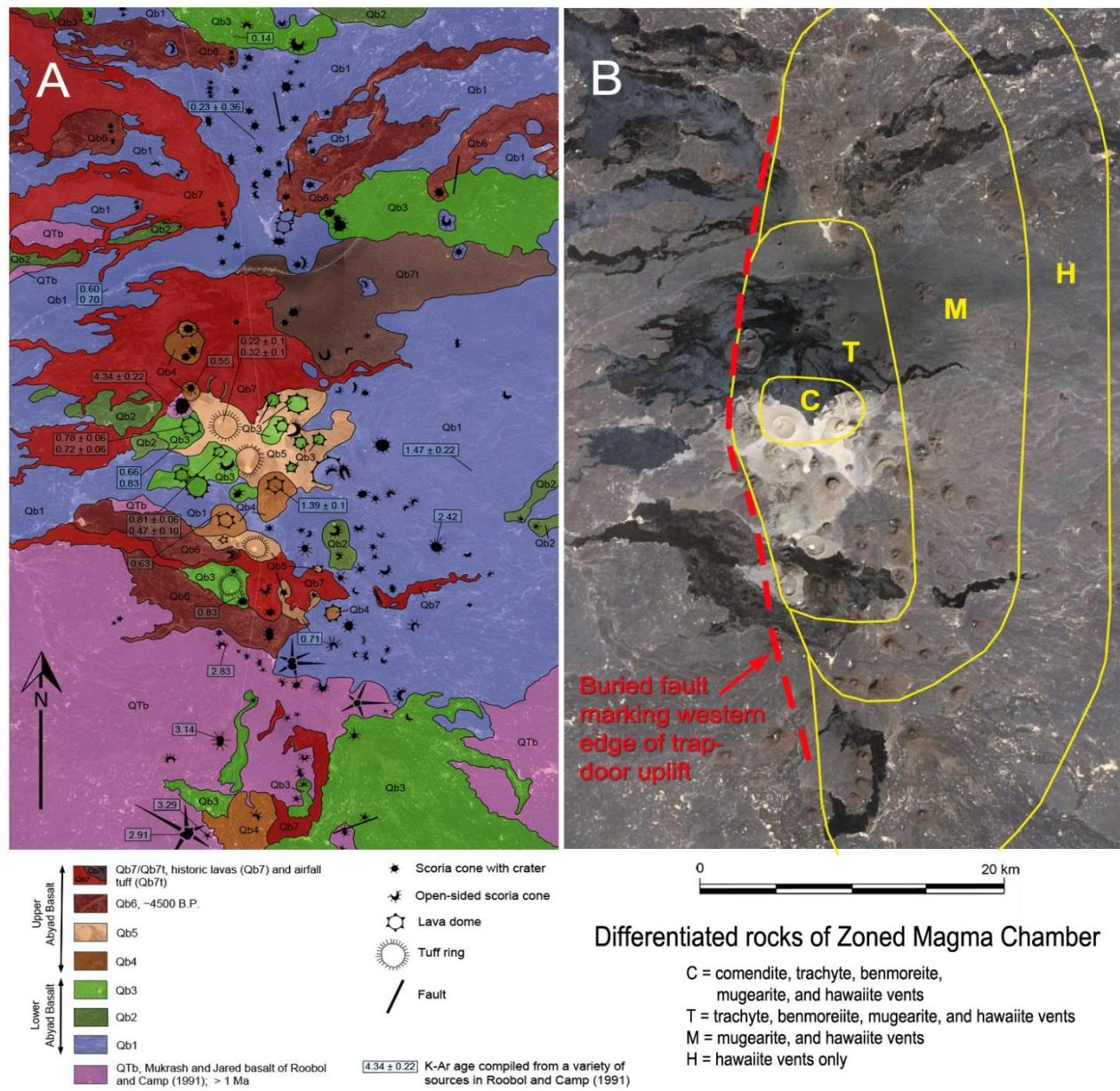


Figure 9. The high central vent system of Harrat Khaybar, at an elevation between 1700 m and 2000 m a.s.l., reduced and modified from Plate 2 (map data from Roobol and Camp, 1991b). A. Most of the exposed vents fed volcanic rocks of Abyad Basalt (< 1 Ma) along a broad (50 x 20 km), north-south trend. Here, more evolved, non-basaltic lavas of mugearite, benmoreite, trachyte, and comendite erupted from a variety of vent types that include scoria cones, tuff cones, tuff rings and lava domes. Several post-Neolithic lavas are present in the central vent area (Qb6), but the youngest subunit (Qb7) is historic and consists of the Jabal Qidr stratovolcano as well as eight lava flows (3 to 55 km long) that erupted from scoria cones. Jabal Qidr is the only known stratovolcano in the Arabian harrat province. B. Concentric zonation of vents and domes reflecting a near-surface zoned magma chamber with an east-dipping chamber roof created by faulting and trap-door uplift.

Scoria cones are the most common vent type on the harrat. Basaltic shield volcanoes are also present, but most common in oldest stratigraphic units (Jarad and Mukrash Basalt). Previously undescribed features, referred to as “whaleback” lava flows by *Roobol and Camp* (1991b), appear to occur as chains of coalesced shield volcanoes. In reality, these features are composed of a sinuous chains of coalesced rootless shield-like volcanoes lying above main arterial lava tubes. These unusual features are restricted to the western side of the harrat, where they radiate outward from a major fault delineated the western edge of the central vent system (Figure 9B). The more evolved lavas erupted from a variety of landforms: mugearites mostly from scoria cones, and benmoreiite, trachyte, and comendite from light-colored lava domes and a variety of phreatomagmatic vents in the form of light-colored tuff cones and tuff rings.

The field and chemical data from Harrat Khaybar are consistent with the development of a shallow magma chamber forming beneath its central vent system. The unusual whaleback lava flows described by *Roobol and Camp* (1991b) are thought to be generated by voluminous outwelling of basalt from a fault associated with trap-door uplift of a near surface magma chamber (Figure 9B). Once the fault was sealed, sidewall crystallization and convective fractionation resulted in the near-surface magma chamber being compositionally zoned. This is reflected in progressively more evolved magmas also erupting at the surface in a compositionally zoned fashion, with comendites restricted to the central most part of the vent system and progressively less evolved lavas erupting over wider areas (*Roobol and Camp*, 1991b; *Camp et al.*, 1991).

The occurrence of numerous Neolithic and historic products on Harrat Khaybar suggest that a large, shallow magma chamber is still present beneath its central vent system. The occurrence of phreatomagmatic vent types in the along the center axis of the vent system, together with contemporary steam fumaroles seen on cool winter days (Figure 10), and numerous fresh-water springs in the vicinity of present-day Khaybar village on western Harrat Khaybar suggest that there is an active, relatively warm groundwater system at the base of the harrat lava flows. These criteria suggest that Harrat Khaybar has a high potential as a geothermal resource, worthy of further exploration. The major question is whether permeable zones exist in sufficient quantities.



Figure 10. Steam fumarole on Harrat Khaybar in 1992, when measured air temperature was 6°C and steam temperature was 25°C (from Roobol et al., 2007).

Harrat Ithnayn

Basaltic lavas from Harrat Ithnayn cover about 4000 km² immediately north of Harrat Khaybar at the northernmost end of the MMN volcanic line (Figure 11). Its central vent system is offset slightly northeast of the Harrat Khaybar central vents, similar to the *en echelon* offset of linear vent systems found throughout the volcanic line. The Ithnayn vents, however, are much more scattered and not as well aligned as those found on Harrat Khaybar. Only basaltic rocks are present (olivine transitional basalt, alkali olivine basalt, and hawaiiite), with a distinct lack of differentiated lavas like those present on Harrat Khaybar. There are no known radiometric dates for Harrat Ithnayn so that all stratigraphic ages are based on flow erosion, weathering and dust-pond development. On this basis, relatively young lavas flows are present, including some flows with surface textures equivalent to post-Neolithic lavas, but there are no clearly historic flows that have the distinct unweathered appearance and lack of dust ponds. As noted in the discussion above, the reported historic eruption of 1800 CE (*Simkin et al.*, 1998) was most likely on Harrat Khaybar rather than Harrat Ithnayn.

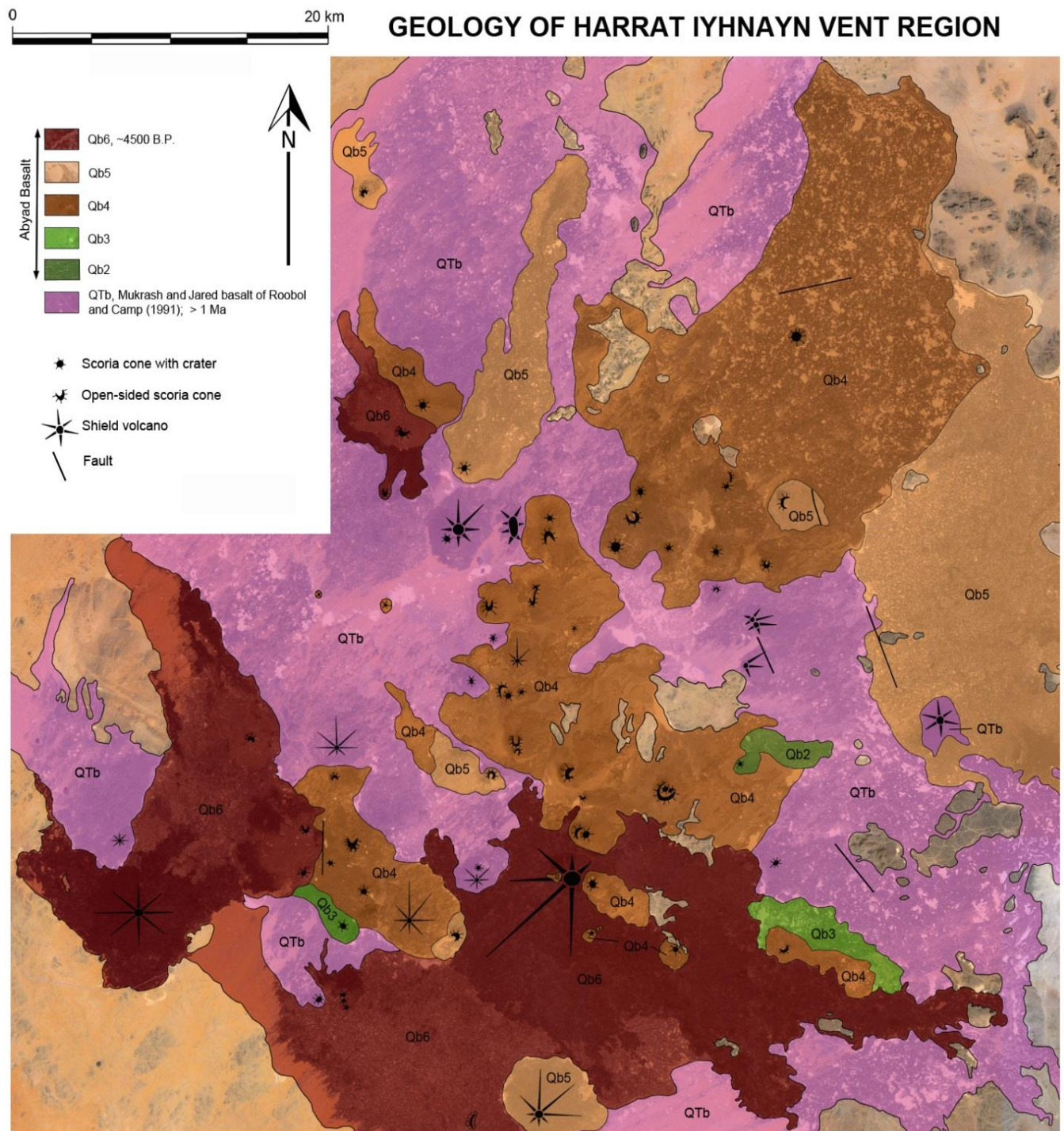


Figure 11. Lava flows and vents of Harrat Ithnayn (map data from Roobol and Camp, 1991b).

Based on the primitive, non-fractionated composition of the Harrat Ithnayn, there is unlikely to be a contemporary shallow magma chamber associated the harrat. Cold fumaroles have been reported from Harrat Ithnayn (*Roobol et al.*, 2007), but without the presence of historic lavas and the lack of evidence for a shallow magma chamber, we suggest that the geothermal potential for the harrat is relatively low in comparison to the other harrats considered here.

Harrat Hutaymah

Harrat Hutaymah covers an area of about 900 km² and is the smallest of the harrat fields considered here (Figure 12). The lava field contains alkali olivine basalts and basanites, many of which contain an abundance of mantle- and crustal-derived xenoliths (*Pallister*, 1985; *Thorner*, 1990; *Duncan et al.*, 2016). The primitive, undersaturated character of the lavas is compositionally more akin to Harrat Lunayyir than to the other harrats along the MMN volcanic line. The lava field was fed from at least 57 relatively small scoria and spatter cones, and at least 22 tuff rings and maars (*Pallister*, 1985). The high concentration of these phreatic and phreatomagmatic vents, about a third of the total vent population, is exceptional when compared to the other harrats, and could indicate the presence of significant meteoric water as sub-surface or surface sources during the time of the eruptions. Although a phreatic component to the maar eruption is likely, *Pallister* (1985) suggests that the tuff rings may not have involved significant meteoric component, but rather result from a diatreme origin.

Much of the harrat lavas are covered by aeolian deposits which makes it difficult to identify erosional and weathering surface characteristics. The surfaces that are observable do not show significant morphological differences, which may suggest a relatively short time span for the eruptions with no significant time gaps between successive flows and vents. In fact, *Duncan et al.* (2016) note that paleomagnetic field measurements all show normal polarity consistent with a relatively young age within the Brunhes interval (≤ 780 ka), and their new ⁴⁰Ar-³⁹Ar ages on 14 lava flows fall within a relatively narrow age range of 850 to 260 ka.

GEOLOGY OF HARRAT HUTAYMAH VENT REGION

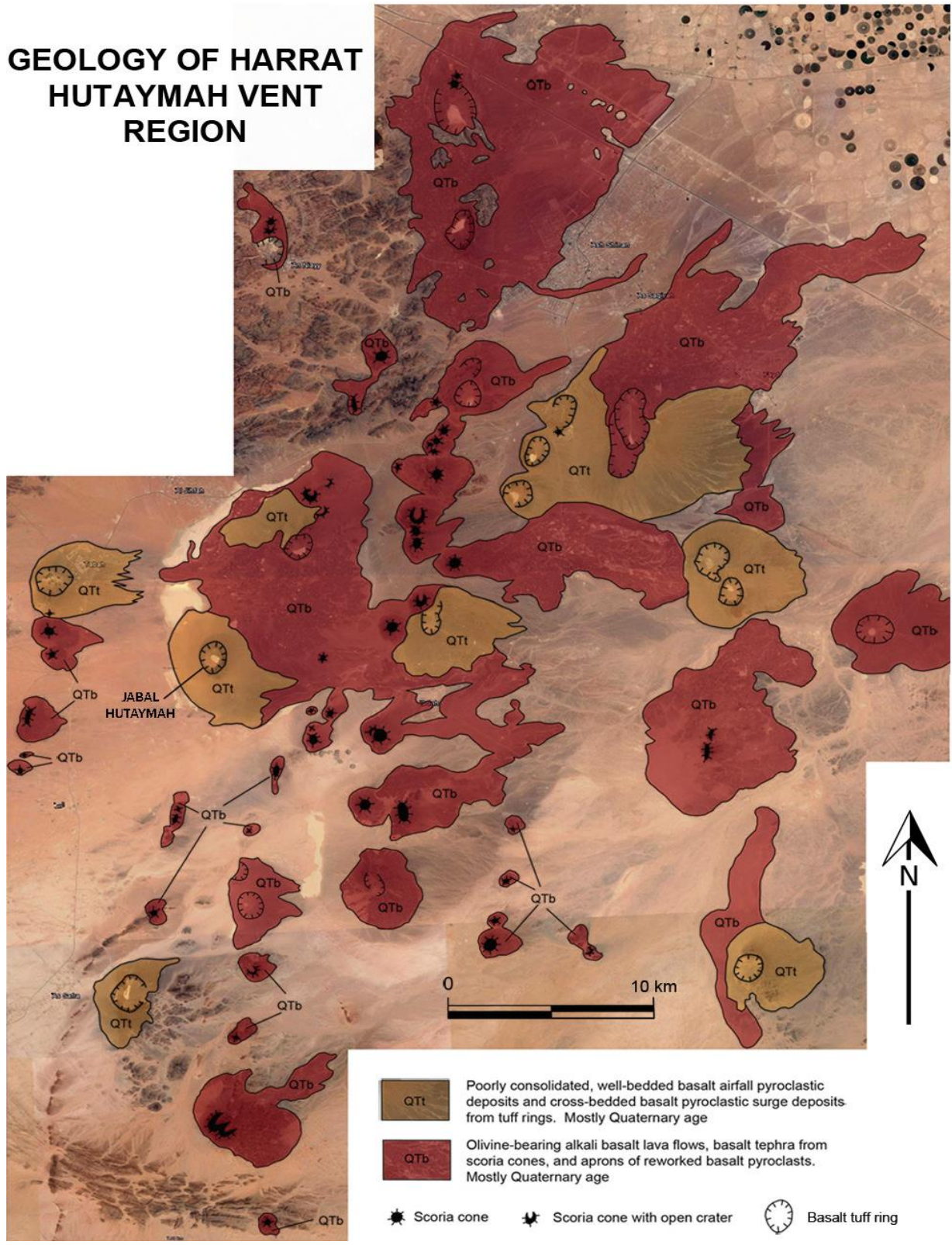


Figure 12. Lava flows, pyroclastic deposits, and vent types of Harrat Hutaymah, (map data from Pallister, 1985 and Thornber, 1990).

Today, a significant but localized amount of sub-surface water exists as cylindrical groundwater reservoirs at considerable depths beneath tuff-ring craters filled with Quaternary alluvium (*Pallister, 1985*). There is no indication of excessive temperature in well-water extraction, however. The lack of young volcanic products (< 250 ka), including post-Neolithic and historic eruptions suggest that Harrat Hutaymah may not hold as much promise for geothermal exploration as the other harrats considered here.

Geothermal Potential of northern Harrat Rahat

Harrat Rahat has a large aerial extent of about 19,800 km², elongated in a north-south direction for 310 km along the MMN volcanic line. It is a composite of four smaller harrats that coalesced during extrusion, each of which has an elongate shield-like shape with a central area marked by linear vent systems. The northernmost of these coalesced harrats was called Harrat Rashid by *Camp and Roobol* (1989, 1991) and Harrat Al Madinah by *Moufti* (1985). This well-studied northern region contains the youngest flows on Harrat Rahat. We first assess here, the geothermal potential of northern Harrat Rahat, based on geologic constraints, and later use advanced geophysical capabilities to detect and characterize potential anomalous zones of high thermal energy beneath the harrat surface.

Geological Constraints

Camp and Roobol (1989, 1991) recognized two prominent lateritic disconformities in the volcanic succession of Harrat Rahat which they used to subdivide the harrat stratigraphy into three main stratigraphic units, the Shawahit (10-2.5 Ma), Hammah (2.5-1.7 Ma), and Madinah (1.7 Ma to recent) basalts, comprising 68%, 19%, and 13% of the harrat volume, respectively. This lava succession sits above an irregular surface on the Proterozoic basement where aeromagnetic and gravity data indicate that it varies in thickness from 100 m near the margins of the harrat to as deep as 300 to 500 m in the center (*Blank and Sadek, 1983; Aboud et al., 2015*). A northward volcanic migration with time is evident in the stratigraphic evolution, with younger Madinah basalt eruptions becoming more prevalent in the northern part of the harrat (Figure 13). Olivine transitional basalt dominates the harrat volume in the older units, but it diminishes in

volume up section. The Madinah basalt in northern Harrat Rahat contains olivine transitional basalt, but the greater basalt volume is alkali olivine basalt and hawaiiite which differentiate along a mildly alkaline trend to produce a smaller volume of mugearite, benmoreiite, and trachyte (Camp and Roobol, 1989, 1991; El Difraway et al., 2013).

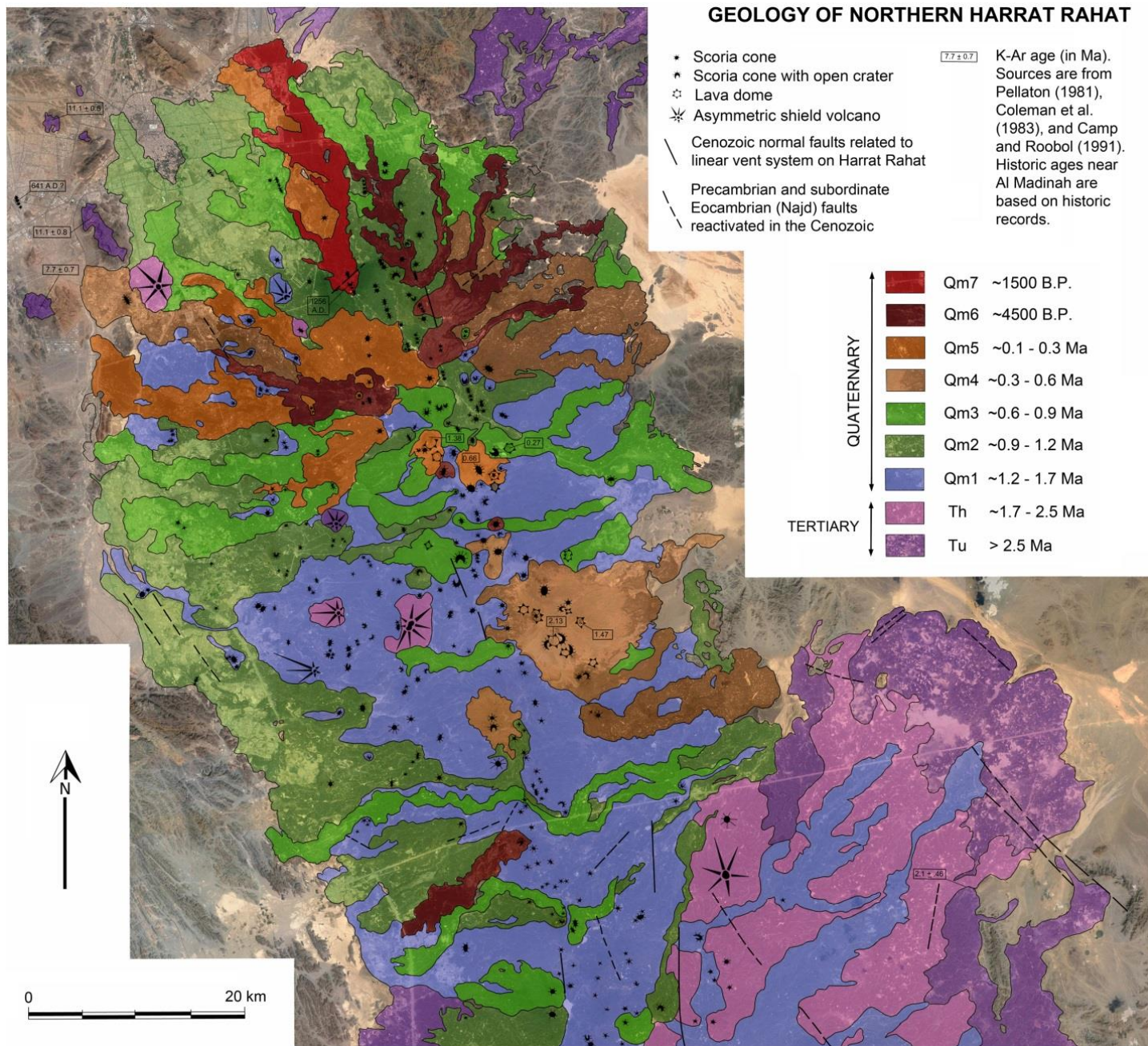


Figure 13. Geologic map of northern Harrat Rahat, (map data from Camp and Roobol, 1991).

Like the other harrats, distinct volcanic landforms on Harrat Rahat reflect different styles of eruptive activity (e.g., *Runge et al.*, 2014). The landscape is dominated by scoria cones and associated lava flows, and prominent shield volcanoes that are particularly common in the older Shawahit basalt. These vent types form the eruption sites for basalt, hawaiite, and mugearite volcanism. Less common are lava domes and pyroclastic deposits associated with benmoreiite and trachyte volcanism. These more differentiated landforms are largely restricted to northern Harrat Rahat where color contrasts on aerial photographs and satellite imagery make them readily identifiable (Figure 14).

The Madinah basalt was subdivided into seven subunits by *Camp and Roobol* (1989, 1991). The four youngest of these comprise the upper Madinah basalt (Qm4 to Qm7). They are defined by their lack of erosion, but vary from one another in surface color due to weathering and in the volume of surface dust ponds. Based on a compilation of K-Ar ages from *Camp and Roobol* (1989) together with new ^{40}Ar - ^{39}Ar ages from *Moufti et al.* (2013), approximate age constraints for these four subunits are: Qm4 (late Pleistocene; mostly < 500,000 yrs. BP), Qm5 (latest Pleistocene to Holocene; < 30,000 yrs. BP), Qm6 (post-Neolithic < 4,500 yrs. BP), and Qm7 (historic). The flows and vents for each of these subunits is shown in Figure 14, with vent distribution outlined in light blue. The post-Neolithic lavas are distinct on satellite imagery and lack the abundant Neolithic burial mounds that characterize the harrats of Saudi Arabia, thus indicating that they are younger than ancient peoples. These burial mounds are likely related to a population of people during the last pluvial interval on the Arabian Peninsula, named the Neolithic pluvial period by *Kaiser et al.* (1973), with ^{14}C ages between 7000 and 4,500 yrs. BP. The post-Neolithic lavas are therefore certainly younger than 7000 yrs. BP, and probably younger than 4,500 yrs. B.P.

The youngest subunit on Harrat Rahat (Qm7) is composed of two historic eruptions, both located near the Holy City of Madinah in 641 and 1256 CE (Figure 14). Geologic descriptions of the 1256 CE eruption are given by *Camp et al.* (1987) and *Kawabata et al.* (2015). The eruption lasted for 52 days, producing high Hawaiian fountains and a 23 km-long lava flow that approached the ancient city to within 8 km. The 641 CE eruption site was identified by *Camp and Roobol*, (1989, 1991) through a 1568 CE historic account kept in the Hacmud Library in Al Madinah (*Al-Samhoudy*, 1568), together with the use of surface characteristics derived from

false-colored ratioed satellite imagery and field observations. This eruption site is located west of the main harrat body, only 12 km from the Holy Mosque of Al-Madinah (Figure 14). Here, the eruption occurred along a 0.8 km-long fissure to produce four small pyroclastic cones that varied from phreatomagmatic to magmatic activity (Murcia *et al.*, 2014).

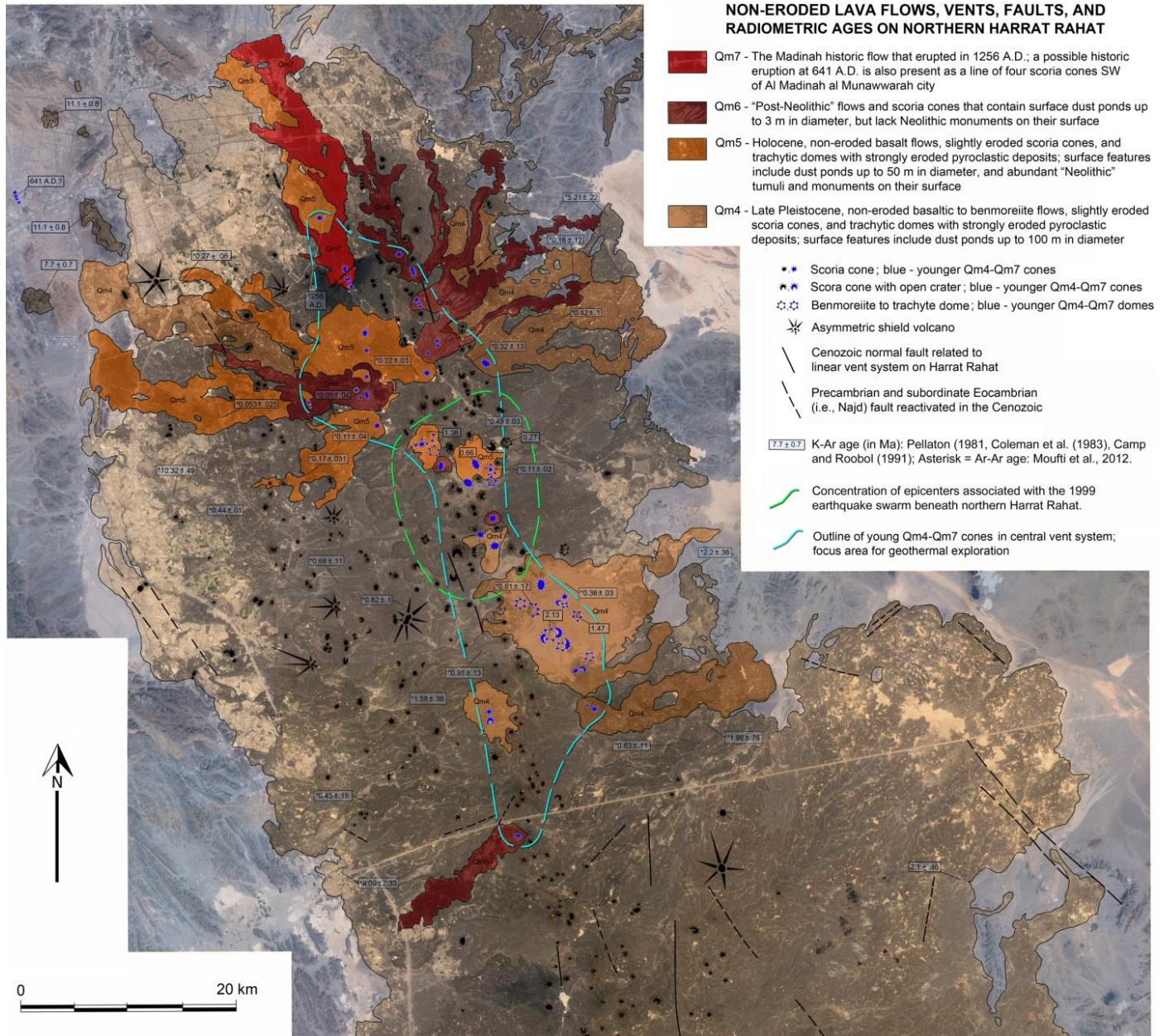


Figure 14. Distribution of non-eroded lava flows of upper Madinah basalt (Qm4 to Qm7) on northern Harrat Rahat. Qm4 to Qm7 vents are outlined in broken blue line, and epicenters for the 1999 earthquake swarm on northern Harrat Rahat are outlined in broken green line.

Northern Harrat Rahat is a young, active magmatic system that appears to have generated 13 eruptions during the past 4,500 years, for a rate of one eruption every 346 years. A recent, high-resolution tomographic study of the crust and upper mantle beneath northern Harrat Rahat revealed strong heterogeneities marked by interconnected low-velocity zones interpreted as a magma reservoir between 40 and 10 km depth (Figure 15; *Abdelwahed et al.*, 2016). This reservoir appears to coincide largely with the NNW-trending Qm4 to Qm7 vents outlined in Figure 14. It extends for about 35 km southeast of the 1256 CE vent area, and encompasses the area of a 1999 earthquake swarm of 145 seismic events, also outlined in Figure 14. Integrated studies of source parameters and focal mechanisms led *Abdelwahed et al.* (2013, 2016) to conclude that the earthquake swarm area consists of significant partial melting material, and that the swarm itself was triggered by rising magma at 40-20 km depth. The distribution of hypocenter depths in *Abdelwahed et al.* (2016) seems exceptionally high and this may bias the tomographic results. The geologically young development of a contemporary crustal magma chamber, or chambers, in northern Harrat Rahat is consistent with differentiated rock types found in upper Madinah basalt, which typically require residence time in crustal reservoirs.

The hydrogeology of northern Harrat Rahat is understood to a much greater degree when compared to other harrat areas, largely because of the importance of groundwater to the ever-increasing population of Al-Madinah. A significant aquifer with a thickness of about 60 m exists beneath the harrat lavas, with the host rock composed of the weathered upper part of the Proterozoic basement and pre-basalt sands and gravels that reach their greatest thickness in paleochannels (*Al-Shaibani et al.*, 1989; *Al-Shaibani*, 2003). *Gorge and Shorbaji* (1987) and *Al-Sahibani* (2003) report a mean temperature of the groundwater system beneath northern Harrat Rahat of 36°C, about 4°C higher than average groundwater measurements of *Bob et al.* (2015) from 20 wells in the Madinah City area, just a few kilometers outside the confines of the harrat. *Roobol et al.* (2007) identified a 3.2-km-long line of weak fumaroles adjacent to the 1256 CE historic lava flow with associated seismic activity from 1986 to 1988. They also reported several individual water wells in the region had anomalously high temperatures up to 53°C, consistent with geothermal processes.

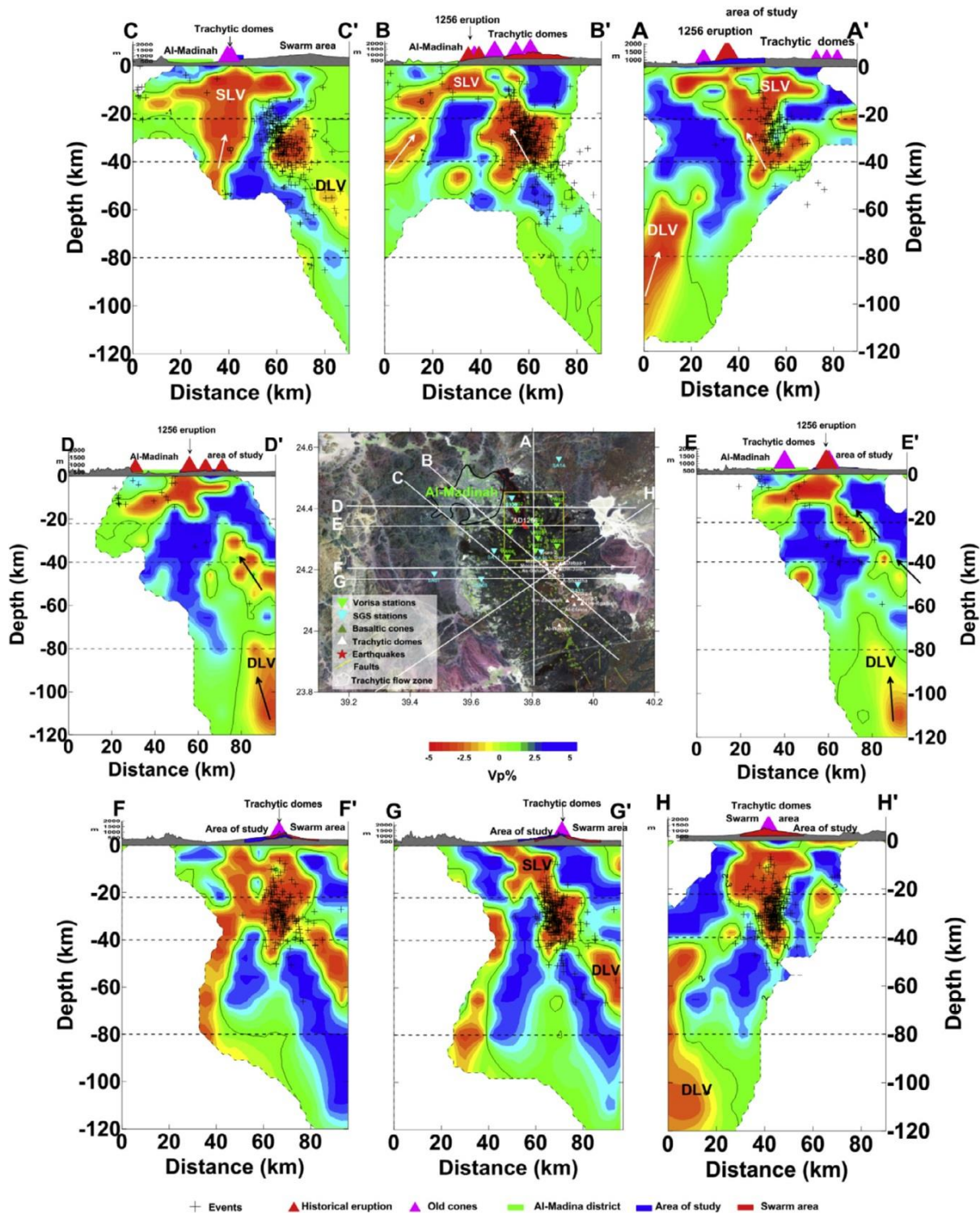


Figure 15. Vertical cross-sections of P-wave tomography beneath northern Harrat Rahat (from Abdelwahed et al., 2016). Profile locations are shown in inset map. Red and blue colors represent low and high velocities, respectively, with velocity perturbation scale shown below inset map. Purple and red triangles denote basaltic scoria cones and trachytic domes, respectively. Hypocenters for the 1999 earthquake swarm are denoted by small plus signs.

Fluid flow in geothermal areas can be enhanced and localized by deep-seated faults. Faults in the Precambrian basement surrounding northern Harrat Rahat conform to three region trends (Figure 16): (1) northwest faults are the dominant trend largely related to the major left-lateral Najd wrench-fault system that formed in the Eocambrian by collision-related intracratonic deformation (*Davies, 1984; Stoesser and Camp, 1985*), (2) enigmatic east-west faults that have are of considerable lengths, and minimal horizontal offset (*Camp and Stoesser, 1985; Ramsay, 1986*), and northeast-trending faults which appear to have formed during late Proterozoic island-arc collision (*Camp, 1984*).

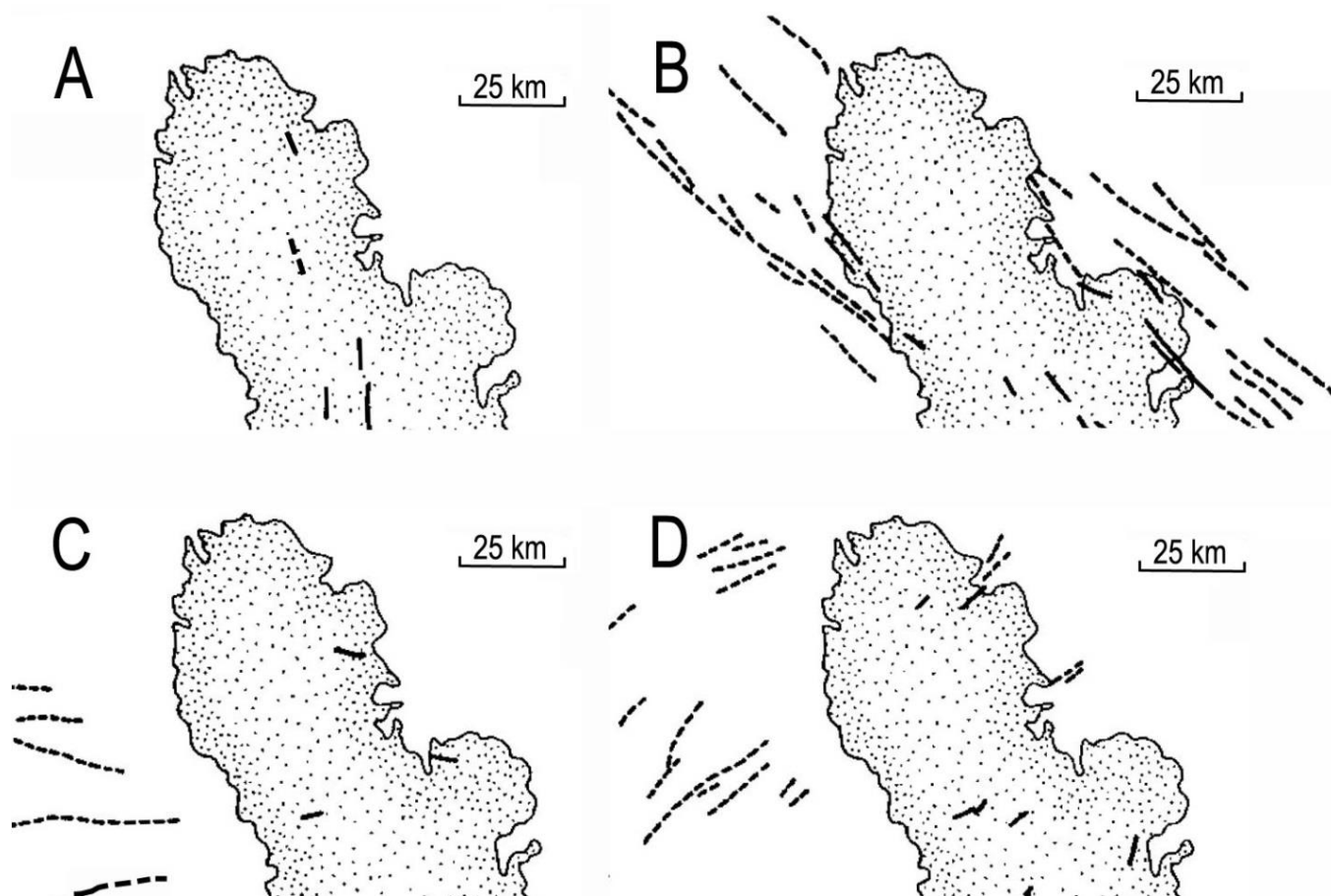


Figure 16. Fault trends on northern Harrat Rahat and in the surrounding Precambrian basement. A. north to north-northeast trends restricted to the central vent area of the harrat, B. Northeast-trends related to the Eocambrian Najd fault system, C. East-west trends of unknown origin, and D. northeast-trends associated with sutured boundaries and reverse/thrust faults generated by late Proterozoic island arc-collision.

In addition, north- to north-northwest-trending faults that are generally absent in the basement rocks, but nevertheless present along the central crest of the northern Harrat Rahat vent system. These latter faults may well be associated with dike intrusion, similar to that generated on Harrat Lunayyir in 2009 (Figure 17). *Aboud et al.* (2015) use filtered magnetic and gravity data from northern Harrat Rahat to delineate all three of the older basement trends, as well as the younger trend coincident with central vent axis.

In summary, the apparent crest of mantle upwelling beneath the MMN volcanic line is the site of abundant magmatic activity with geothermal potential. Groundwater temperatures are about 100°C at Al Lith hot springs, south of Harrat Rahat, where the MMN line crosses the Red Sea coastal plain above thin crust of about 15 km depth. Slightly elevated groundwater temperatures, weak fumaroles, and post-Neolithic to historic eruptions sites are present above thicker crust (about 40 km depth) coincident with the central vent axes of northern Harrat Rahat and Harrat Khaybar. These same areas show geological and/or seismic evidence for young, magma chambers where geothermal systems most commonly develop. An environment of geothermal potential is certainly present in these areas, but a more accurate assessment of this potential warrants further geothermal exploration.



Figure 17 Ground fissures in northern Harrat Rahat, near Al Madinah, from the Saudi Geological Survey. These examples are similar in length, width and character to the dike-induced fracture generated on Harrat Lunayyir in 2009.

3.2 Event Detection Processing

As mentioned earlier, we use advanced detection algorithms in an attempt to detect and identify small earthquakes that were not detected by the processing used to construct the standard catalog released by network operators. These new locations may help to identify faults and areas of high strain associated with possible areas of high permeability needed for an economically viable geothermal area. The idea is motivated by analogy with the seismicity recorded at the Tres Virgines field prior to geothermal exploitation. Here we summarize the results of the detection processing. The processing takes two steps: identification of anomalous events (detectors) and then application of these detectors as matched filters to identify repeating events (multiple detectors) and finally local events. Table 2 summarizes the number of detectors created by the autonomous system for each of the four stations, the number of detectors that had multiple detections, and the number of detectors developed on local events based on visual inspection of the event waveforms. As we are primarily concerned with Harrat Rahat, only stations in Harrat Rahat were used. Seismic data from other harrats was not available.

Table 2. Framework detectors.

Station	Number of detectors created	Number of multiple detectors	Number of local event detectors
RHT01	370	45	13
RHT04	2290	40	9
RHT14	486	9	3
RHT15	572	22	5

Station RHT01 was the top performer in producing detectors constructed from local events, and, thereby, in producing large numbers of local event detections. However, most of the detections appeared to be related to quarry operations. One group of events was very likely to be a pair of earthquakes (Figure 18 and 19). These events were selected for the second correlation detection step. We refer to them as a group by the identification number (673576) assigned by the autonomous system to the detector that found them.

Again, because the number of local detectors is modest, we provide plots of the waveforms from the events comprising the groups for stations RHT04, RHT14 and RHT15 in Appendices B, C, and D, respectively. Summary data (detection time, detector, detection statistics) for the

detections for just those events deemed to be local are provided in Appendix E. No attempt has been made as yet systematically to reconcile the detections among the stations. Detectors were run independently on the four stations, and the detections frequently overlap among them (e.g. RHT01:674249 and RHT04: 680028).

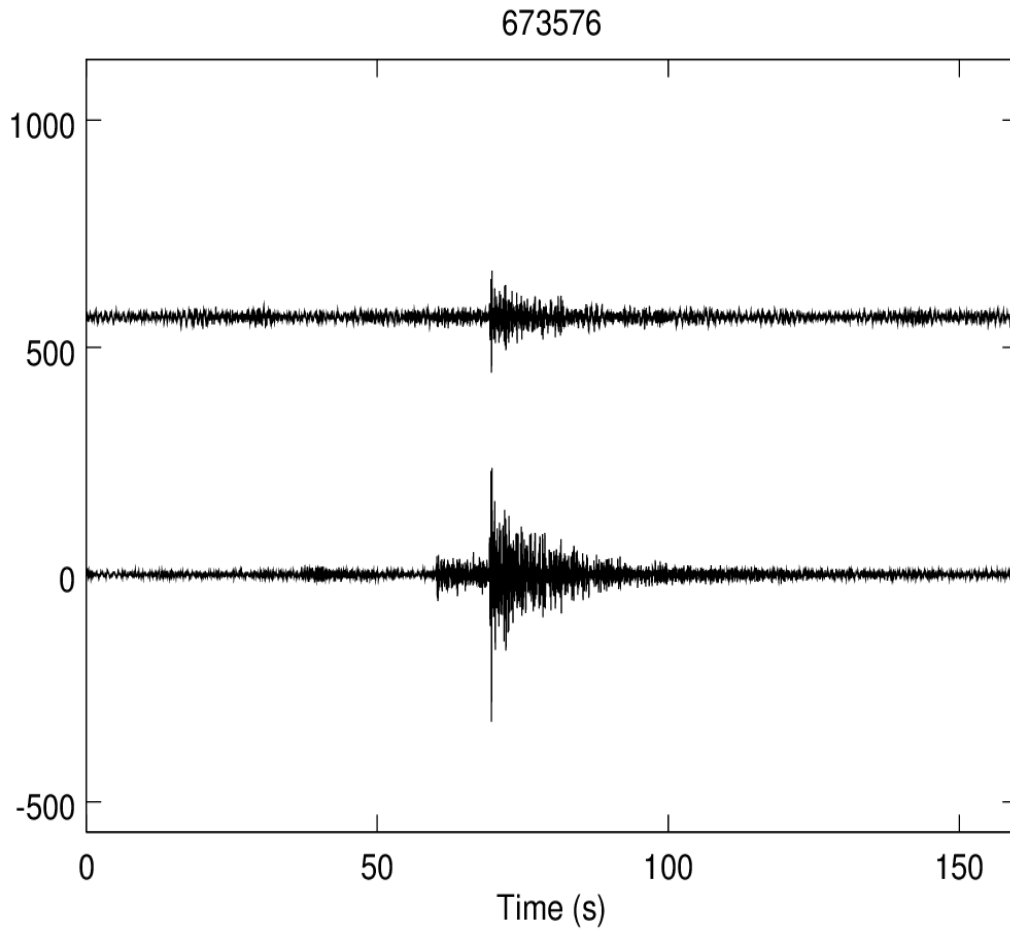


Figure 18. Local earthquakes selected for a second pass of correlation detection.

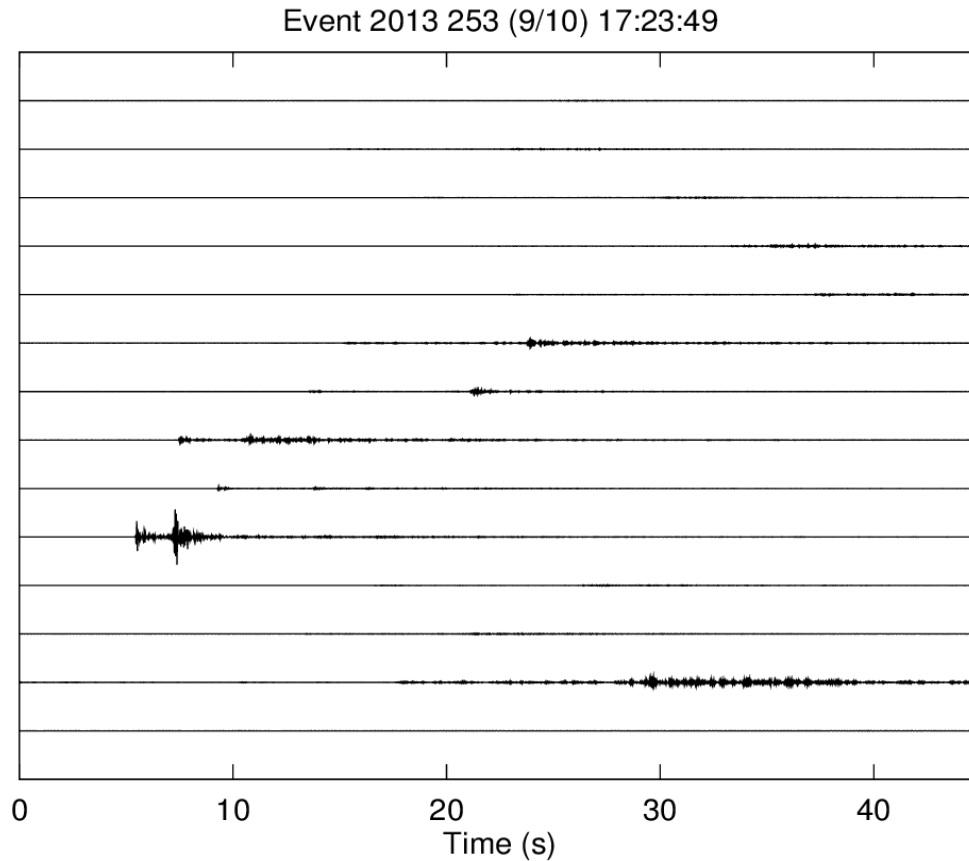


Figure 19. Vertical-component waveforms from all stations of the network for the first event in the 673576 pair. The large waveform (10th trace) is the recording at station RHT11. This station is closest to the source and was selected for high-frequency correlation processing.

We configured a subspace detector (*Harris, 2006*), a type of generalized correlation detector, to operate on the three channels of station RHT11, using the detector 673576 event pair to construct a rank-one detector. The detection statistic produced by the subspace detector in the high-frequency band (4-20 Hz) is shown in Figure 20. This detection statistic produced twelve valid event detections, which are displayed in Figure 21. Most of the events are quite small, with corresponding low SNR signals. These smaller events are properly considered to be microseismic, since they were detected only at station RHT11.

These events are events of the correct size that we seek to understand volcanic processes and potential geothermal sites in the Harrat Rahat. Unfortunately, these particular events occurred to

the north of the Harrat, and, therefore, may not be associated with volcanic processes. The procedure was successful in finding events of the right type, if not in the high-interest location.

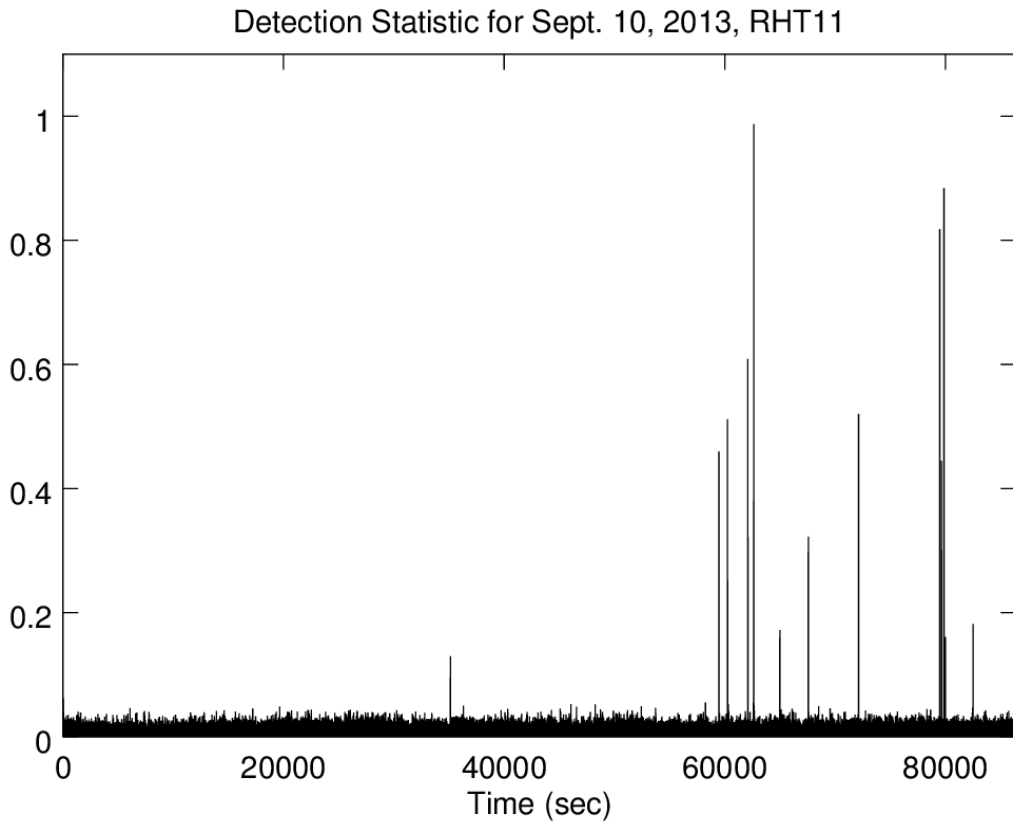


Figure 20. Detection statistic produced by the subspace detector constructed from the large events. Twelve valid event detections resulted in this time period, with an additional detection on 10/24/2013 (corresponding to the second large event of Figure 18). Many of these events are much smaller than the two large design events and would properly be considered microseismicity.

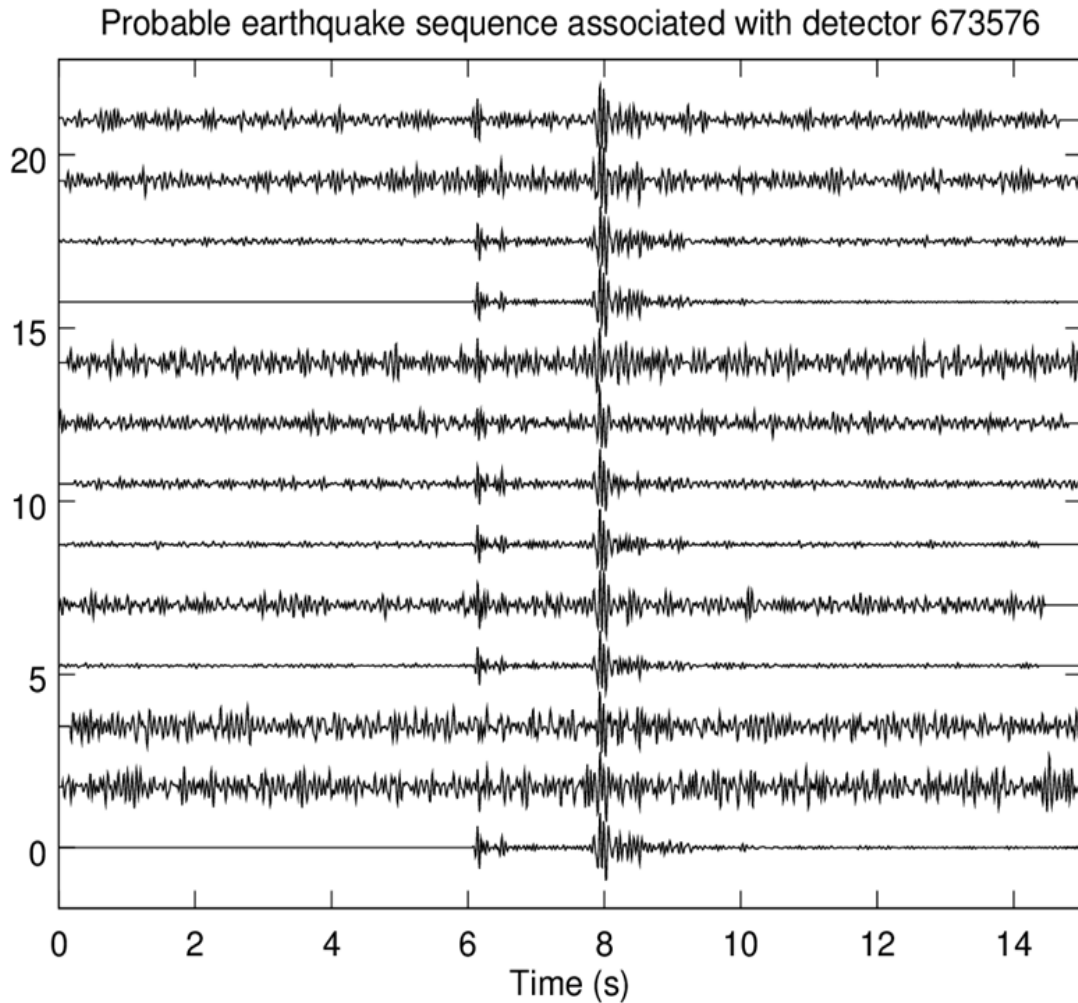


Figure 21. The collection of vertical-component event waveforms found in the RHT11 continuous stream by the high-frequency subspace detector. The events clearly are highly repetitive, consistent with a small source region.

Correlators built with catalog event templates

In an attempt to improve the results, an alternate detection method was also tested. We had at our disposal waveforms from 50 events from the time period 2010/2/13 - 2014/6/15. We selected 39 of these for high signal-to-noise ratio and used them as templates to process the network data stream from July 1, 2013 – July 1, 2014. Whereas with the autonomous processing individual stations were selected for correlation detection, this time multiple stations were selected for each event. A single multichannel correlator was used for each event in a frequency band chosen to maximize signal-to-noise ratio (SNR), either 1-10 Hz or 2-20 Hz depending on the individual

event. For each event, the stations contributing to the correlation were chosen to maximize the number of channels with approximately similar signal amplitudes, in an attempt to minimize the false alarm rate. Each event had a unique network footprint on which its signals were well recorded. Appendix A provides detail on each of the multichannel templates producing new event detections, describing the channels selected for each template and the frequency band used for detection processing.

The continuous data (July 2013 – July 2014) were processed for each template event, using the channel configuration chosen for that event. Frequently, the correlation detector produced no new detections. Several of the detectors were “runaway” detectors generating a large number of detections unrelated to the template event. Screening these two cases out, we obtained 9 detectors that produced interesting new collections of events (Appendix A).

The map of Figure 22 shows the catalog locations of the 39 events used as templates, in light grey, if they produced no usable new detections, in red, if they produced new detections and were judged to be associated with mining, and in green, if they produced new detections and were judged to be earthquakes. Six of the nine productive events probably were from explosion sources and 3 were probable earthquakes. Altogether, the nine productive templates found an additional 36 events in the time period July 1, 2013 – July 1, 2014, adding to the original 16 catalog events that we had during that time period (total after detection processing: 52). Five of the new events were probable earthquakes; it happens that two of the earthquakes in the catalog list were from the same source and produced duplicated new events. The remaining 31 new events were explosions, all from two source regions. Figure 22 shows the locations of the productive template events.

Appendix A provides detail on the multichannel templates and detections from the nine productive events. The other 30 events are not discussed, as they produced no new information.

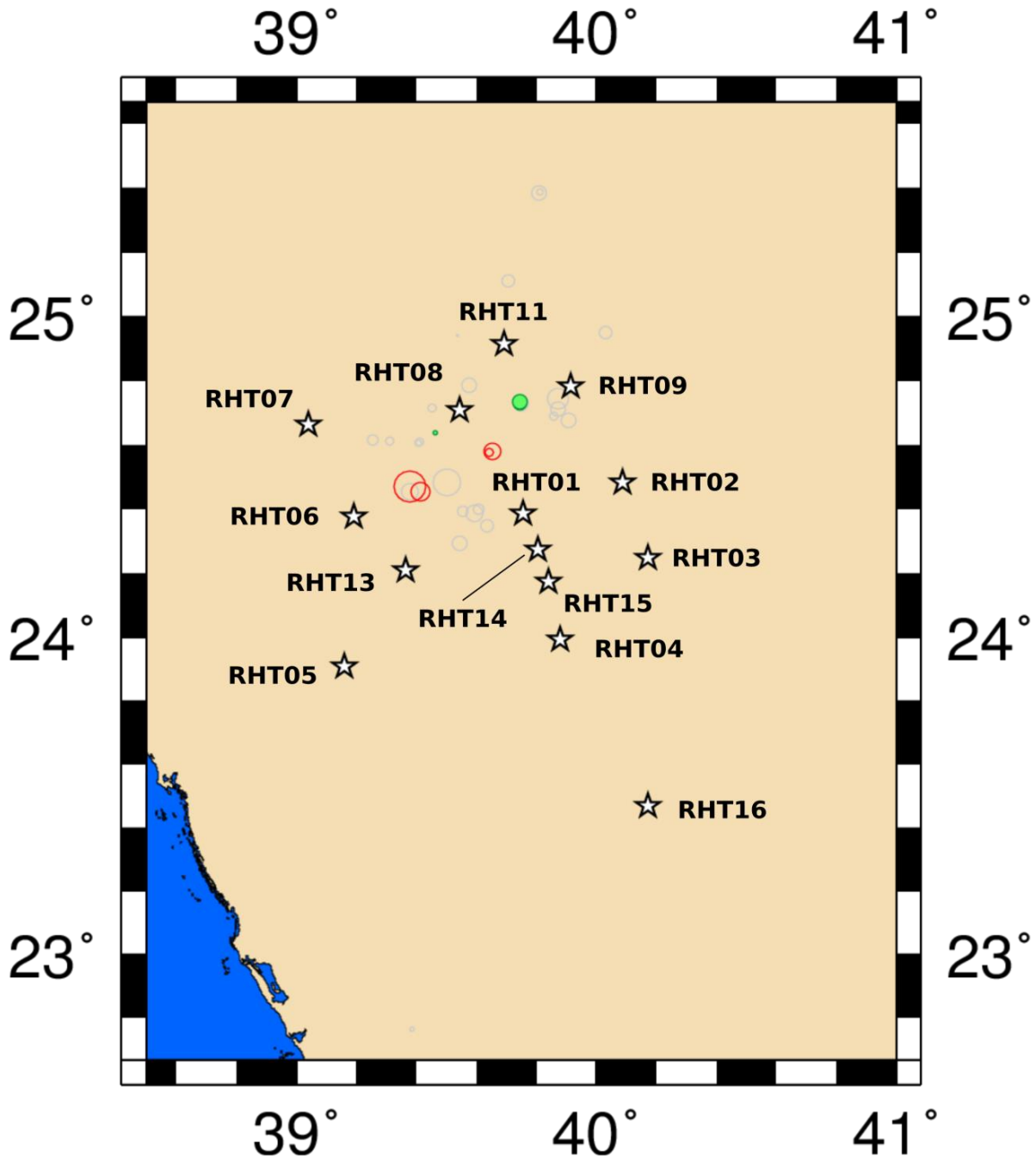


Figure 22. Map of events from the catalog used as templates for correlation detection. The locations are those of the catalog. The events are indicated as circles, with symbol size proportional to the reported magnitude, and the stations are shown as black stars. The events are confined to the northern part of the Harrat Rahat, except for one small event toward the bottom of the map. Light grey circles indicate events that were not used or failed to produce additional detections. Red circles indicate events that produced additional detections and were judged to be explosions. Green filled circles indicate events that produced additional detections and were judged to be earthquakes.

3.3 Ambient noise analysis

In parallel, we use ambient noise cross-correlation to estimate crustal velocity structure (Figure 23). This method uses the seismic noise background to infer crustal velocity structure (*Shapiro and Campillo, 2004; Bensen et al., 2007*). Ambient noise correlation has been widely used to create surface wave tomography maps in numerous regions (*Bensen et al., 2009*). Recently, this technique has been applied to geothermal areas and other regions of high heat flow and has successfully identified seismic velocity anomalies (*Brenguier et al., 2007, Stankiewicz et al., 2010, Seats and Lawrence, 2014*). We apply it to the area around Harrat Rahat (Figure 23).

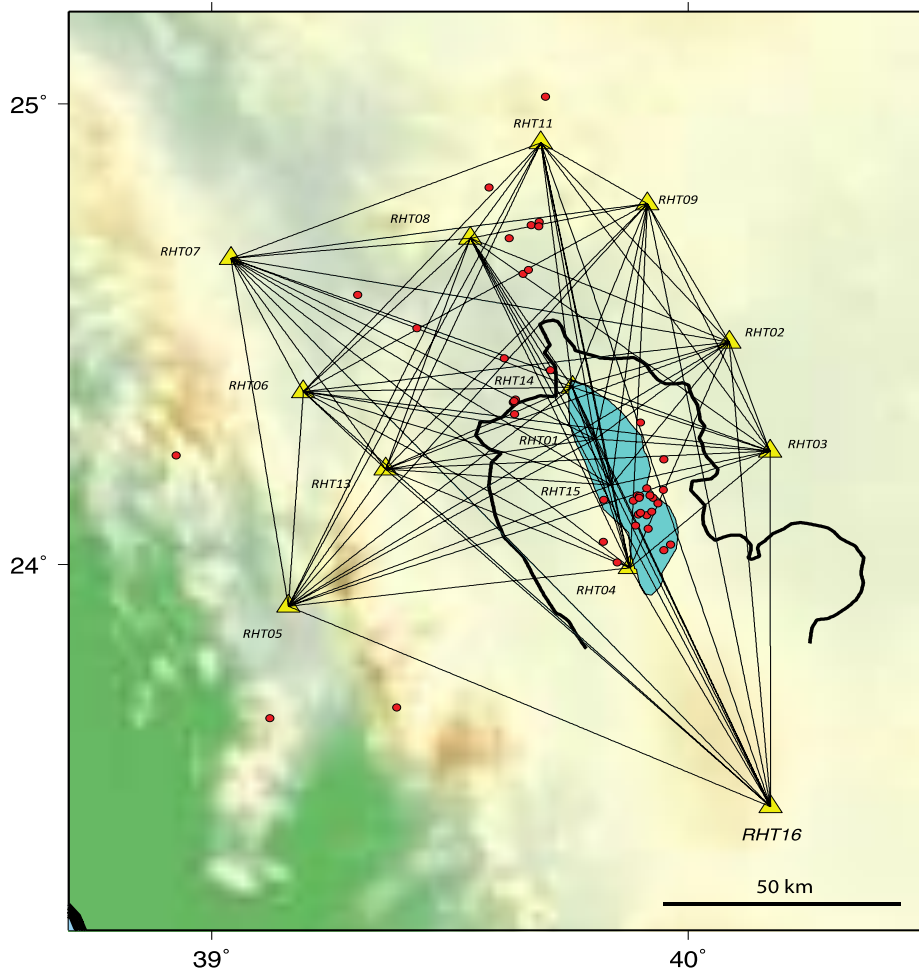


Figure 23. Raypaths covered by the ambient noise correlation showing seismic stations and outline of the northern Harrat Rahat. The blue area denotes the area of likely high subsurface heat flow based on the young volcanics as mapped based on surface geology. Velocity models have been generated for each path.

In brief, correlation of long time periods of seismic noise recorded at a pair of stations will yield the Green's function response of the path between the two stations. Once Green's functions have been calculated for each station pair, the next step is to convert them into representations of the velocity structure. Typically, the velocities are obtained by inverting the dispersion curves for 1D structure along the path. We expect that the area directly under Harrat Rahat will show anomalous velocity structure due to high temperatures and zones of magma when compared with the surrounding crust.

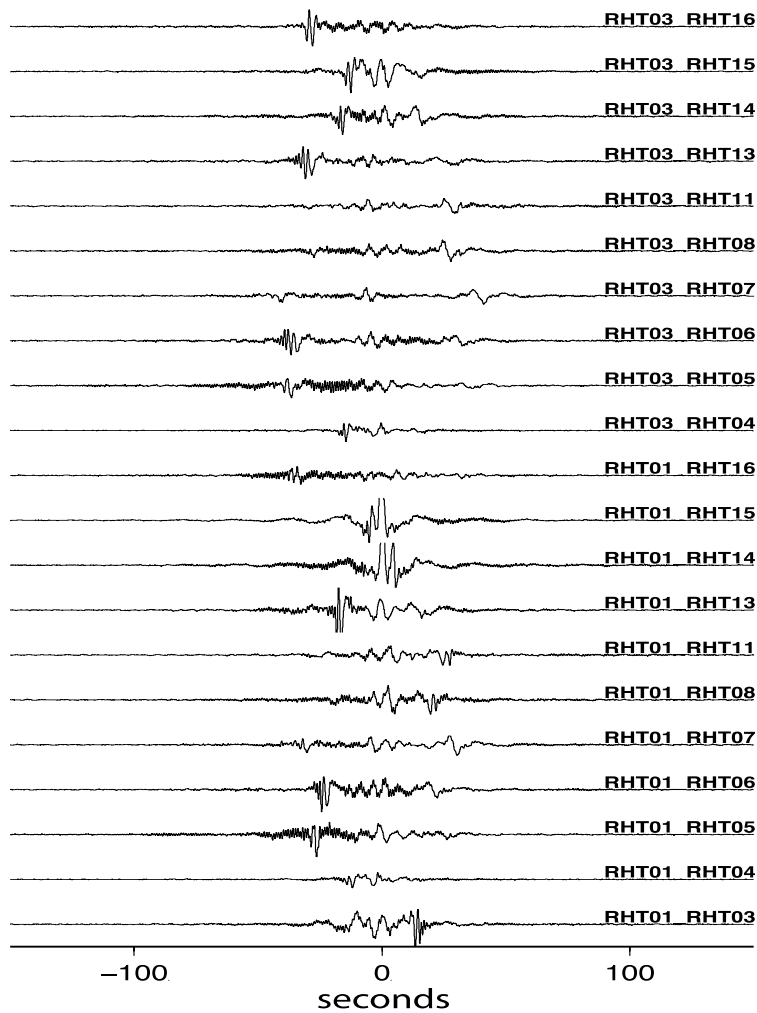


Figure 24. Example of Green's functions generated for various stations pairs. Several of the functions are asymmetric indicating azimuthal varying noise sources.

The available data is from 14 stations that comprise a local network in the region around the Harrat Rahat. 18 months of continuous data is available from August 2013 to September 2014. In general it is best to use a year or more of data as the technique is sensitive to seismic noise, which varies in amplitude seasonally (*Al-Amri et al.*, 1999). The data was converted to seismic analysis format (SAC), the instrument response was removed, and then divided up into day-long files, one for each station (Z component) and decimated to a 5 Hz sample rate.

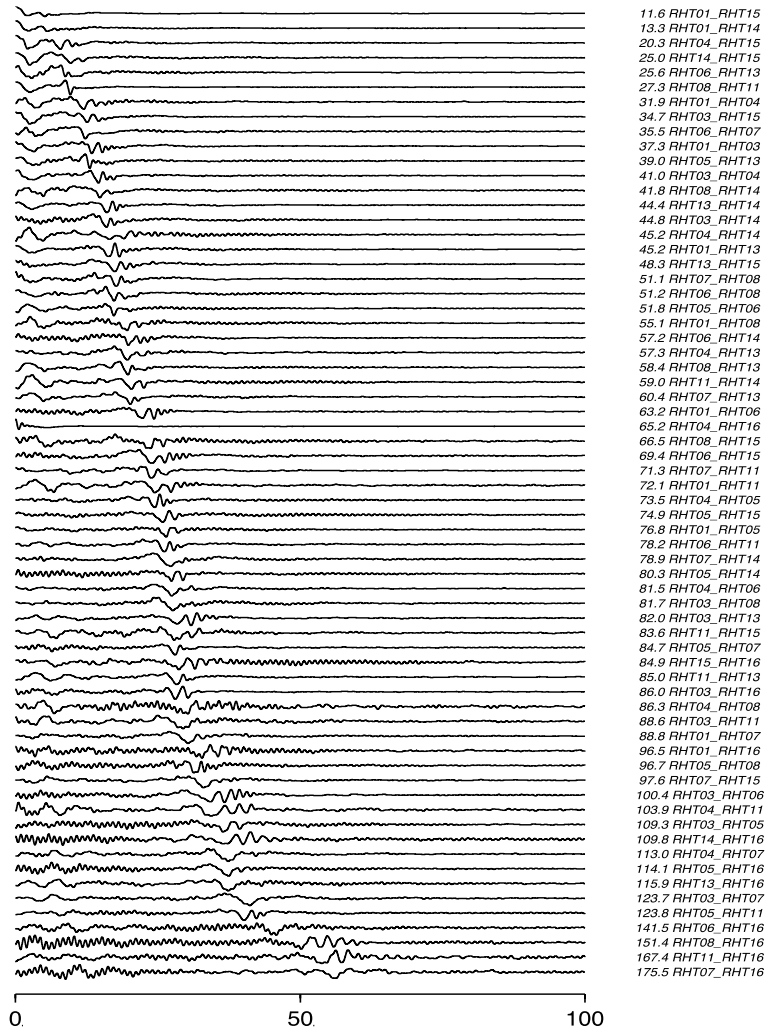


Figure 25. Green's function displayed as a function of distance.

Processing followed the general procedure of Bensen et al., (2007) although a running average was used rather than a signbit procedure to normalize outliers. Cross-correlations for each day/station pair were calculated and then stacked by months. These stacks were then manually examined for artifacts due to instrument problems or large signals. All month stacks were then

stacked for each station pair. 67 stations pairs were calculated. Processing the entire dataset required approximately 700 Gb of disk space and one week of CPU time on a 12 core Linux machine. Several runs were made to test different normalization routines (e.g. signbit) and filter parameters. Auto-correlations were also calculated to validate processing. The Green's functions show clear differences between station pairs indicating substantial differences in velocity structure and possibly attenuation. A drawback is that several show clear asymmetry (Figure 24), which indicates that the noise is not azimuthally balanced, which will bias results. The stacks were then folded and summed to eliminate asymmetry and displayed in order by distance between stations (Figure 25). This showed a clear pattern and showed that the Green's function were well resolved with a high signal-to-noise. The next step was to examine the paths with respect to the known geology. Pairs that were entirely inside the volcanic region were compared with path outside the volcanic region and in the shield (Figure 26).

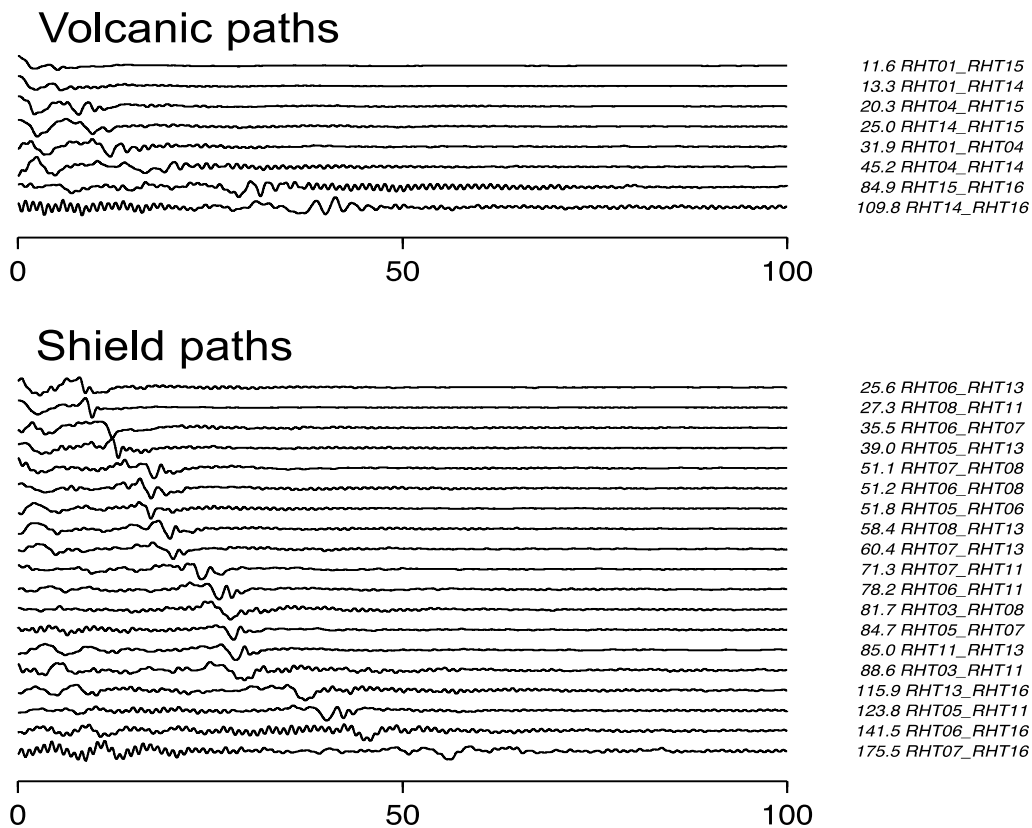


Figure 26. Comparison of paths inside the volcanic region with shield paths.

The Green's functions were then converted to velocity versus depth for each pair. A simulated annealing algorithm was used and matched a 1D synthetic with the envelope (Hilbert transform) of the observed Green's function. The starting point the same for all data paths (solid red and blue) so no bias towards the initial model is included. Figure 27 shows all profiles for P and S velocities.

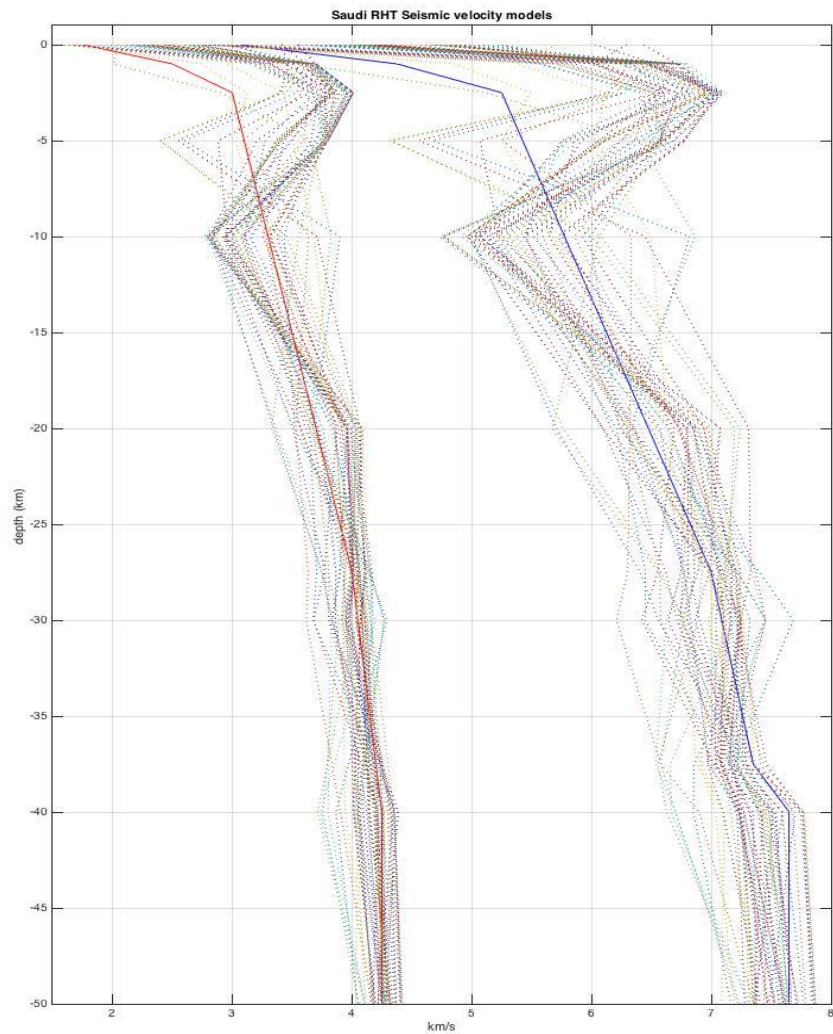


Figure 27. All velocity profiles generated from the Green's functions.

Following the selection in Figure 26, the average volcanic velocities were compared to the average shield velocities for the upper 4 km, as this is the depth of most interest. Figure 28 shows the results. A clear distinction is obvious to a depth of approximately 3 km. A velocity profile from a refraction conducted on the shield is added for comparison and velocities at depth match fairly well.

Red – average volcanic
Black – average shield
Green – refraction line on shield

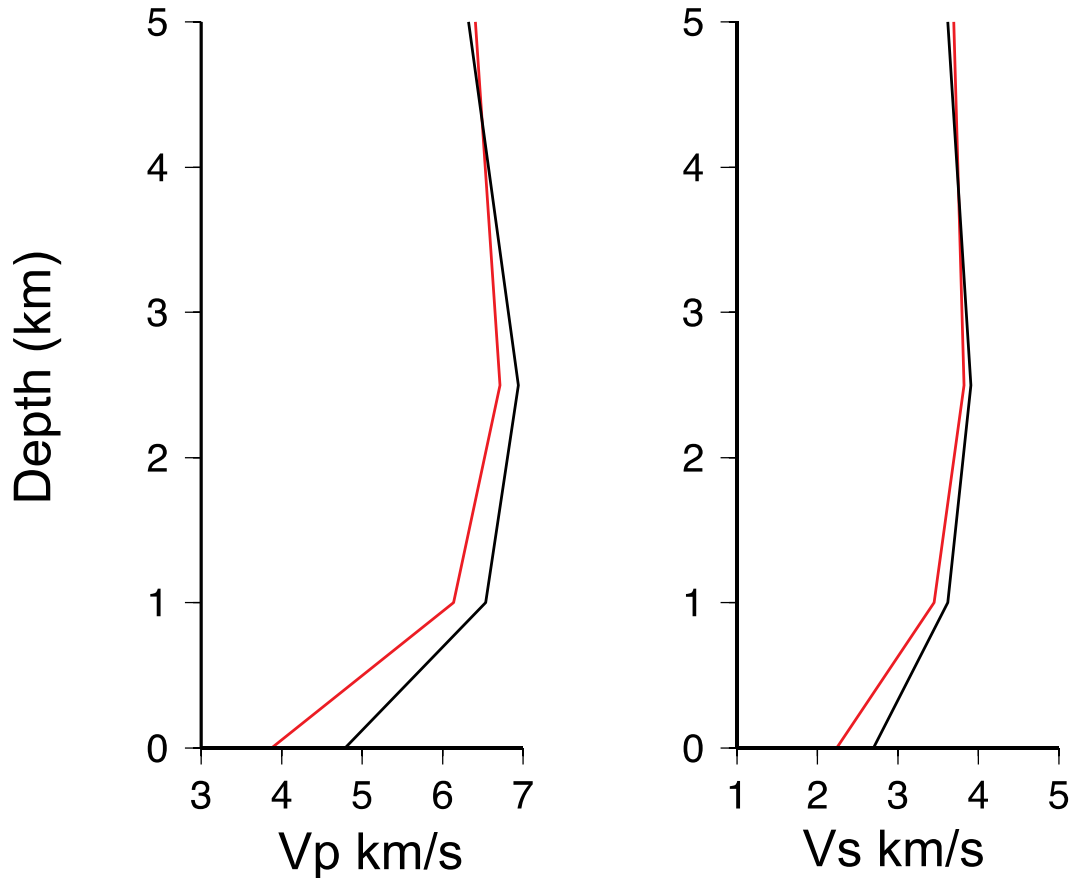


Figure 28. Comparison of velocities for shield (black) and volcanic (red) for P (left) and S velocities (right).

To confirm the difference, ray with an average velocity above the median are mapped and compared with ray paths below the median (Figure 29). We chose median but very similar results were obtained by using the mean. Ray paths that included more than 50% of the volcanic area were substantially lower velocity. This indicates that ambient noise tomography is effective at mapping areas of low velocity induced by volcanism. Some indications of low velocities to the north of the volcanic region appear but resolution is inadequate to make a definite conclusion. Nevertheless, it does confirm low velocities and likely elevated geothermal gradient throughout the region and would be useful to apply to the other harrats. Currently, this data is not available.

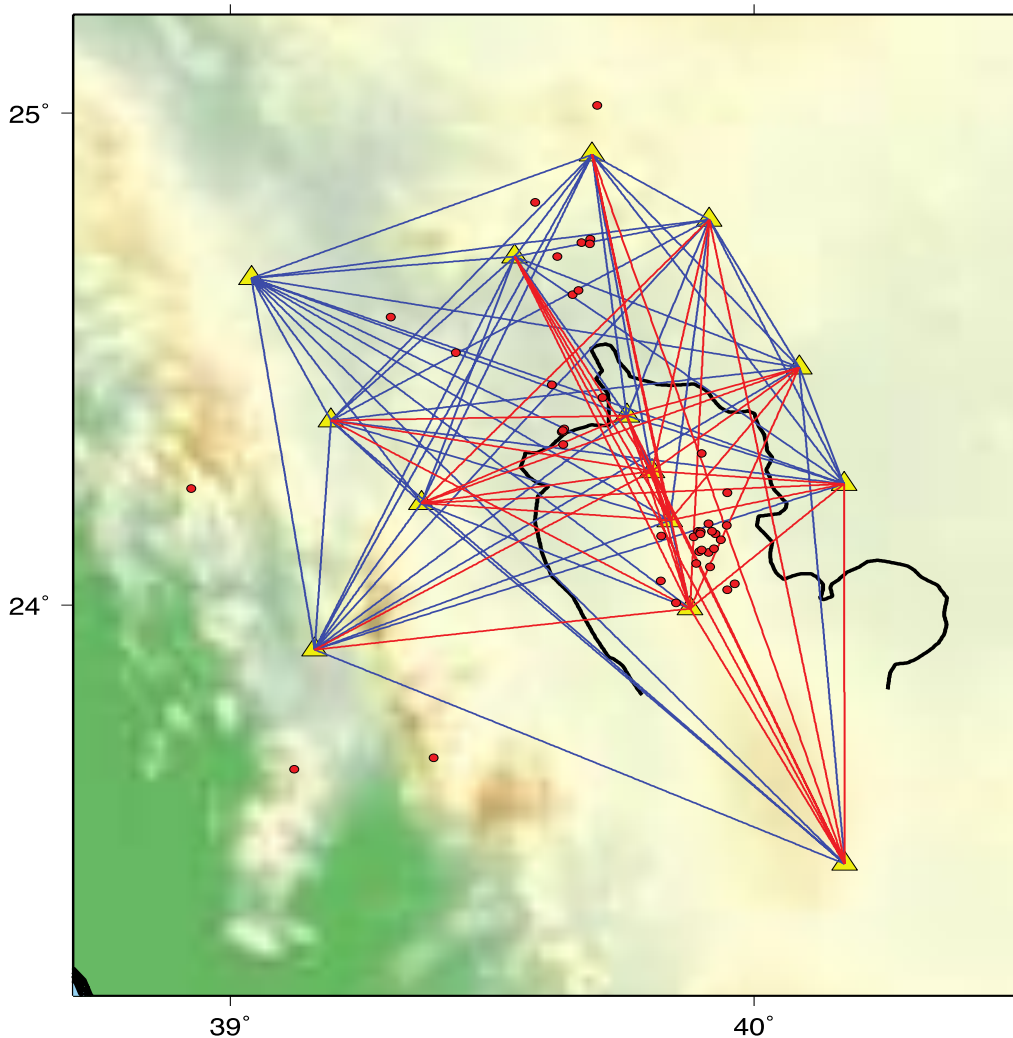


Figure 29. Map of ray with below median velocity (red) and above (black). The black outline marks the approximate edge of the volcanics.

3.4 Earthquakes, faults, and permeability

Sub-surface permeability is the most difficult parameter to estimate, especially from the available data. Following the observations made at the proposed analog field, we examine the relationship between seismicity (Figure 30 and 31) and known faults (Figure 32). The seismicity trends roughly along the orientation of the northerly basement faults (set B in Figure 32), as is noted previously. Areas where these faults are dense would be a priority to investigate. We also examined the frequency content of the available event data to look for differences in attenuation. No obvious differences were observed.

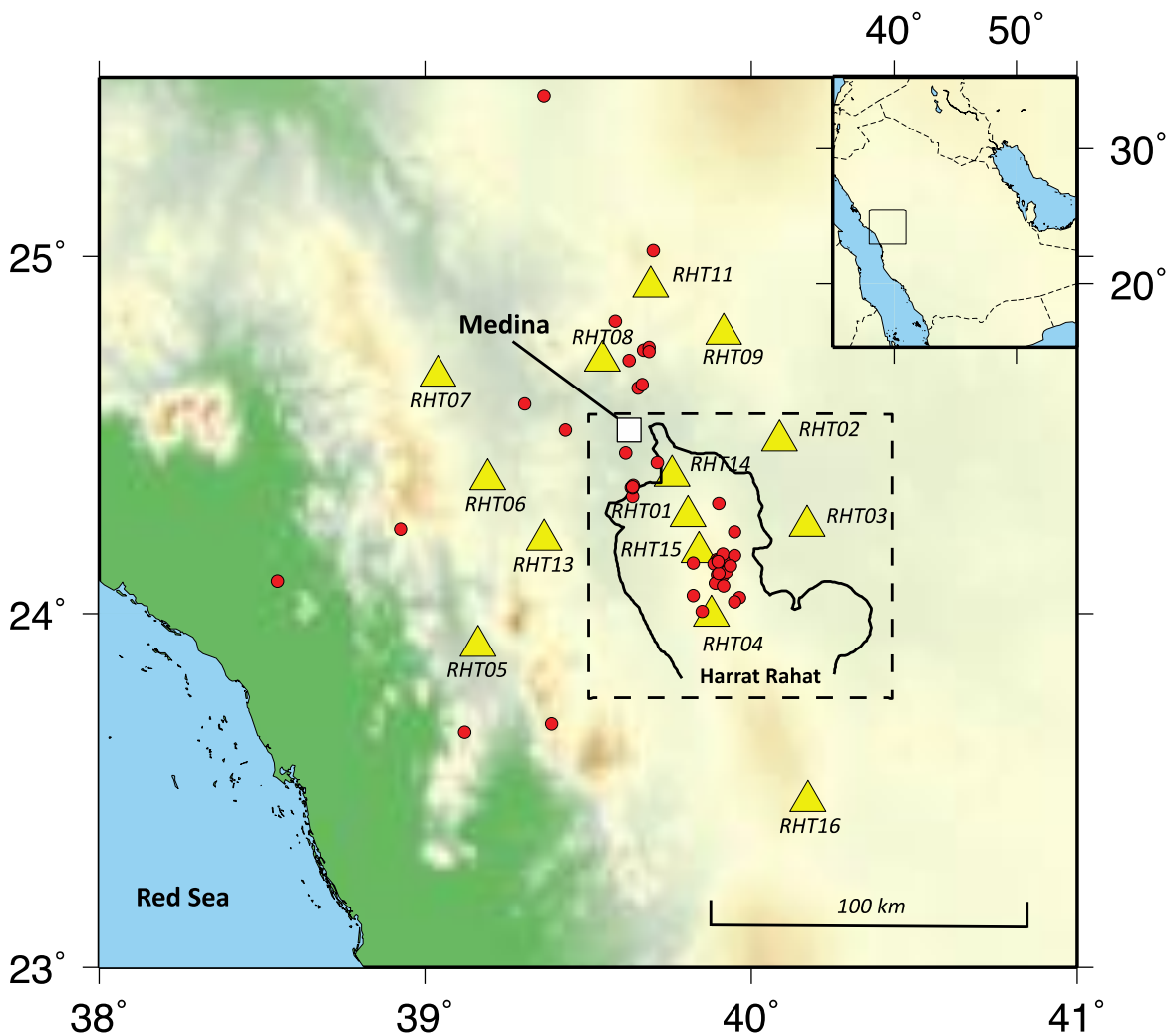


Figure 30. Map of seismic stations and earthquakes from available data.

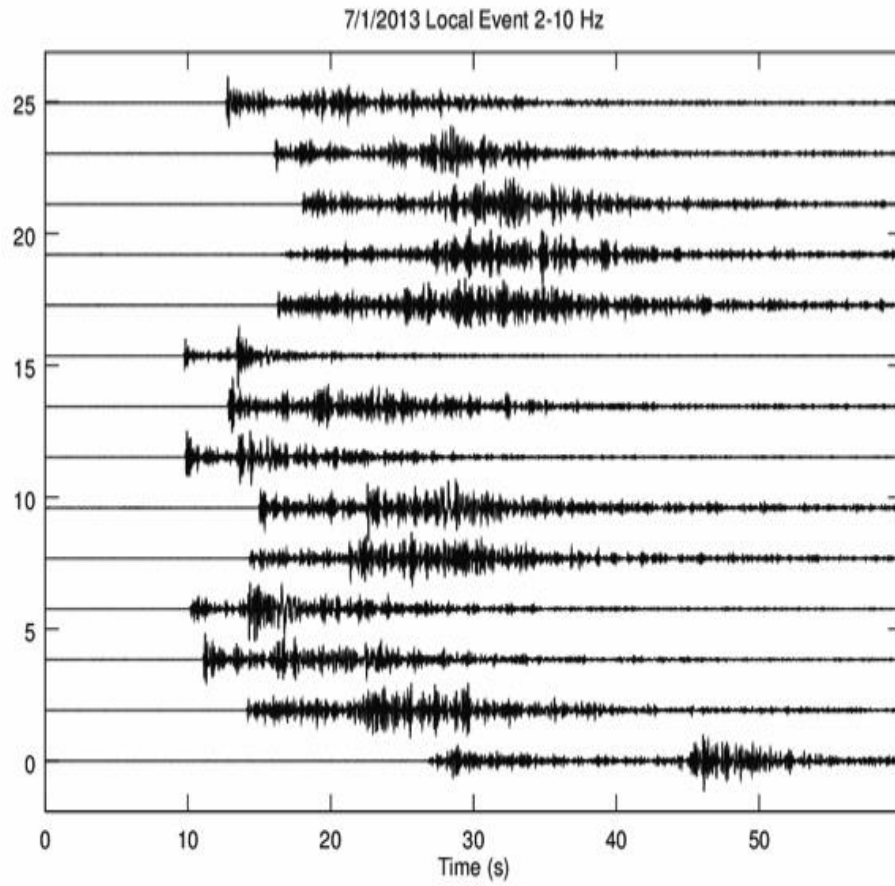


Figure 31. Example of local earthquake showing clear signal-to-noise.

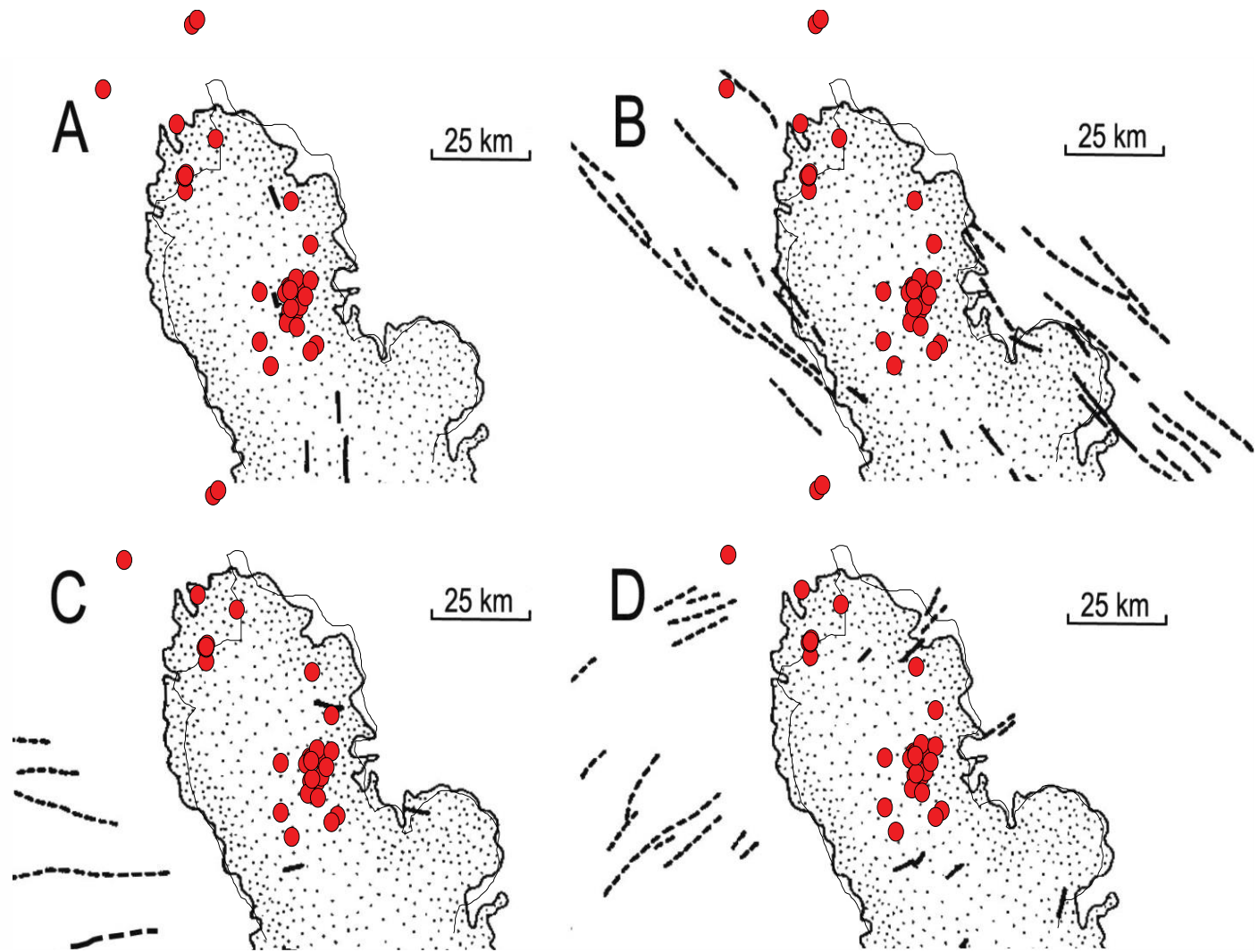


Figure 32. Earthquakes plotted on fault map and volcanics

4.0 Discussion & Interpretation

Most of the harrat volcanic fields erupted from northerly trending linear vent systems that lie oblique to nearly all basement trends. There is no evidence of prevailing east-west extension in the western Arabian Shield. The main zone of mantle upwelling beneath the harrats appears to be reflected in the Makkah-Madinah-Nafud volcanic line, a linear system of vents that extends in a northerly direction over a distance of ~600 km (*Camp and Roobol, 1992*). This volcanic line marks the main eruption sites for Harrats Rahat, Khaybar and Ithnayn. Petrologic data suggest that this feature delineates the axis of mantle upwelling with lavas along its length generated by higher degrees of partial melting when compared to the harrat lavas lying farther to the west and east (*Camp and Roobol, 1992*). This main axis of upwelling is consistent with seismic

tomography that has resolved a large north-south prong of hot mantle with an axis coincident with the Makkah-Madinah-Nafud volcanic line (*Chang and van der Lee, 2011; Chang et al., 2011*).

All of these harrats contain common Quaternary lava flows, many of which are Holocene in age. Two of these harrats (Khaybar and Hutaymah) are notable in containing abundant, young phreatomagmatic tuff rings, indicating the availability of water from sub-surface sources. There is no indication that such sources lie beneath Harrats Lunayyir or Ithnayn; however, both of these harrats show evidence of very young Holocene activity. In fact, the entire volcanic history at Harrat Lunayyir may be less than 600 ka (*Duncan and Al-Amri, 2013*), with the most recent event being a near eruption between April and June, 2009 (*Pallister et al., 2010*). Although Harrats Lunayyir and Ithnayn lack any clear evidence for presence of significant subsurface meteoric water, the very young age of volcanism on these harrats suggest that their central vent systems may be areas of high heat flow but low fluid flow that could be rendered geothermally viable through the creation or exploitation of enhanced geothermal systems (EGS).

Extensive geological mapping and historic eruptions in Harrat Rahat indicate active volcanic activity. The youngest unit (Qm7) is historic in age and includes the only two historic eruptions in Saudi Arabia for which eyewitness accounts exist: the 1256 AD eruption southeast of Al Madinah (*Camp et al., 1987; El-Masry et al., 2013*), and a small eruption in 641 AD expressed as four small pyroclastic cones located in the southwest corner of Al-Madinah City (*Murcia et al., 2014*). Subunit Qm6 is considered post-Neolithic in age because the lavas lack abundant Neolithic burial mounds that characterize the upper surface of other flows. These burial mounds appear to have a ^{14}C ages between 7,000 and 4,500 years B.P (*Kaiser et al., 1973*). However, *McClure (1978)* notes that the Neolithic pluvial period ceased on the Arabian Peninsula at ~6000 years B.P with the onset of a hyper-arid climate. We therefore believe that all of the units of Qm6 are at least as young as 6000 years B.P., and possibly younger than 4500 years B.P. Since this time, there have been 13 post-Neolithic and historic eruptions on northern Harrat Rahat. If we assume that all are younger than 4,500 years, the average eruption rate since that time has been one per 346 years. Eroded vents older than Qm4 are spread across a wide region of northern Harrat Rahat. However, all of the young non-eroded vents (Qm4-Qm7) lie within a distinct northwest-trending linear axis in the central part of the harrat, the only exception being

the 641 A.D eruption SW of Al-Madinah. The geologic data suggest that this central area should be the focus of geothermal exploration.

In addition, we processed a year of seismic data from thirteen stations within and near the Harrat Rahat using sensitive correlation detection software. After removing redundant groups, this process found 29 groups of repeating events, 22 of which appear to be in the neighborhood of the Harrat. It appears that most of the events are surface explosions. However, of the 22 groups local to the Harrat, it appears that 7 are small groups of possible natural events based upon earthquake-like waveform and population characteristics. Our more detailed correlation operation on one of these groups of events resulted in discovery of a brief swarm of 13 events near the northern edge of the Harrat.

Ambient noise tomography indicates that the entire Harrat Rahat is underlain by a region of low velocity and likely above average geothermal gradient and that this region may extend north of the highly volcanic region. A search for anomalous attenuation proved inconclusive.

5.0 Conclusions

A preliminary evaluation of a selection of harrats suggest that several, based on likely subsurface heat, groundwater, and possible permeability are reasonable prospects for future evaluation. It should be noted that proximity to major metropolitan areas is a significant consideration in developing geothermal resources for power production, as this ensures a nearby market without the need for extensive power lines, as these lines add to the cost. Proximity to a city also reduces the cost and effort required for construction although locations near the coast may be useful in terms of providing energy for desalination. Harrats Rahat, Lunayir, and Khaybar appear to be the most promising. A major uncertainty is the distribution of permeability, which is essential.

Table 3. Summary of results and geothermal promise.

Location	subsurface heat source	permeability	water	proximity to major areas of use	overall assessment
Lunayir	good	perhaps good	yes	fair	good
Khaybar	good	uncertain	yes	good	good
Ithnayn	poor	uncertain	unclear	fair	poor
Hutaymah	poor	uncertain	yes	fair	fair
Rahat	good	possibly good	yes	good	good

In general, the harrats are comparable in setting to the Tres Virgines geothermal plant in Baja California, Mexico. This plant currently produces 10 MW but is estimated to overlie a resource capable of 40 MW. As the harrats cover a much larger area, the associated resources may be much larger.

A preliminary investigation based on available seismic data at Harrat Rahat showed that advanced detection algorithms could increase the number of detected events although the increase was not sufficient to improve geothermal exploration. Ambient noise tomography is effective at estimating crustal velocities on a regional scale. It was not possible to evaluate attenuation due to sparse data.

Geology indicates that the volcanism and seismicity roughly correlates with the northerly trending faults, which may be associated with higher permeability, as is the case in Mexico. Work in other areas suggests that intersecting fault are often productive and especially at a high angle. Ideally, areas with dense northerly trending faults intersecting with northeast trending faults would be the preferred areas to investigate further. The flow of groundwater in the region is unknown but it is possible that it flows outward from the slightly higher volcanic. Therefore, areas at the edge may be preferable as well as easier logistically for drilling equipment and power lines.

This investigation could be based on detailed remote sensing combined with spectral analysis to detect zones of surface alteration, which are frequently associated with geothermal fluids. A high density deployment of seismometers on the Harrat would be useful to improve resolution of potential resources.

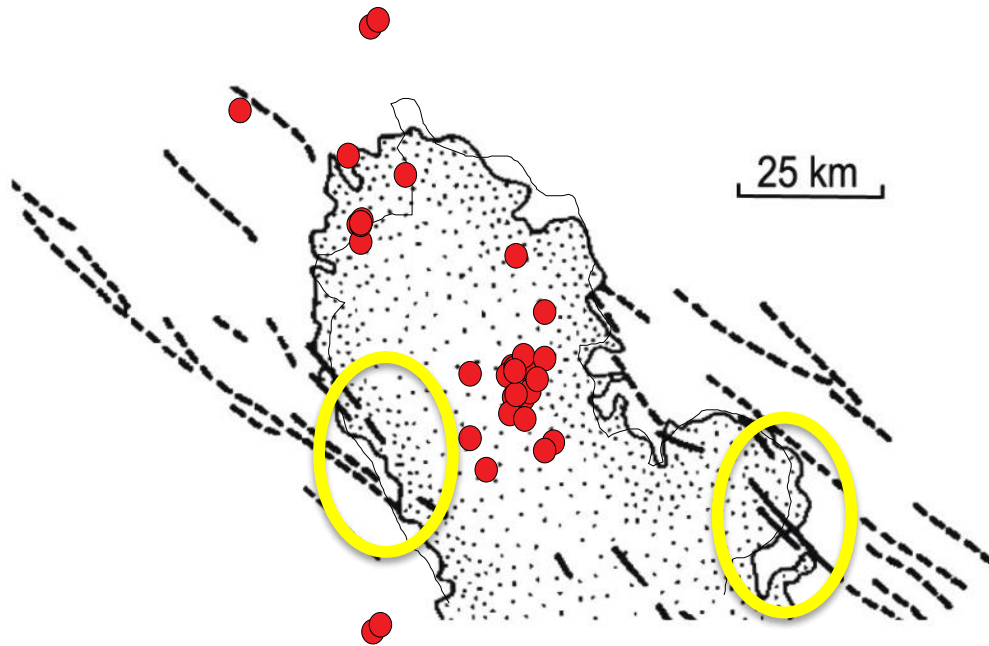


Figure 33. Possible areas for further investigation (in yellow).

6.0 Publications resulting from this work

Mellors, R. J., E. Matzel, V. Camp, D. Harris, and A. Al-Amri, 2015, Using seismic networks to explore for geothermal resources in western Saudi Arabia, 2016 GRC Transactions (extended abstract and oral presentation).

Mellors, R. J., V. Camp, D. Harris, and A. Al-Amri, 2015, Investigating Potential Geothermal Resources in Western Saudi Arabia, 2015 GRC Transactions (extended abstract and poster presentation).

7.0 References

- Abdelwahed, M.F., El-Masry, N., Moufti, M.R., Kenedi, C.L., Zhao, D., Zahran, H., and Shawali, J., 2016, Imaging of magma intrusions beneath Harrat Al-Madinah in Saudi Arabia: *Journal of Asian Earth Sciences*, v. 120, p. 17-28.
- Aboud, E., El-Masry, N., Qaddah, A., Alqahtaini, F., and Moufti, M.R.H., 2015, Magnetic and gravity data analysis of Rahat Volcanic field, El-Madinah city, Saudi Arabia: *Journal of Astronomy and Geophysics*, v. 4, p. 154-162.
- Al-Amri, A.M., Fnais, M.S., Abdel-Rahman, K., Mogren, S., and Al-Dabbagh, M., 2012, Geochronological dating and stratigraphic sequences of Harrat Lunayyir, NW Saudi Arabia, *International Journal of Physical Sciences*, v. 7, p. 2791-2805, doi:10.5897/IJPS12.178.
- Al-Dayel, M., Geothermal resources in Saudi Arabia. 1988, *Geothermics*, Vol. 17, No. 2/3, pp. 465-476.
- Al-Masry, N.N., Moufti, M.R., Nemeth, K., Murcia, H., Qaddah, A.A., and Abdelwahed, M.F., 2013, Historic Accounts of the AD 1256 eruption near Al-Madina, Volcanic risk in Saudi Arabia (VORISA) meeting, Extended Abstracts, King Abdul Aziz University, p. 9-13.
- Almond, D.C., 1986, Geologic evolution of the Afro-Arabian dome, *Tectonophysics*, v. 131, p. 301-332.
- Al-Samhoudy, N. Al-D.A.B-A, 1568 (976 A.H.), *Khulasaf Al-Wafa*: Unpublished manuscript, Hacmud Library, Al Madinah, Saudi Arabia.
- Al-Shaibani, A.M., 2003, Lava fields as potential groundwater sources in western Saudi Arabia, in Sherif, S. Singh, V.P., and Al-Rashed, M., editors, *Hydrology and Water Resources: Volume 5, Proceedings of the International Conference on Water Resources Management in Arid Regions (WaRMAR)*, Swets and Zeitlinger, Lisse, ISBN 90-5809-548-7, p. 103-120.

- Artemieva, I.M., and Mooney, W.D., 2001, Thermal thickness and evolution of Precambrian lithosphere: A global study, *Journal of Geophysical Research*, v. 106, p. 16,387-16,414.
- Bayer, H.-J., Hotzl, H., Jado, A.R., Roscher, B., and Voggenreiter, W., 1988, Sedimentary and structural evolution of the northwest Arabian Red Sea margin, *Tectonophysics*, v. 153, p. 137-151.
- Baer, G., and Hamiel, Y., 2010, Form and growth of an embryonic continental rift: InSAR observations and modelling of the 2009 western Arabia rifting episode, *Geophysical Journal International*, v. 182, p. 155-167.
- Blank, H.R., and Sadek, H.S., 1983, Spectral analysis of the 1976 aeromagnetic survey of Harrat Rahat, Kingdom of Saudi Arabia: Saudi Arabian Deputy Ministry for Mineral Resources Open-File Report USGS-OF-03-67, 29 p.
- Blusztajn, J., Hart, S.R., Shimizu, N., and McGuire, A.V., 1995, Trace-element and isotopic characteristics of spinel peridotite xenoliths from Saudi Arabia, *Chemical Geology*, v. 123, p. 53-65.
- Bob, M., Rahman, N.A., Taher, S., and Elamin, A., 2015, Multi-objective assessment of groundwater quality in Madinah City, Saudi Arabia, *Water Quality Exposure Health Journal*, v. 7, p. 53-66.
- Bohannon, R.G., Naeser, C.W., Schmidt, D.L., and Zimmermann, R.A., 1989, The timing of uplift, volcanism, and rifting peripheral to the Red Sea: A case for passive rifting?: *Journal of Geophysical Research*, v. 94, p. 1683-1701.
- Bosworth, W., Huchon, P., and McClay, K., 2005, The Red Sea and Gulf of Aden Basins, *Journal of African Earth Sciences*, v. 43, p. 334-378, doi: 10.1016/j.jafrearsci.2005.07.020.
- Camp, V.E., 1984, Island arcs and their role in the evolution of the western Arabian Shield, *Geological Society of America Bulletin*, v. 95, p. 913-921.
- Camp, V.E., Hooper P.R., Roobol, M.J., and White, D.L., 1987, The Madinah eruption, Saudi Arabia: Magma mixing and simultaneous extrusion of three basaltic chemical types: *Bulletin of Volcanology*, v. 49, no. 2, p. 489-508, doi:10.1007/BF01245475.
- Camp, V.E., and Roobol, M.J., 1989, The Arabian continental alkali basalt province: Part I. Evolution of Harrat Rahat, Kingdom of Saudi Arabia: *Geological Society of America Bulletin*, v. 101, p. 71-95.

- Camp, V.E., Roobol, M.J., and Hooper, P.R., 1991, The Arabian continental alkali basalt province, part II, Evolution of Harrats Khaybar, Ithnayn, and Kura, Kingdom of Saudi Arabia, *Geological Society of America Bulletin*, v. 103, p. 363-391.
- Camp V E, Roobol M J, 1991. Geologic map of the Cenozoic lava field of Harrat Rahat, Kingdom of Saudi Arabia. Saudi Arabia Directorate Gen Min Res, Map GM-123, 1:250,000 geologic maps and text.
- Camp, V.E., and Roobol, M.J., 1992, Upwelling asthenosphere beneath western Arabia and its regional implications, *Journal of Geophysical Research*, v. 97, no. B11, p. 15,255-15,271.
- Camp, V.E., and Stoesser, D.B., 1985, Enigmatic east-west structures of the Arabian-Nubian shield: Saudi Arabian Deputy Ministry for Mineral Resources Open-File Report DGMR-OF-05-58, 11 p.
- Chang, S-J., and Van der Lee, S., 2011, Mantle plumes and associated flow beneath Arabia and east Africa, *Earth and Planetary Science Letters*, v. 302, p. 448-454, doi: 10.1016/j.epsl.2010.12.050.
- Chang, S-J., Merino, N., Van der Lee, S., Steine., S., Stein, C.A., 2011, Mantle flow beneath Arabia offset from opening of the Red Sea, *Geophysical Research Letters*, v. 38, doi: 10.1029/2010GL045852.
- Cochran, J.R., 1983, A model for development of Red Sea, *American Association of Petroleum Geology Bulletin*, v. 67, p. 41-69.
- Cochran, J.R., Gaulier, J.-M., and Le Pichon, X., 1991, Crustal structure and the mechanism of extension in the northern Red Sea: constraints from gravity anomalies, *Tectonics*, v. 10, p. 1018-1037.
- Coleman, R.G., Gregory, R.T., and Brown, G.F., 1983, Cenozoic volcanic rocks of Saudi Arabia, U.S., Geological Survey Open File Report, USGSW-OF-03-93, 82 p.
- Davies, F.B., 1984, Strain analysis of wrench faults and collision tectonics in the Arabian-Nubian Shield: *Journal of Geology*, v. 92, p. 37-54
- Dodge, D. and D. Harris (2015), Large scale test of dynamic correlation processors: Implications for correlation-based seismic pipelines, in review.
- Duncan R.A., and Al-Amri, A.M., 2013, Timing and composition of volcanic activity at Harrat Lunayyir, western Saudi Arabia, *Journal of Volcanology and Geothermal Research*, v. 260, p. 103-116, doi: 10.1016/j.jvoleores.2013.05.006.

- Duncan, R.A., Kent, A.J.R., Thornber, C.R., Schlieder, T.D., and Al-Amri, A.M., 2016, Timing and composition of continental volcanism at Harrat Hutaymah, western Saudi Arabia, *Journal of Volcanology and Geothermal Research*, v. 313, p. 1-14.
- Fairer, H.M., 1986, Geologic map of the Harrat Ithnayn quadrangle, shet 26D, Kingdom of Saudi Arabia: Saudi Arabian Deputy Ministry for Mineral Resources Geoscience Map-106C, scale 1:250,000, with text, 15 p.
- Foulger, G. 1982, Geothermal Exploration and reservoir monitoring using earthquakes and the passive seismic method, *Geothermics*, Vol. 11, No. 4, pp 259-268.
- George, M., and Shorbaji, H., 1987, Explanatory notes to the hydrogeologic and hydrochemical maps of the Al-Madinah quadrangle, Sheet 24D, Kingdom of Saudi Arabia, Directorate General of Mineral Resources, Jiddah, Saudi Arabia, Open-File Report BRGM-OF-23, 23, 65 p.
- Gettings, M.E., 1982, Heat-flow measurements at shot point along the 1978 Saudi Arabian Seismic Deep-Refracton LINE, Part 2: Discussion and interpretation, U.S. Geological Survey Open File Report 82-794.
- Hansen, S.E., Schwartz, S., Al-Amri, A., and Rodgers, A., 2006, Combined plate motion and density-driven flow in the asthenosphere beneath Saudi Arabia: Evidence from shear-wave splitting and seismic anisotropy, *Geology*, v. 34, p. 869-872.
- Hansen, S. E., H. R. deShon, M M. Moore-Driskell, and A. M. S. Al-Amri, 2013, Investigating the P wave velocity structure beneath Harrat Lunayyir, northwestern Saudi Arabia, using double-difference tomography and earthquakes from the 2009 seismic swarm, 118, (9), 4814-4826
- Harris, D. (2006). Subspace detectors: Theory, Lawrence Livermore National Laboratory, report UCRL-TR-222758.
- Harris, D. and D. Dodge (2011). An autonomous system for grouping events in a developing aftershock sequence, *Bull. Seism. Soc. Am.* **101**, 763-774, doi:10.1785/0120100103.
- Hashem, B., Geothermal Development Roadmap for the Kingdom of Saudi Arabia, 2012, *GHC Bulletin*, August.
- Henjes, Kunst, F., Altherr, R., and Baumann, A., 1990, Evolution and composition of the lithospheric mantle underneath the western Arabian peninsula: Constraints from Sr-Ne isotope systematics of mantle xenoliths, *Contributions to Mineralogy and Petrology*, v. 105, p. 460-472.

- Hernandez, A. L., G. H. Garcia Estrada, J. F. Arellano Guardarrama, 1995, Geothermal exploration at Las Tres Virgenes, B.C.S, Mexico, World Geothermal Congress.
- Julia, J., Ammon, C.J., and Herrmann, R.B., 2003, Lithosphere structure of the Arabian Shield from the joint inversion of receiver functions and surface-wave group velocities, *Tectonophysics*, v. 371, p. 1-21.
- Kaiser, K., Kemp, E.K., Leroi-Gouran, A., and Schutt, H., 1973, Quartar-stratigraphische Untersuchungen aus dem Damaskas-Becken und seiner Umgebung, *Zeitschrift fuer Gomorphologic*, v. 17, p. 263-353l, Berlin.
- Kaliwoda, M., Altherr, R., Meyer, H-P., 2007, Composition and thermal evolution of the lithospheric mantle beneath Harrat Uwayrid, eastern flank of the Red Sea rift (Saudi Arabia), *Lithos*, v. 99, p. 105-120.
- Kawabata, E., Cronin, S.J., Bebbington, M.S., Moufti, M.R.H., El-Masry, N., and Wang, T., 2015, Identifying multiple eruption phases from a compound tephra blanket: an example of the AD1256 Al Madinah eruption, Saudi Arabia, *Bulletin of Volcanology*, v. 76, p. 1-13.
- Koulakov, I., El-Khrepy, S., Al-Arifi, N., Sychev, I., and Kuznetsov, P., 2014, Evidence of magma activation beneath the Lunayyir basaltic field (Saudi Arabia) from attenuation tomography, *Solid Earth Discussions*, v. 6, p. 1401-1421.
- Koulakov, I., S. El-Khrepy, N. Al-Arifi, P. Kuzetsov, and E. Kasatkina, 2015, Structural cause of a missed eruption in the Harrat Lunayyir basaltic field (Saudi Arabia) in 2009, *Geology*, doi: 10.1130/G36271.1
- Kuo, L-C., and Essene, E.J., 1986, Petrology of spinel harzburgite xenoliths from the Kishb Plateau, Saudi Arabia, *Contributions to Mineralogy and Petrology*, v. 93, p. 335-346.
- Lashin, A., N. A. Arifi, D. Chandrasekharam, A. Al Bassam, S. Rehman and M. Pipan, 2015, Geothermal Energy Resources of Saudi Arabia: Country Update, *Proceedings World Geothermal Congress 2015*, Melbourne, Australia, 19-25 April.
- Lashin, A., N. Al Arifi, 2014, Geothermal energy potential of southwestern of Saudi Arabia "exploration and possible power generation": A case study at Al Khouba area– Jizan, *Renewable and Sustainable Energy Reviews*, 30, 771-78.
- Marone, F., van der Lee, S., Glardini, D., 2004, Three-dimensional upper mantle S-veolcity model for the Eurasia-Arfica plate boundary region, *Geophysical Journal International*, v. 158, jp. 109-130.

- McClure, H.A., 1978, Ar Rub' al Khali, *in* Al-Sayari, S.S., and Zotl, J.G., eds., Quaternary period in Saudi Arabia: Springer-Verlag, New York, p. 252-263.
- McGuire, A.V., 1988a Petrology of mantle xenoliths from Harrat al Kishb: The mantle beneath western Saudi Arabia, *Journal of Petrology*, v. 29, p. 73-92.
- McGuire, A.V., 1988b, The mantle beneath the Red Sea margin: Xenoliths from western Saudi Arabia, *Tectonophysics*, v. 150, p. 101-119.
- Moufti, M.R.H., 1985, The geology of Harrat Al Madinah volcanic field, Harrat Rahat, Saudi Arabia, Unpublished Ph.D Dissertation, Department of Environmental Science, University of Lancaster, United Kingdom, 476 p.
- Moufti, M.R., Moghazi, A.M., and Ali, K.A., 2012, $^{40}\text{Ar}/^{39}\text{Ar}$ geochronology of the Neogene-Quaternary Harrat Al-Madinah intercontinental volcanic field, Saudi Arabia: Implications for duration and migration of volcanic activity, *Journal of Asian Earth Sciences*, doi:10.1016/j.jseas.2012.09.027.
- Muksin, U., K. Bauer, and C. Haberland, 2013, Seismic Vp and Vp/Vs structure of the geothermal area around Tarutung (North Sumatra, Indonesia) derived from local earthquake tomography, *Jour. Vol. Geo. Res.*, 260, June, 27-43.
- Murcia, H., Nemeth, K., El-Masry, N., Wameyo, P., Moufti, M.R., Lindsay, J., Cronin, S., Smith, I., and Kereszturi, G., 2014, Phreatomagmatic to magmatic activity in the 641 AD historical eruption in Al-Madiah City, Kingdom of Saudi Arabia, *in* Carrasco-Nunez, G., Aranda-Gomez, J.J., Ort, M.H., Silva-Corona, J.J., eds., 5th International Maar Conference, Abstracts Volume: Juriquilla, Queretaro, Mexico, Universidad Nacional Autonoma de Mexico, Centro de Geosciences, p. 212-213.
- Nasir, S., 1992, The lithosphere beneath the northwestern part of the Arabian plate (Jordan): Evidence from xenoliths and geophysics, *Tectonophysics*, v. 201, p. 357-370.
- Pallister, J.S., 1984, Reconnaissance geologic map of the Harrat Hutaymah quadrangle, sheet 26/42A, Kingdom of Saudi Arabia, U.S. Geological Survey Open-File Report USGS-OF-04-461, 77 p.
- Pallister, J.S., 1987, Magmatic history of Red Sea rifting, *Geological Society of America Bulletin*, v. 98, p. 4000-417.
- Pallister, J.S., McCauland, W.A., Jonsson, Sigurjon, Zhong L., Zahran, H.M., Haddidy, S.E., Aburukbah, A., Stewart, I.C.F., Lundgren, P.R., White, R.A., and Moufti, M.R.H., 2010, Broad accommodation of rift-related extension recorded by dyke intrusion in Saudi Arabia, *Nature Geoscience*, v. 3, p. 705-712, doi: 10.1038/NGE0966.

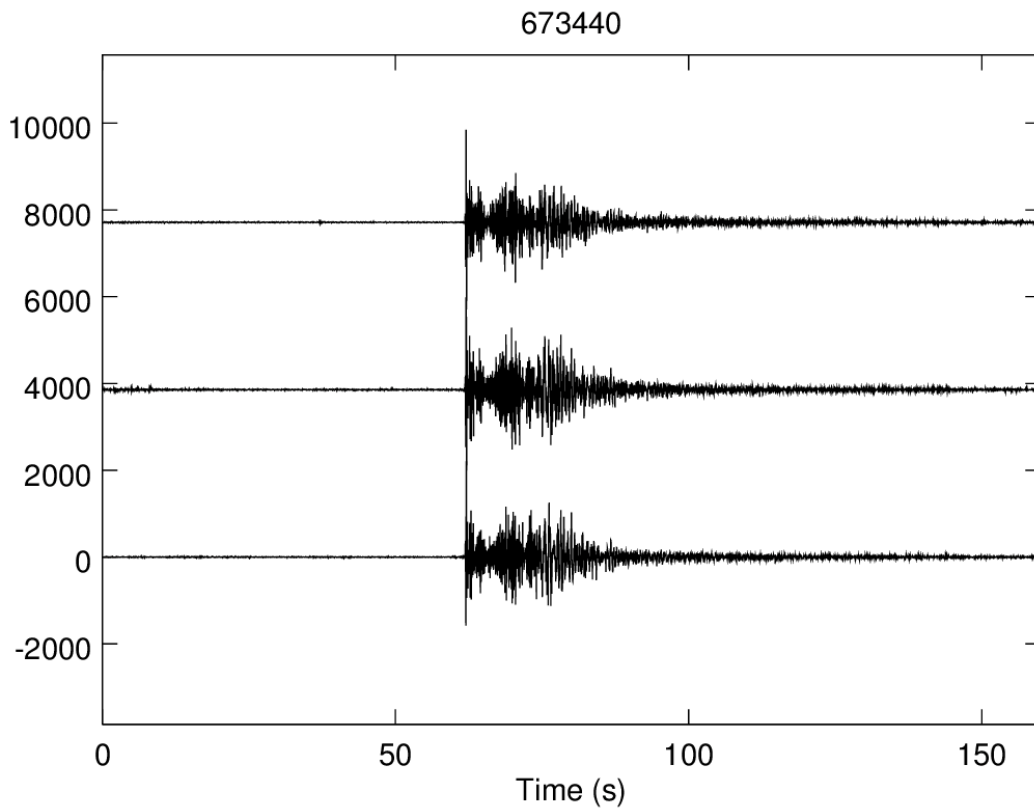
- Park, Y., Nyblade, A.A., Rodgers, A.J., Al-Amri, A., 2007, Upper mantle structure beneath the Arabian Peninsula and northern Red Sea from teleseismic body wave tomography: Implications for the origin of Cenozoic uplift and volcanism in the Arabian Shield, *Geochemistry, Geophysics, Geosystems*, v. 8, p. 1-15.
- Ramsay, C.R., 1986, Geologic map of the Rabigh quadrangle, sheet 22D, Kingdom of Saudi Arabia: Saudi Arabian Deputy Ministry for Mineral Resources, Geoscience Map GM-84, scale 1:250,000, with text, 49 p.
- Rehman, S., 2010. Saudi Arabian geothermal energy resources – an update. Proceedings of the 2010 World Geothermal Congress, Bali, Indonesia, April 25–29, paper No. 0107, 6 pp.
- Rehman S, Shash A. Geothermal resources of Saudi Arabia, Country update report. Proceedings World Geothermal Congress, Antalya, Turkey, 2005: 7
- Richard, J.J., van Padang, M.N., and Geze B., 1957, Catalogue of the Active Volcanoes of the World. Part IV. Catalogue of the Active Volcanoes and Solfara Fields of Africa and the Red Sea, International Volcanological Association.
- Robinson, F.A., Foden, J.D., Collins, A.S., and Payne, J.L., 2014, Arabian Shield magmatic cycles and their relationship with Gondwana assembly: Insights from U-Pb and Hf isotopes, *Earth and Planetary Science letters*, v. 408, p. 207-225, doi: 10.1016/epsl.2014.10.010.
- Roobol, M.J., and Camp, V.E., 1991, Geology of the Cenozoic lava field of Harrats Khaybar, Ithnayn, and Kura, Geoscience Map GM-131, 1:25,000-scale, with text, 776 p., Saudi Arabian Directorate General of Mineral Resources, Jiddah.
- Roobol, M.J., and Camp, V.E., 1991a, Geology of the Cenozoic lava field of Harrat Kishb, Geoscience Map GM-132, 1:250,000-scale, with text, Saudi Arabian Directorate General of Mineral Resources, 63 p.
- Roobol, M.J., and Camp, V.E., 1991b, Geology of the Cenozoic lava field of Harrats Khaybar, Ithnayn, and Kura, Geoscience Map GM-131, 1:250,000-scale, with text, Saudi Arabian Directorate General of Mineral Resources, 76 p.
- Roobol MJ, Bankher K, Bamufleh S., 2007, Geothermal anomalies along the MMN volcanic line including the cities of Al Madinah Al Munnawwarah and Makkah Al Mukkarramah. Jeddah: Saudi Geological Survey.
- Runge, M.G., Bebbington, M.S., Cronin, S.J., Lindsay, J.M., Kenedi, C.L., and Moufti, M.R.H., 2014, Vents to events: determining an eruption event from volcanic vent structures for the Harrat Rahat, Saudi Arabia, *Bulletin of Volcanology*, v. 76, p. 1-16.

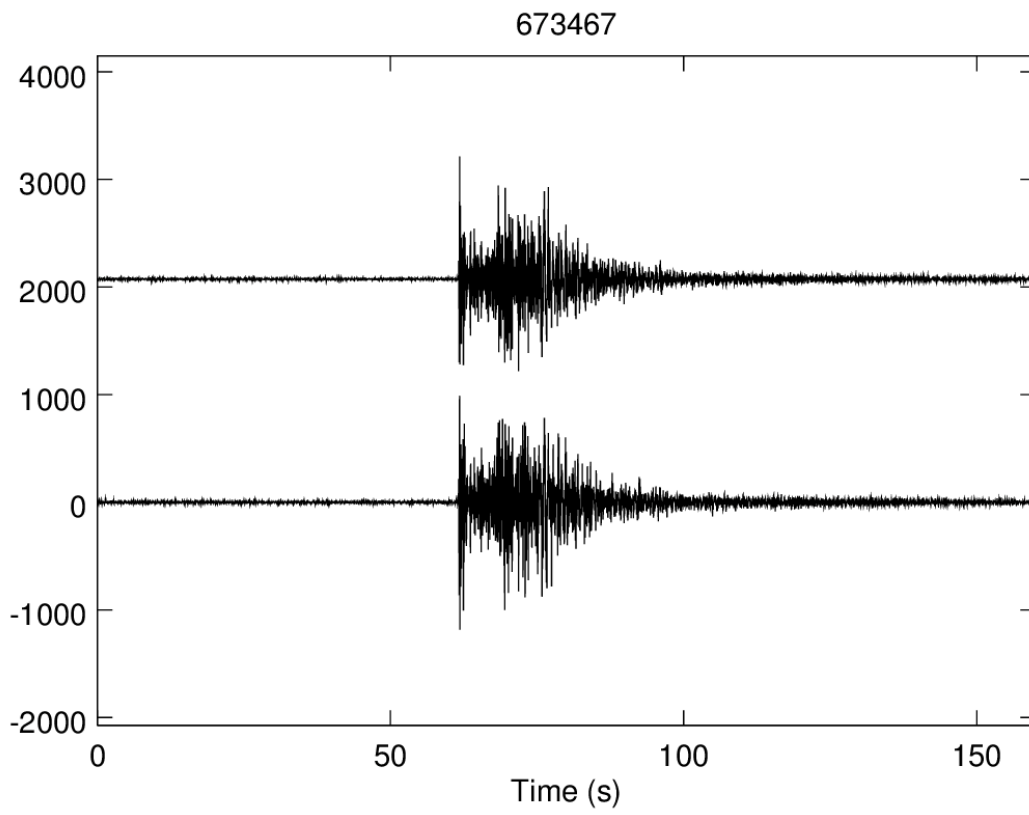
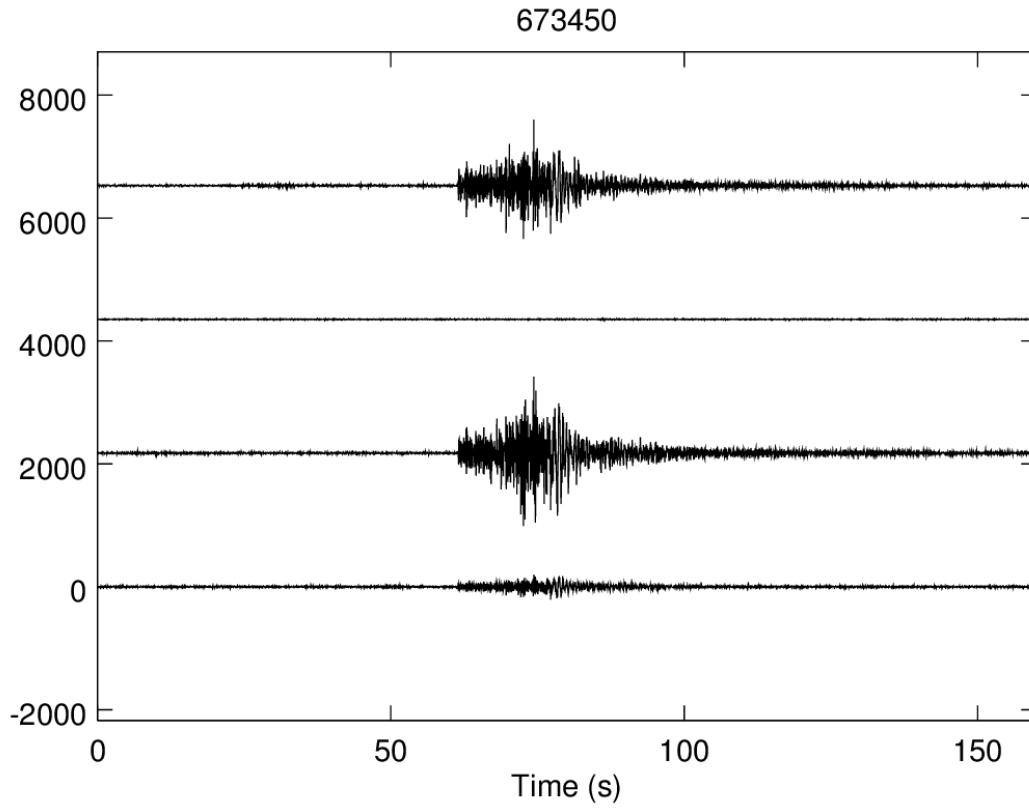
- Sengor, A.M.C., and Burke, K., 1978, Relative timing of rifting and volcanism on Earth and its tectonic implications, *Geophysical Research Letters*, v. 5, p. 419-421.
- Schmidt, D.L., and Hadley, D.G., 1984, Stratigraphy of the Miocene Baid formation, southern Red Sea Coastal plain, Kingdom of Saudi Arabia, U.S. Geological Survey Technical Record, USGS TR-04-23, Saudi Arabian Deputy Ministry of Mineral Resources, Jiddah, 46 p.
- Sebai, A., Zumbo, V., Feraud, G., Bertrand, H., Hussain, A.G., Giannerini, G., Campredon, R., 1991, $^{40}\text{Ar}/^{39}\text{Ar}$ dating of alkaline and tholeiitic magmatism of Saudi Arabia related to the early Red Sea Rifting, *Earth and Planetary Science Letters*, v. 104, p. 473-487.
- Siebert, L., Simkin, T., and Kimberly, P., 2010, *Volcanoes of the World*, 3rd edition, Berkeley, University of California Press, 568 p.
- Simkin, T., Siebert, L., and McClelland, L., 1984, *Volcanoes of the world; 1984 supplement and volcano reference file master list*: Washington D.C., Smithsonian Institution.
- Stankiewicz, J., Ryberg, T., Haberland, C., Fauzi, Natawidjaja, D., 2010a. Lake Toba volcano magma chamber imaged by ambient seismic noise tomography. *Geophysical Research Letters* 37 (17), L17306.
- Stern, R.J., 1985, The Najd fault system, Saudi Arabia and Egypt: a late Precambrian rift-related transform system, v. 4, p. 497-511, doi: 10.1029/TC004i005p00497.
- Stoeser, D.B., and Camp, V.E., 1985, Pan-African microplate accretion of the Arabian Shield, *Geological Society of America Bulletin*, v. 96, p. 817-826.
- Stoeser D.B., and Stacey, J.S., 1988, Evolution, U-Pb geochronology, and isotope geology of the Pan-African Nabitah orogenic belt of the Saudi Arabian Shield, *in* El-Gaby, S., Greiling, R.O.E., eds., *The Pan-African Belt of northeast Africa and adjacent areas: tectonic evolution and economic aspects of a Late Proterozoic orogeny*, Friedrich Vieweg and Son, p. 227-288.
- Stoeser, D.B., and Frost, C.D., 2006, Nd,Pb, Sr, and O isotopic characterization of Saudi Arabian Shield terranes, *Chemical Geology*, v. 226,p. 163-188.=
- Thornber, C.R., 1990, Geologic map of Harat Hutaymah, with petrologic classification and distribution of ultramafic inclusions, Saudi Arabia, U.S. Geological Survey Miscellaneous field studies map MF-2129.
- Thornber, C.R., and Pallister, J.S., 1985, Mantle xenoliths from northern Saudi Arabia, *Eos Transactions, American Geophysical Union*, v. 66, p. 393.

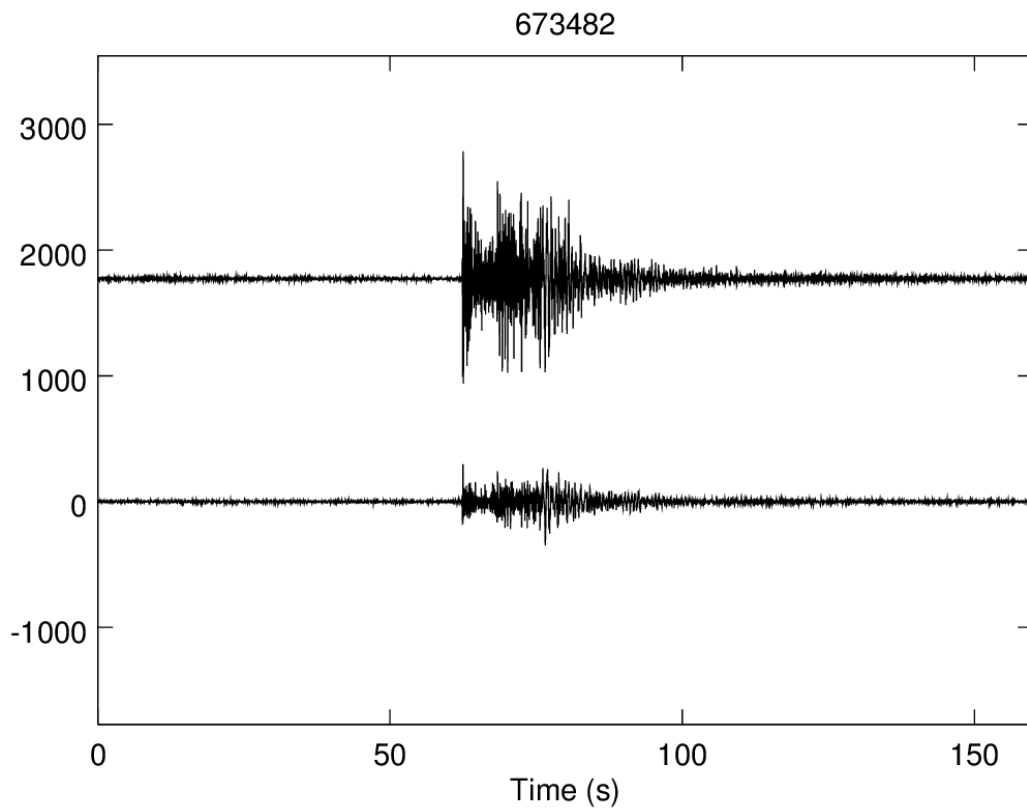
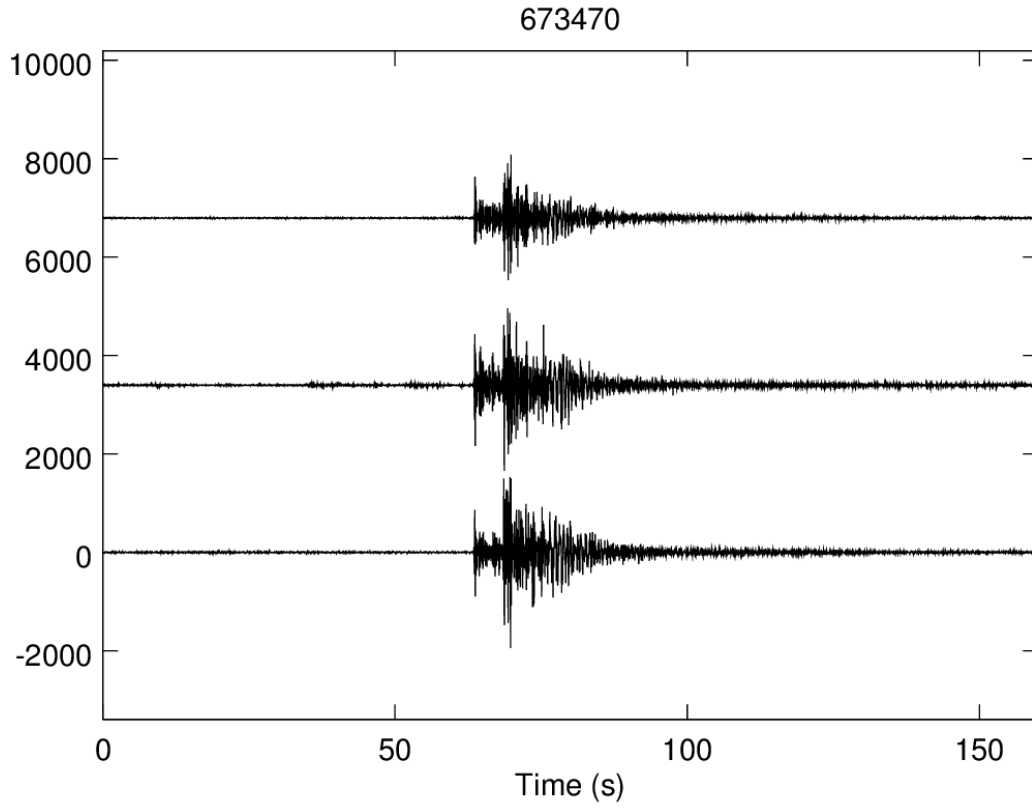
- Voggenreiter, W., Hotzl, H., and Mechie, J., 1988, Low-angle detachment origin for the Red Sea Rift System?, *Tectonophysics*, v. 150, p. 51-75.
- Wilson, C. K., and C. H. Jones, 2004, Geothermal Resource Mapping Using Teleseismic Conversions, *Geothermal Resources Council Transactions*, Vol. 28, August 29 - September 1.
- Wilson, C.K., C.H. Jones, and H.J. Gilbert, Single-Chamber Silicic Magma System Inferred from Shear Wave Discontinuities of the Crust and Uppermost Mantle, Coso Geothermal Area, California, *J. Geophys. Res.*, 108, art. no.-2226, 2003
- Wong, V. and L. Munguia, Seismicity, focal mechanisms, and stress distribution in the Tres Virgenes volcanic and geothermal region, Baja California Sur, Mexico, 2006, *Geofisica International*, 45, 1, 23-37.
- Wong, V., C. J. Rebolgar, and L. Munguia, 2001, Attenuation of Coda Waves at the Tres Virgenes Volcanic Area, Baja California Sur, Mexico, *Bull. Seismo. Soc, Amer*, 91, 4, 683–693.
- Zucca, J.J., Hutchings, L.J., Kasameyer, P.W., 1994. Seismic velocity and attenuation structure of the Geysers geothermal field, California. *Geothermics* 23 (2), 111–126.

Appendix A

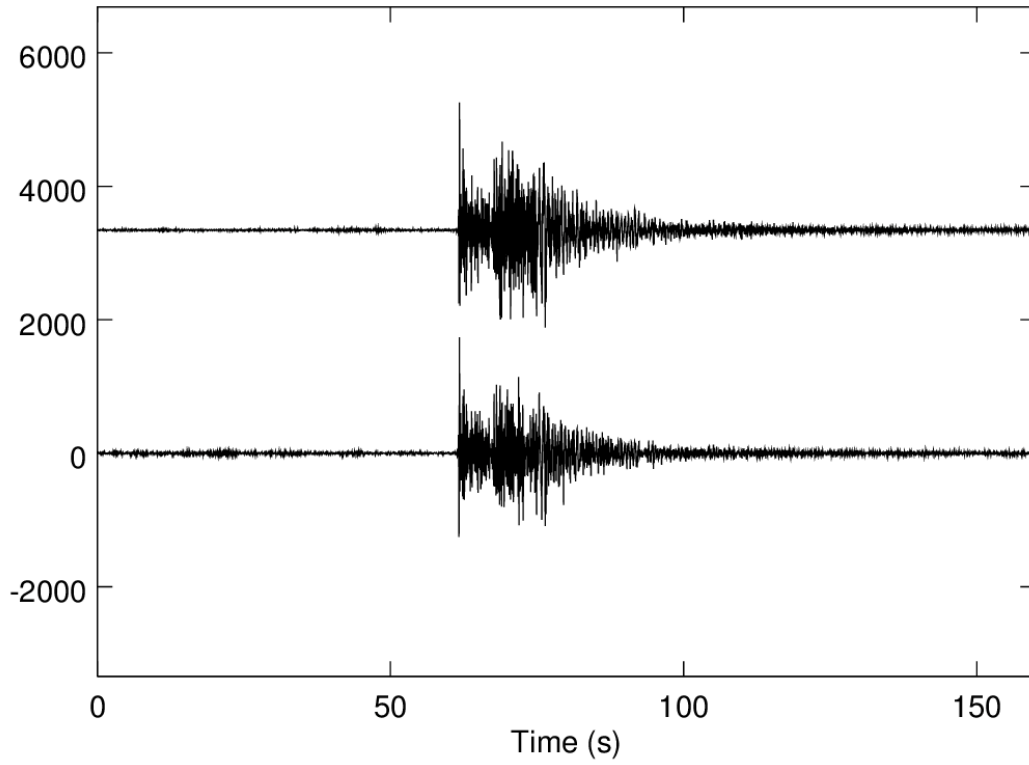
Local event groups detected at RHT01



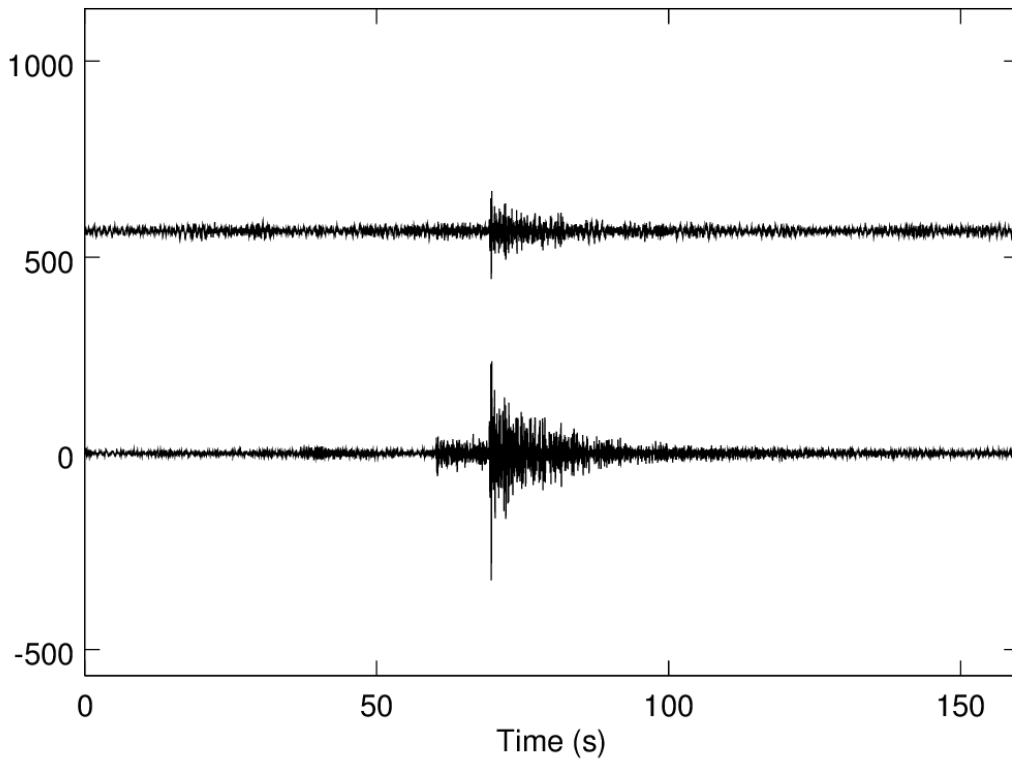




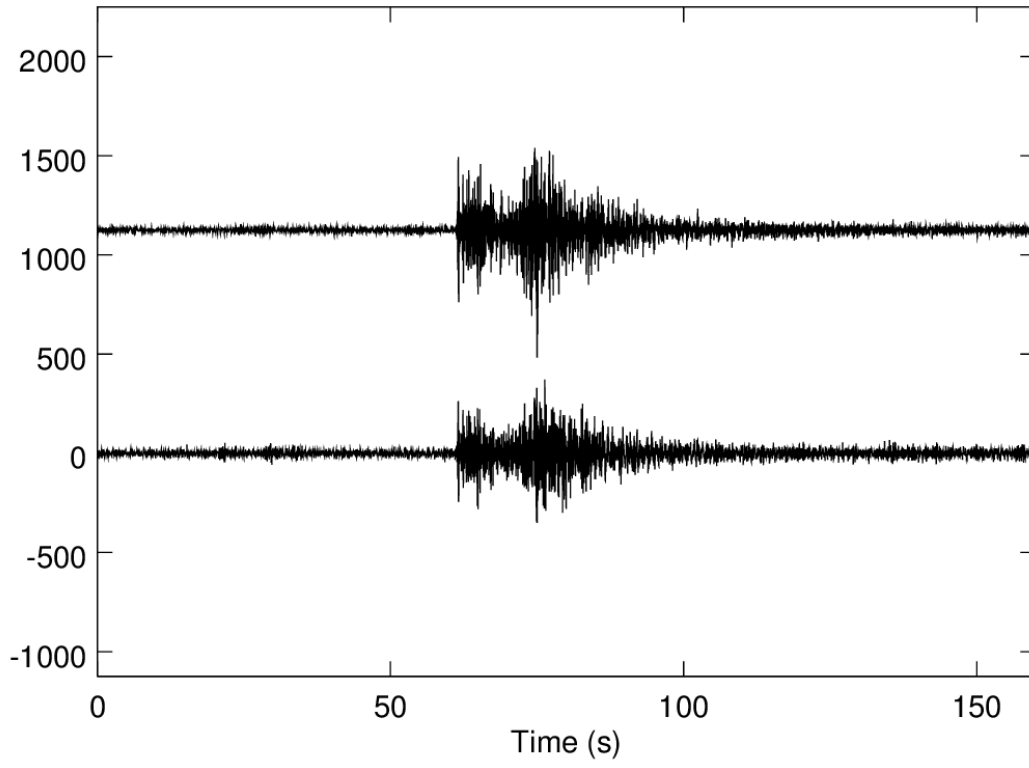
673521



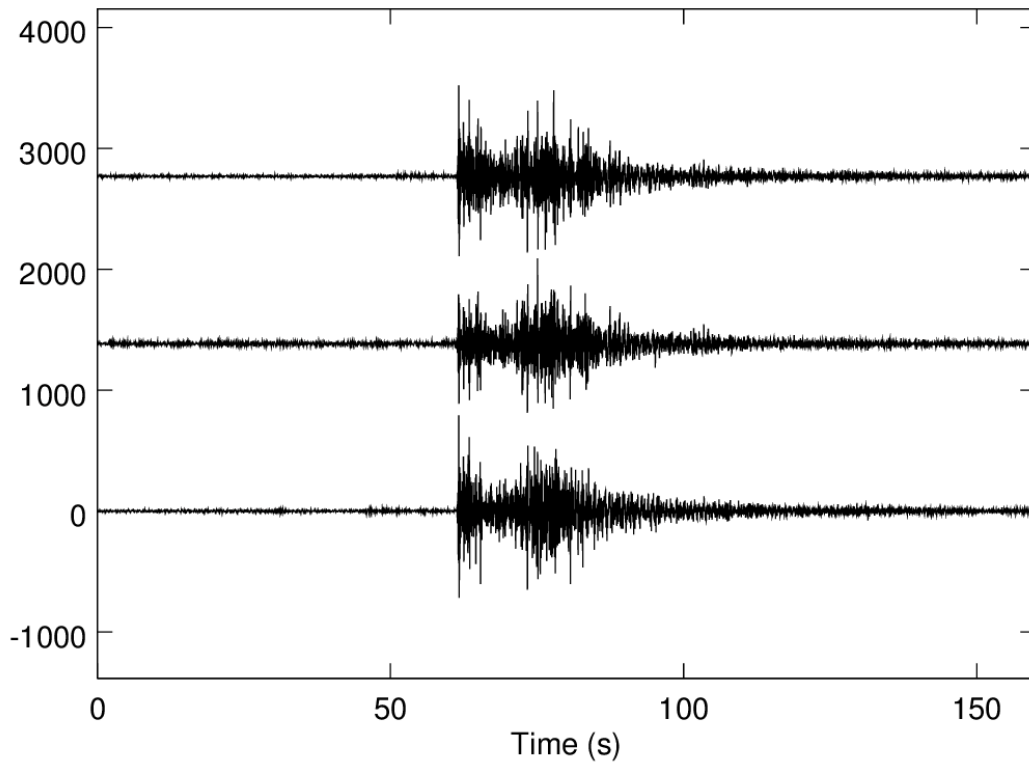
673576

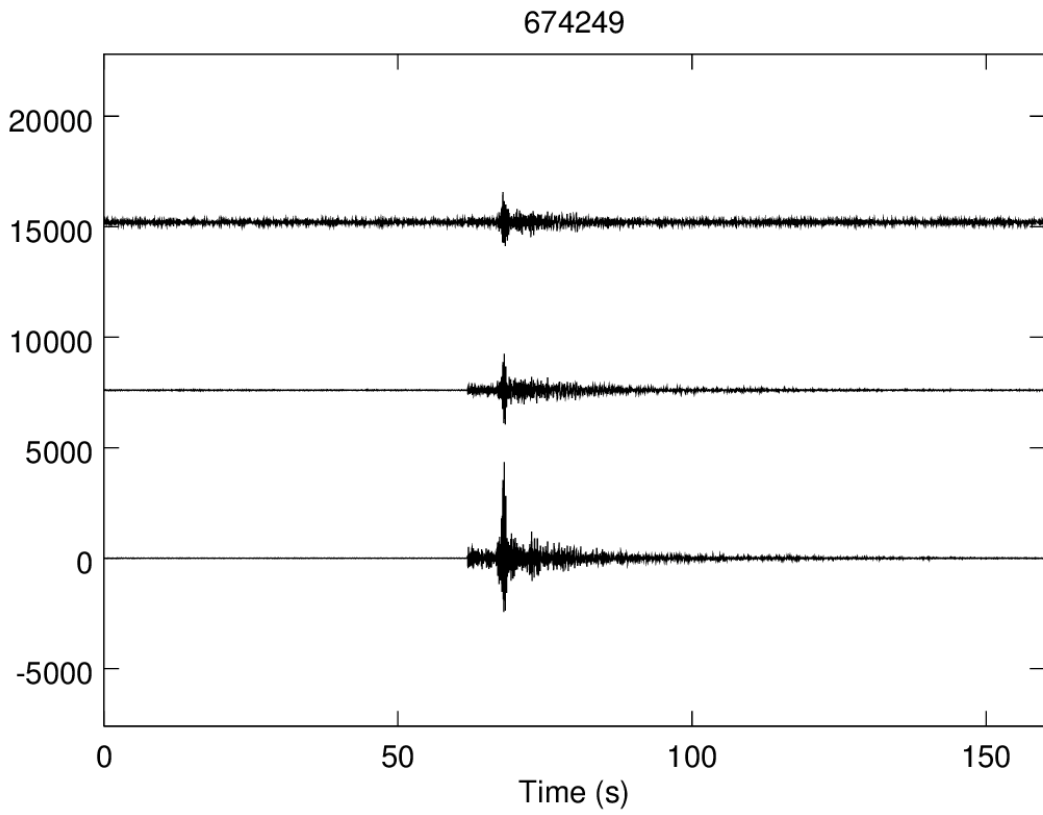
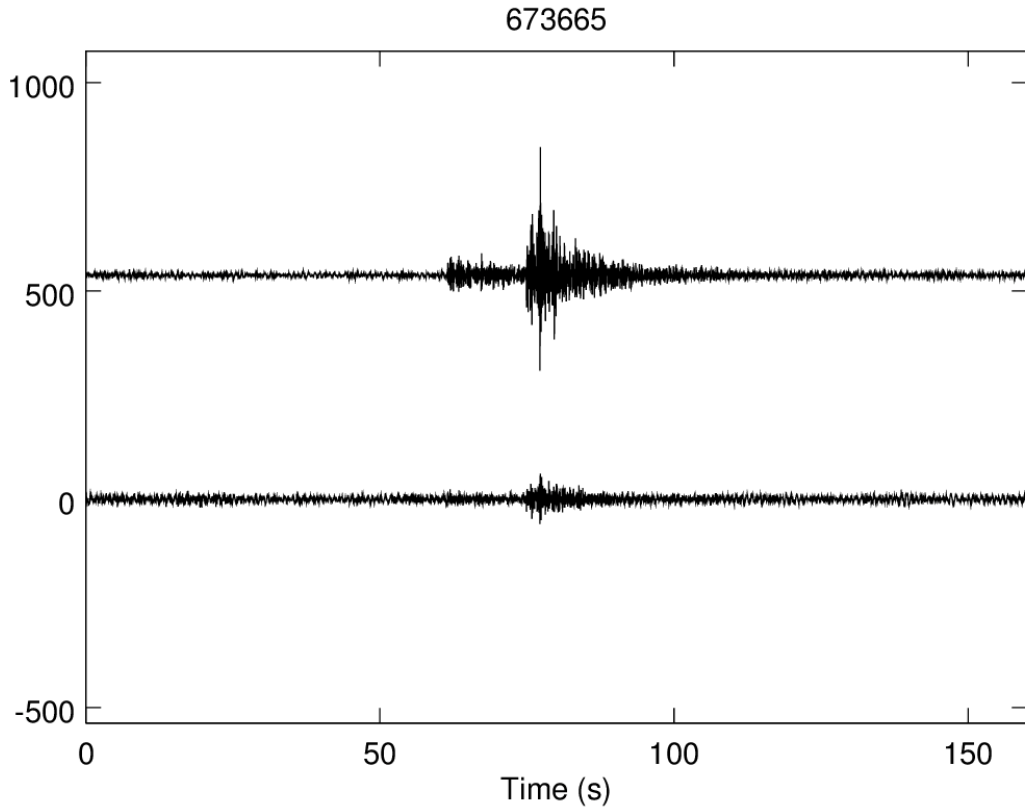


673598

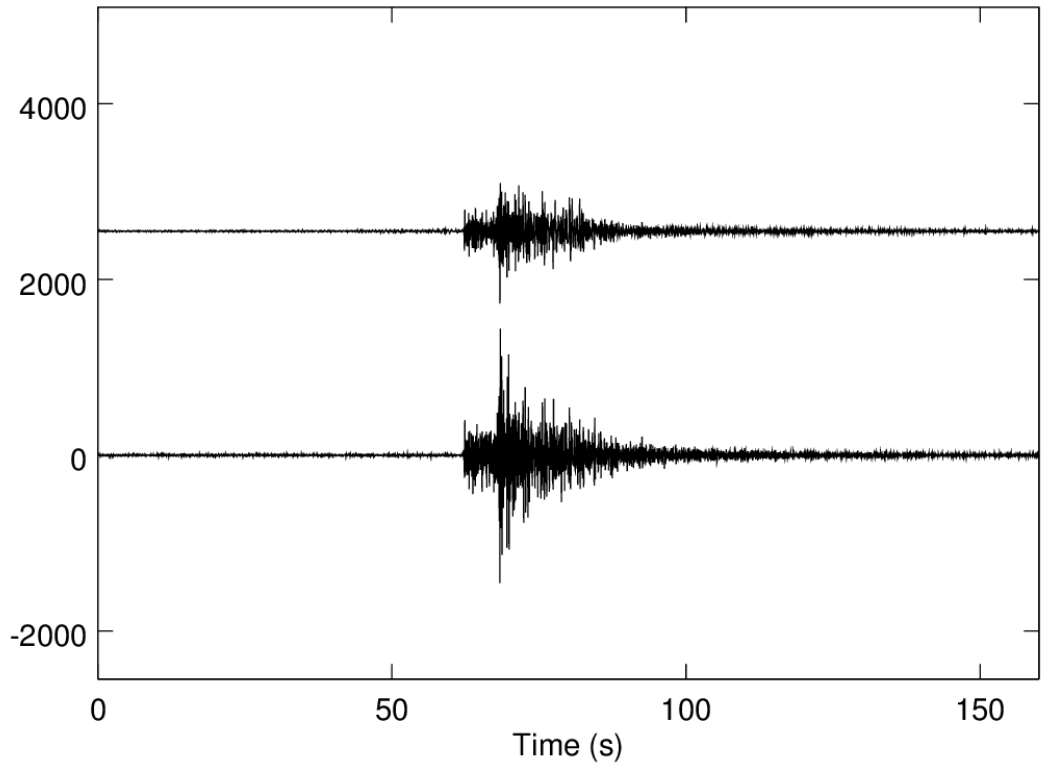


673619

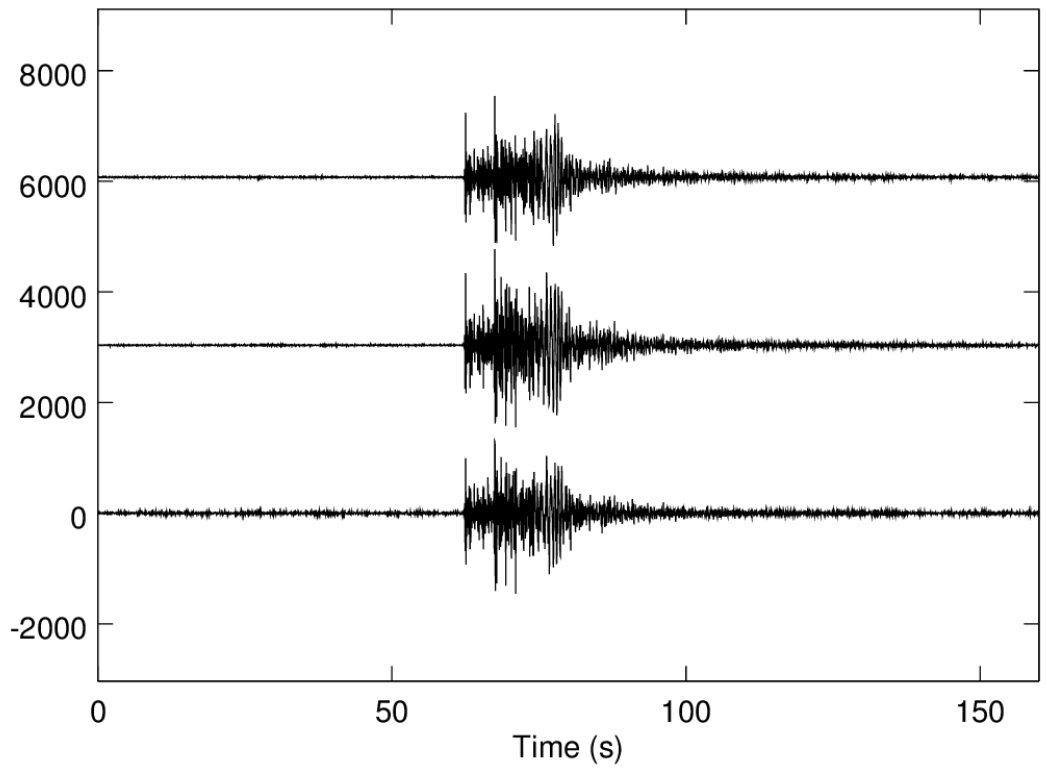




674427

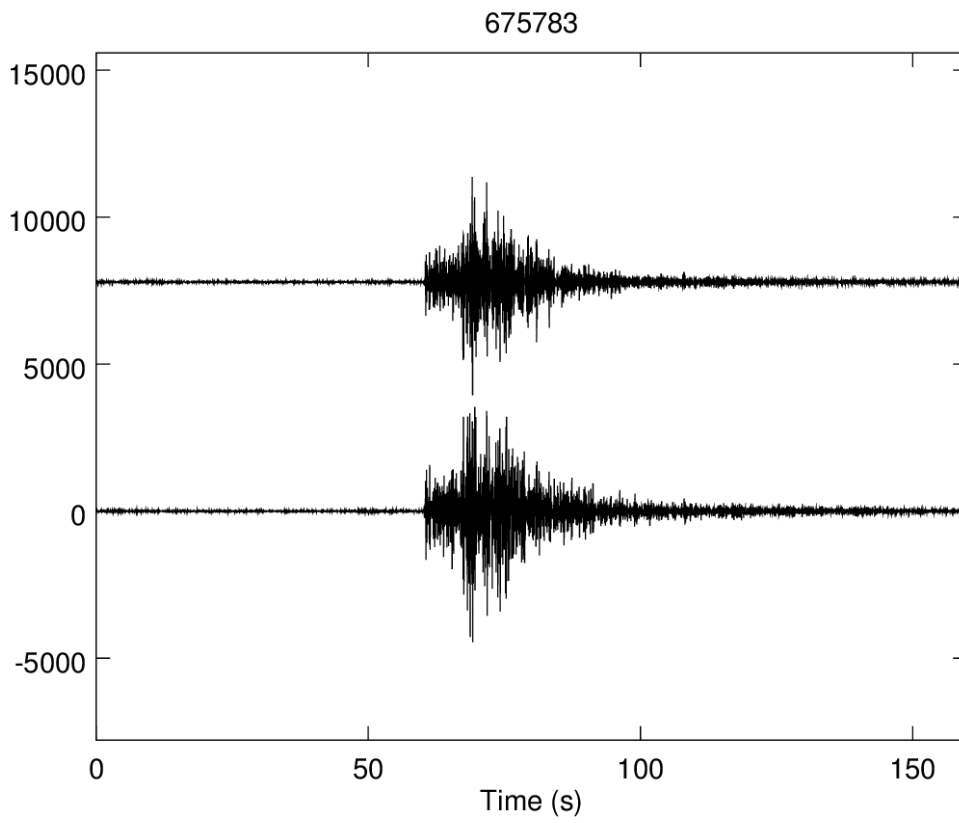


674549

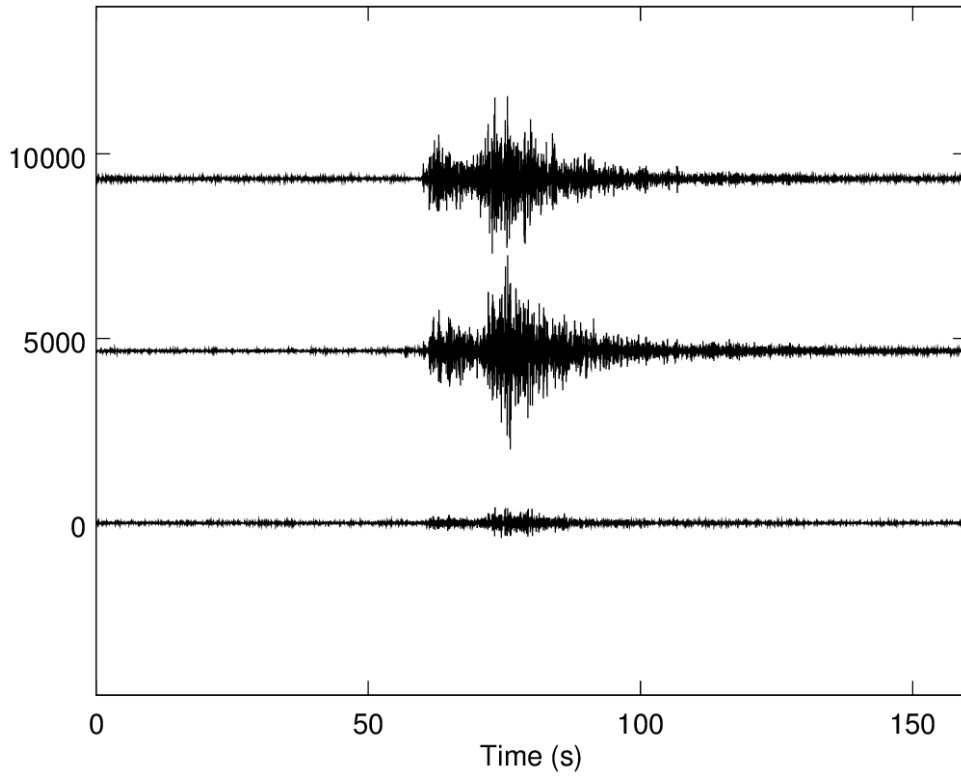


Appendix B

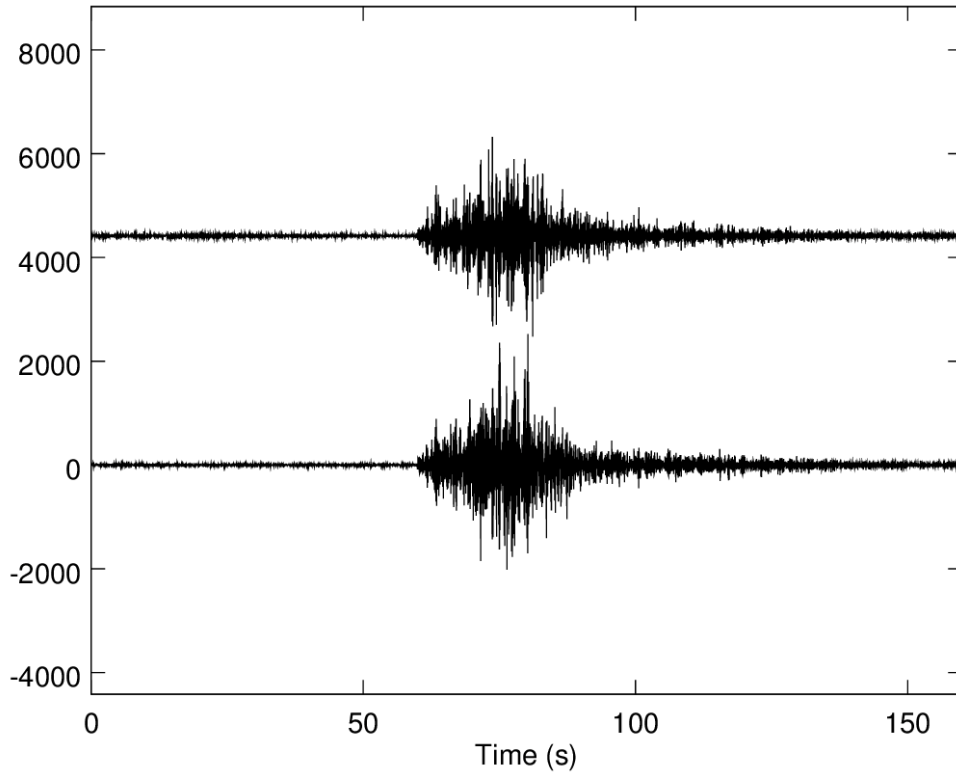
Local event groups detected at RHT04

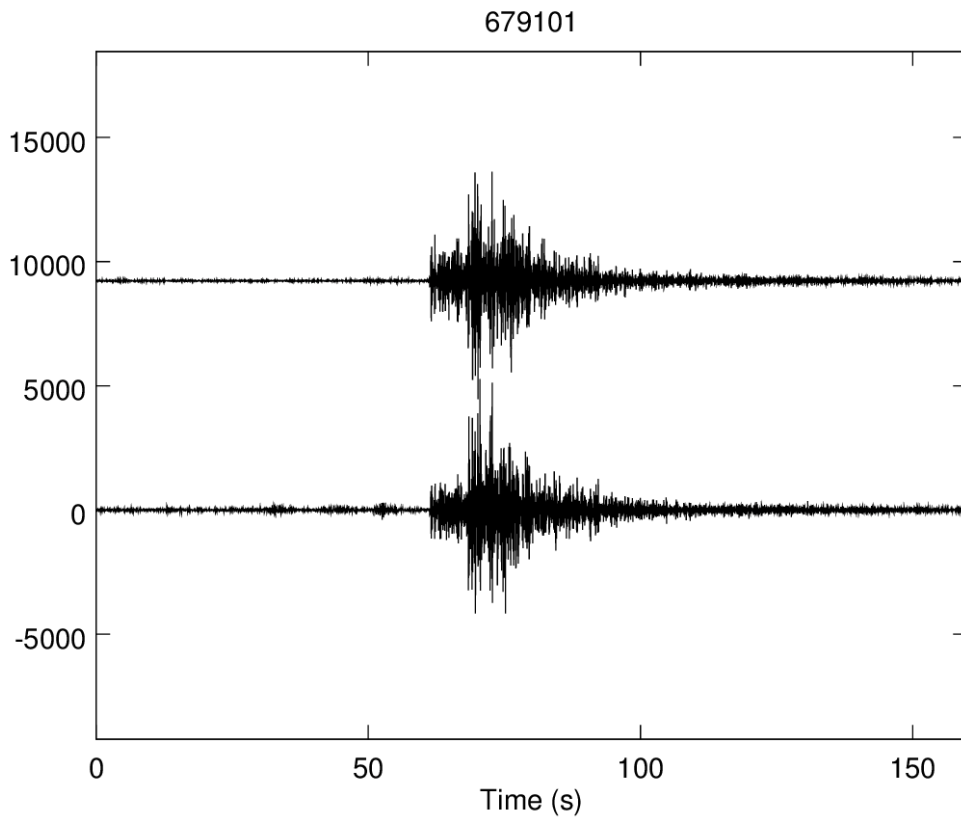
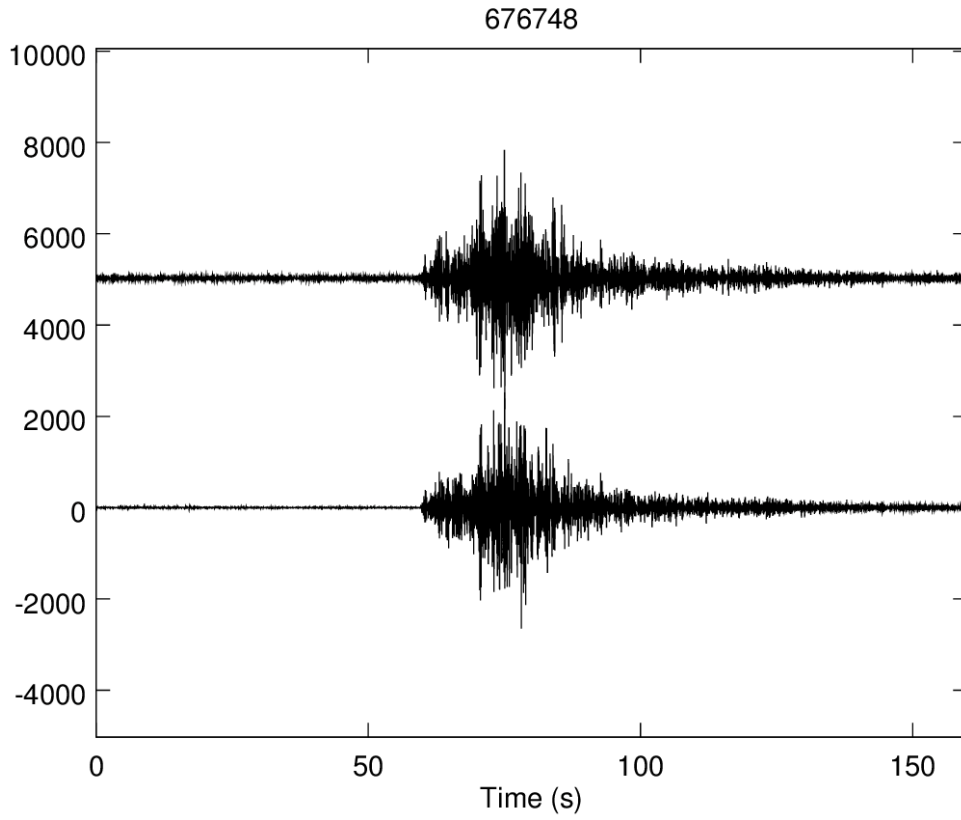


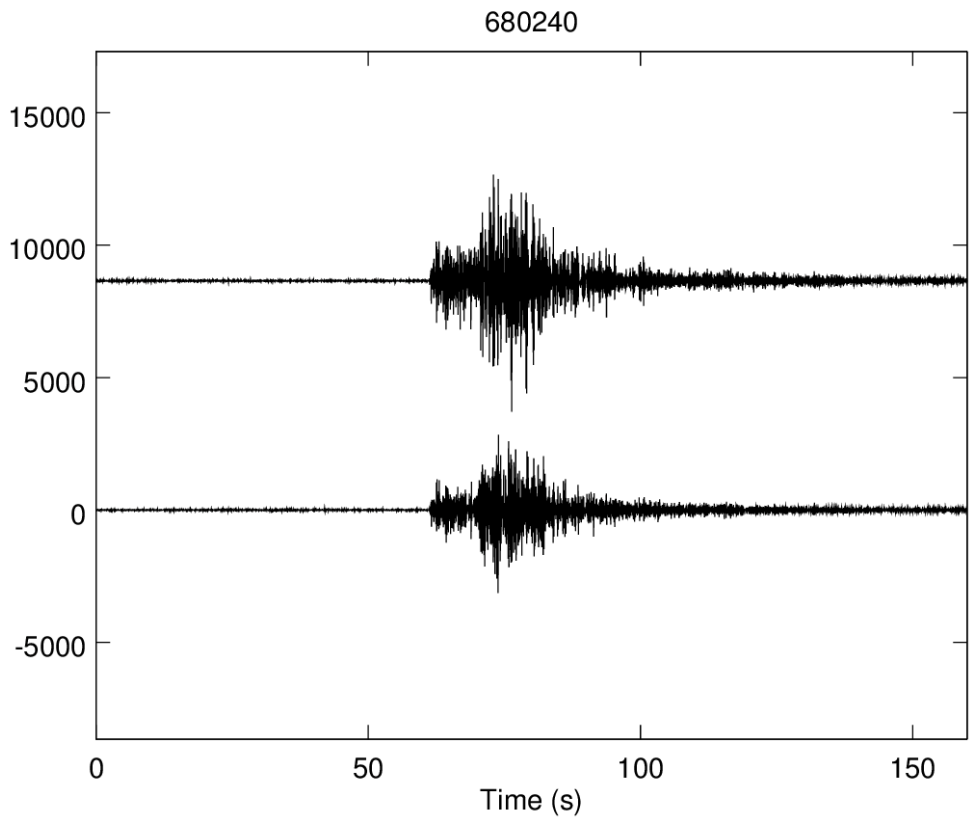
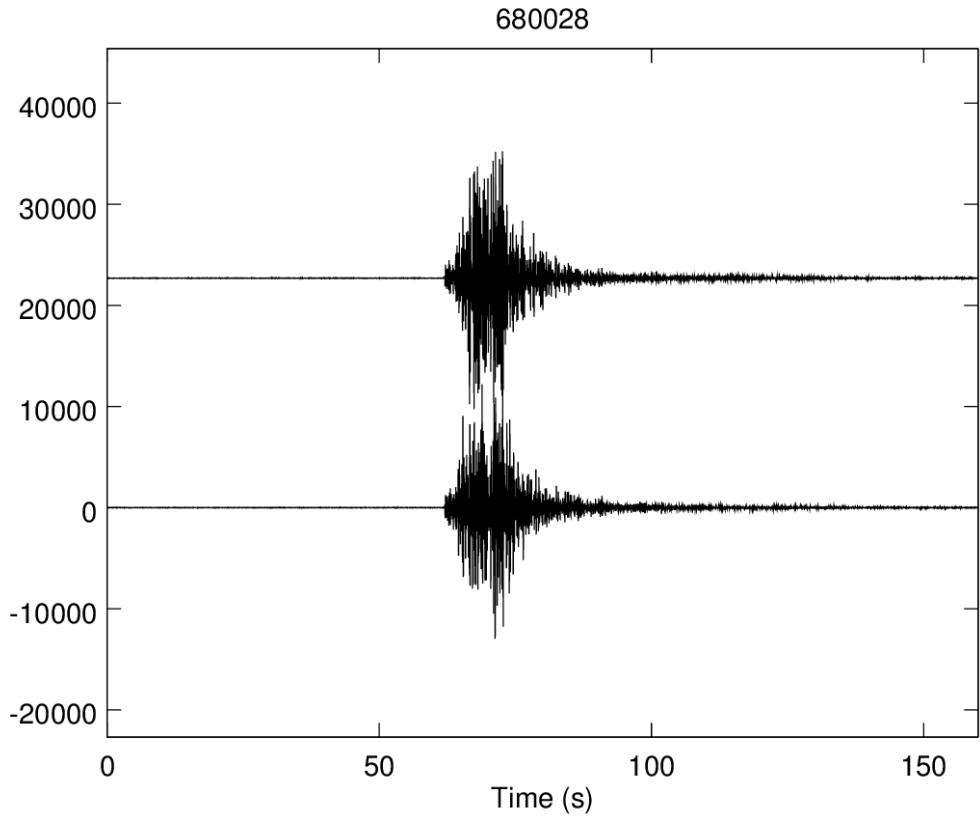
675784

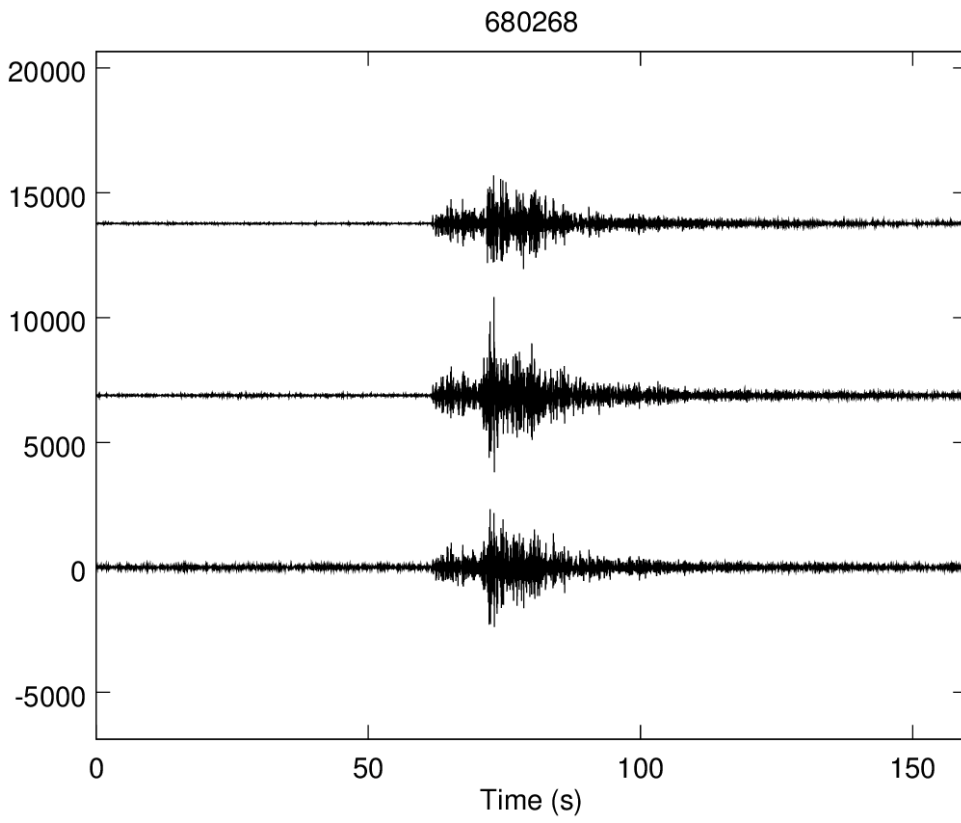
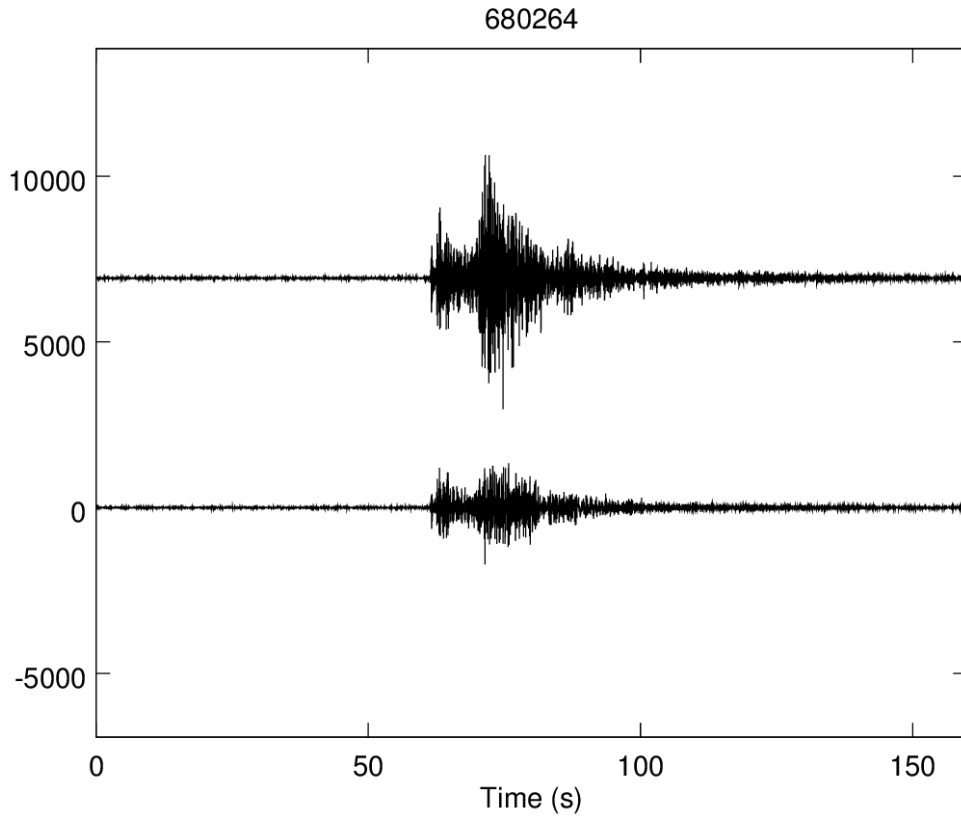


675871



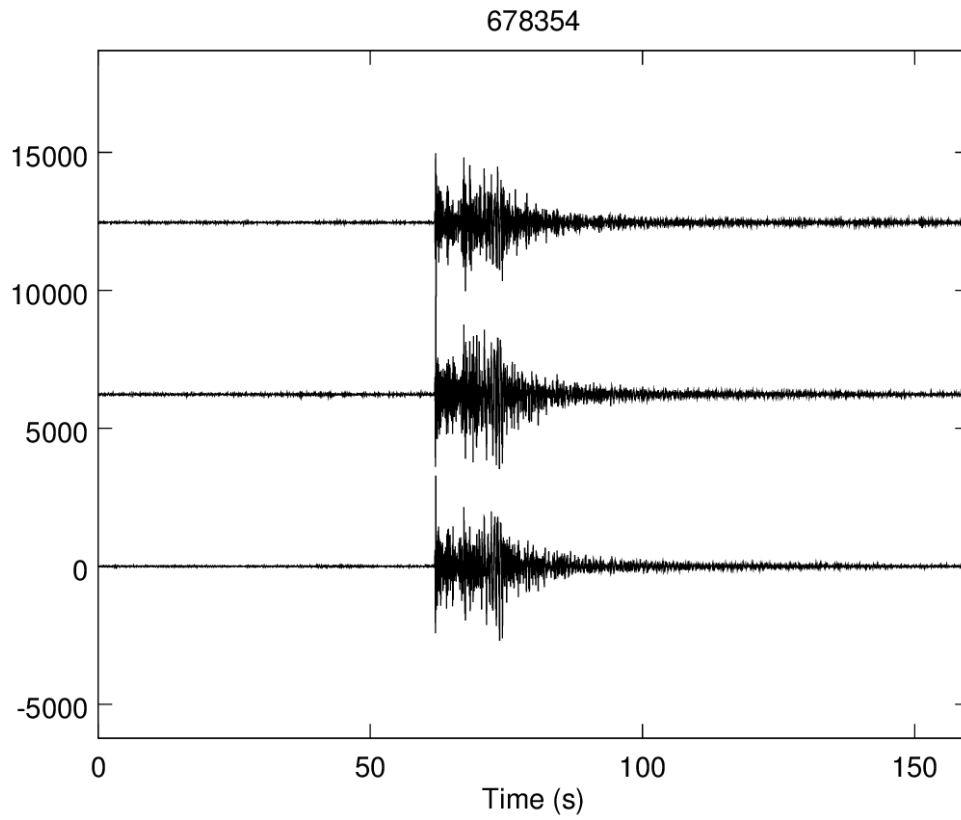




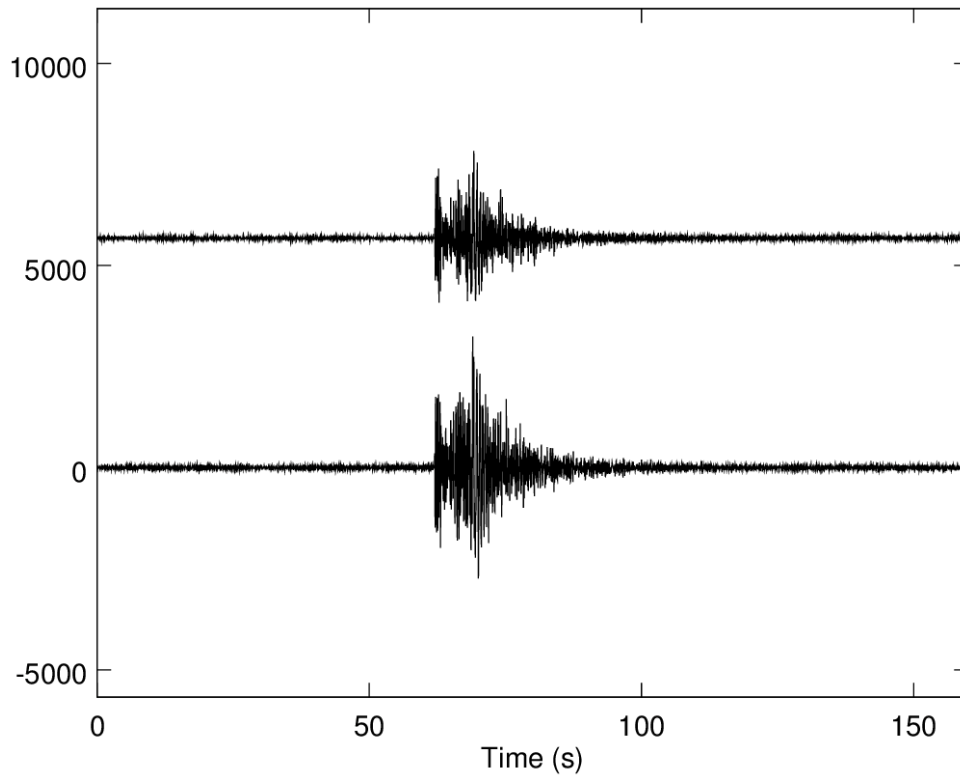


Appendix C

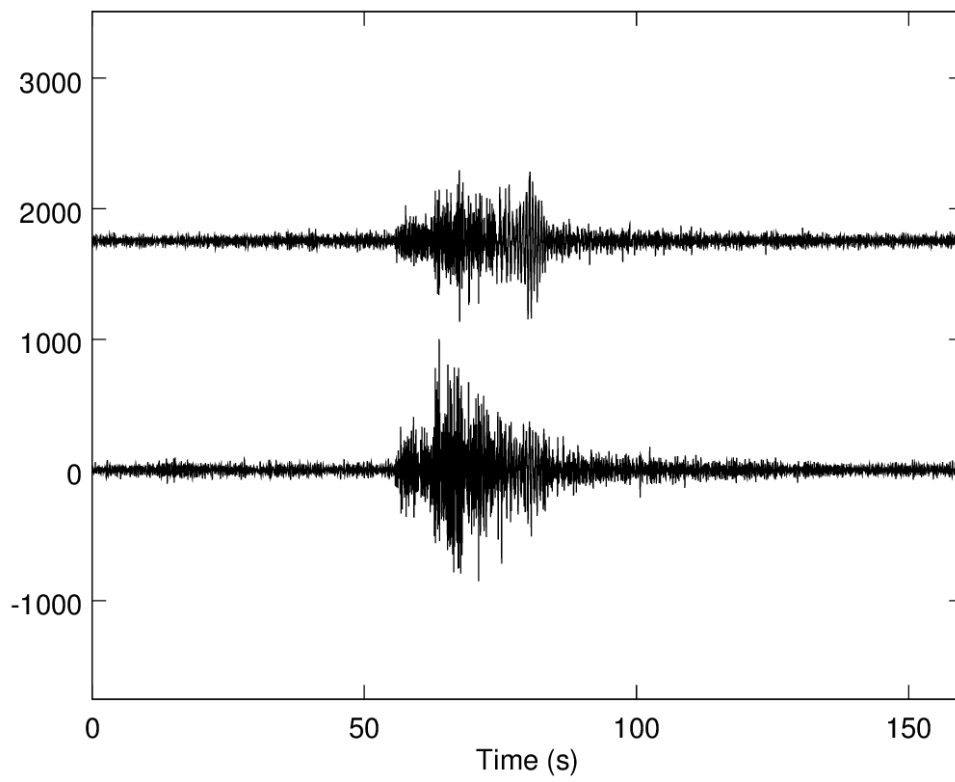
Local event groups detected at RHT14



678370

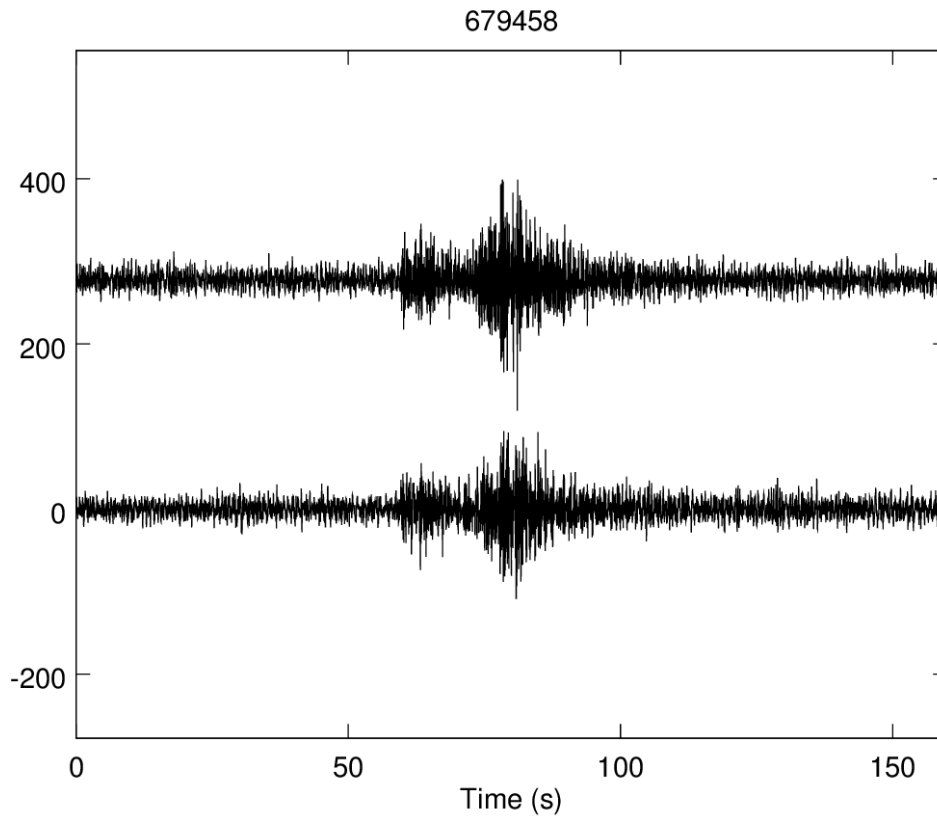


679005

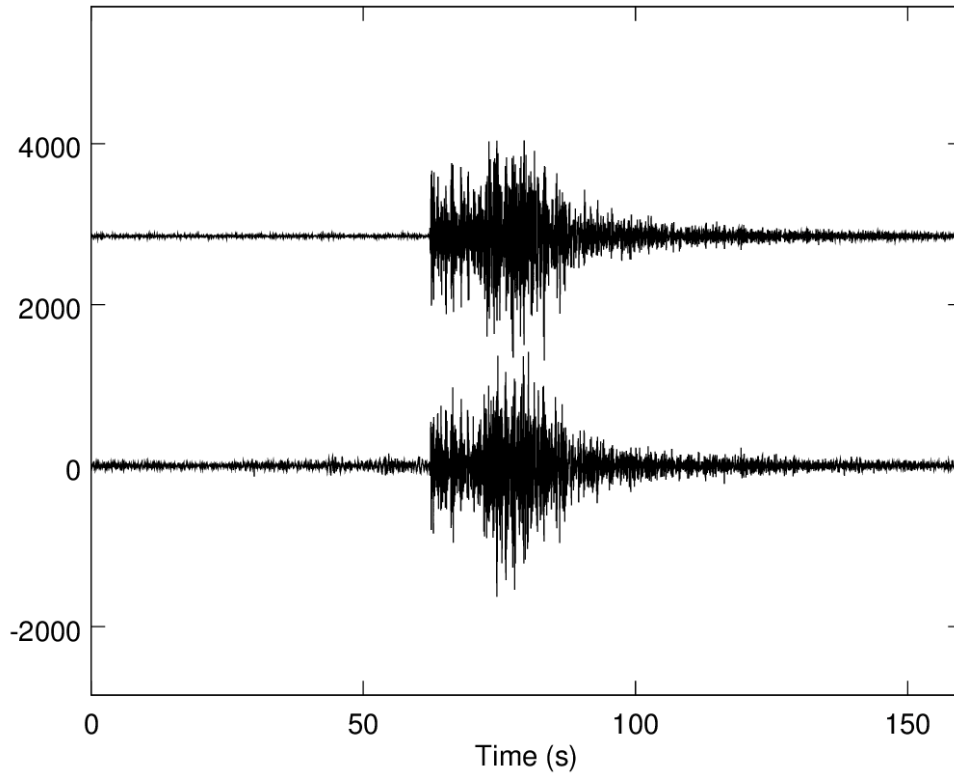


Appendix D

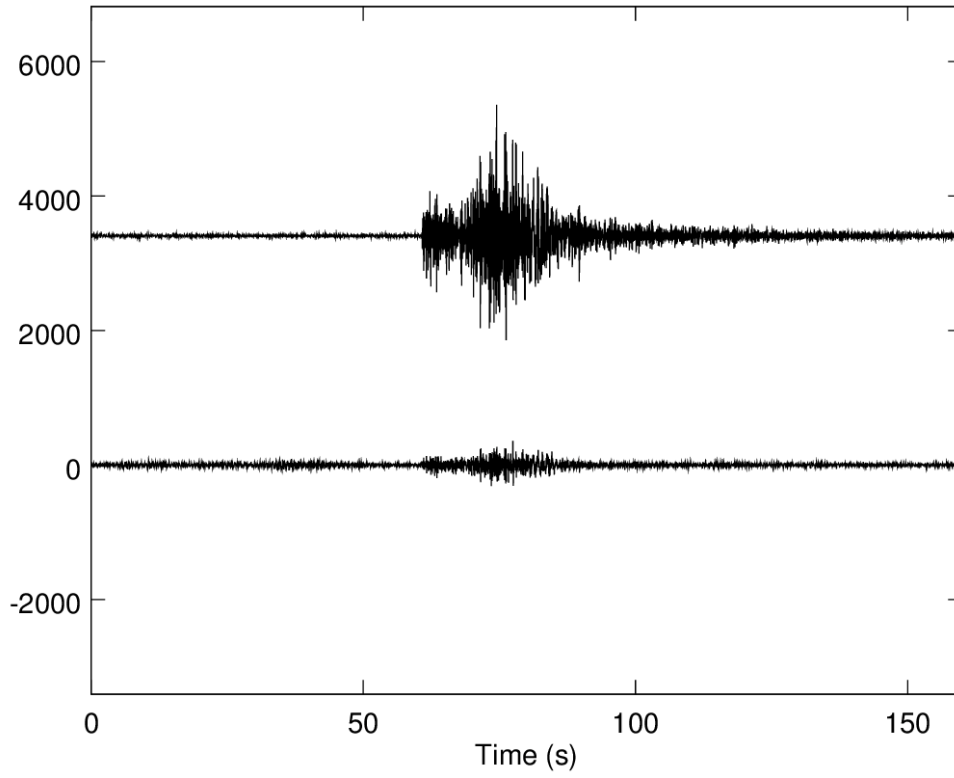
Local event groups detected at RHT15

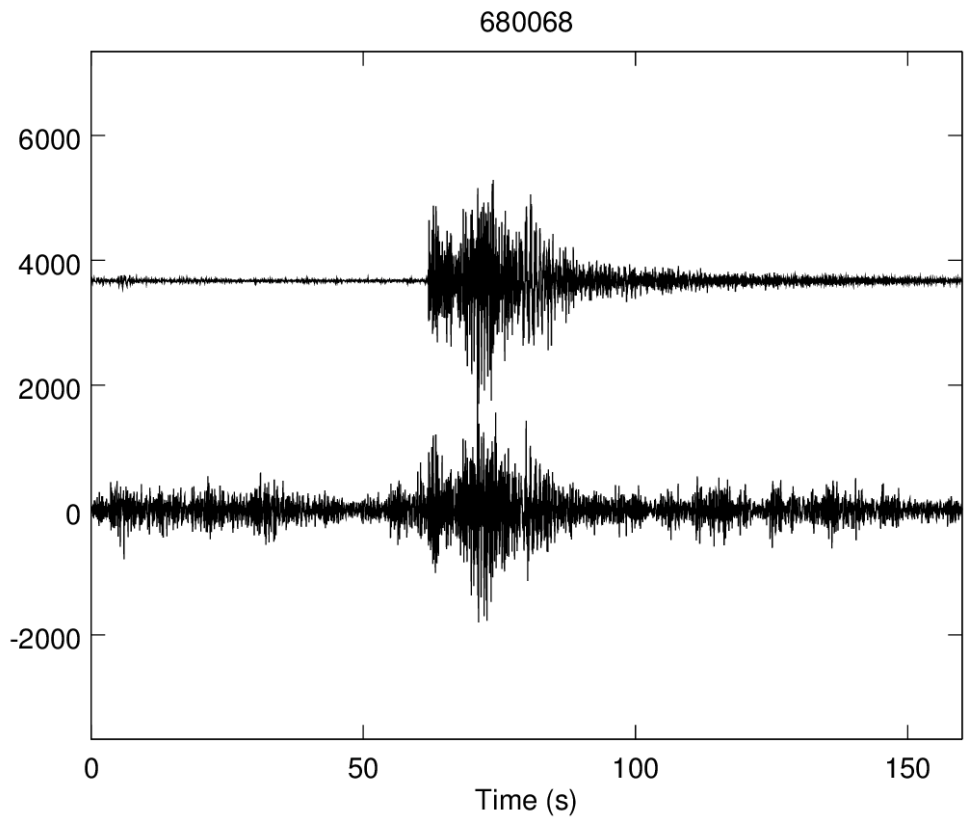
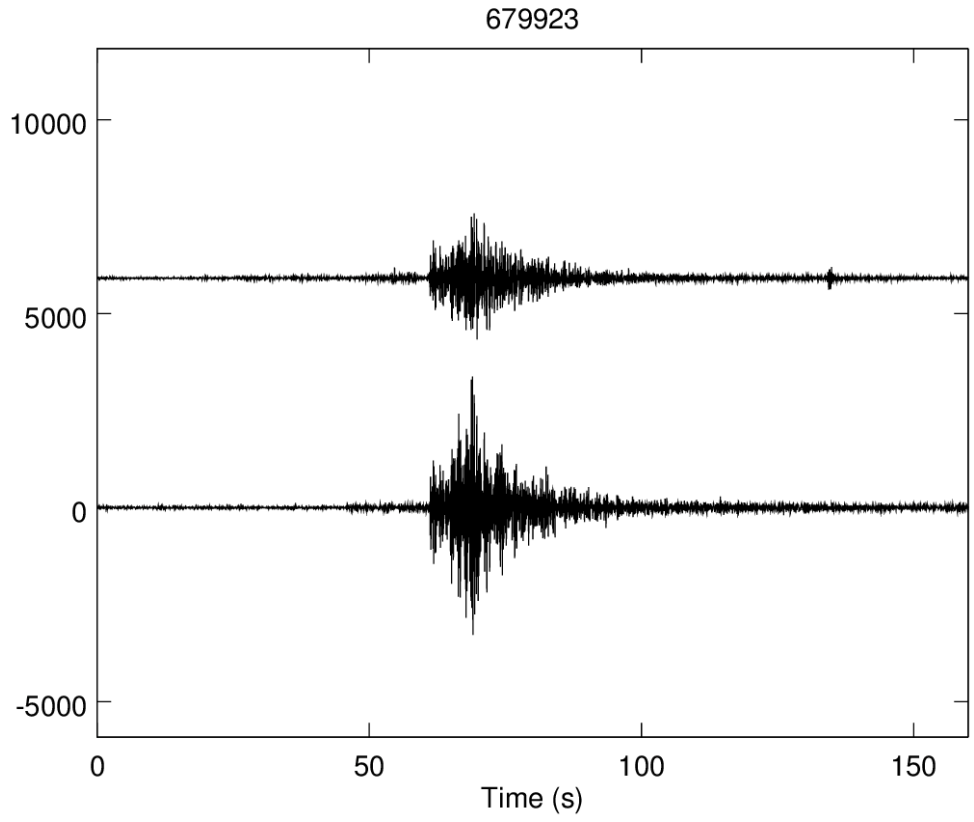


679632



679717





Appendix E

Detection Times of Local Group Events by Station

RHT01

<u>Detector</u>	<u>Epoch Time</u>	<u>Human readable time</u>	<u>detection statistic</u>
673440	1372658120.78	2013/07/01 (182) 05:55:20.780	1.00000011920929
673440	1376900668.14	2013/08/19 (231) 08:24:28.140	0.525095224380493
673440	1379410836.32	2013/09/17 (260) 09:40:36.320	0.500747323036194
673450	1373182471.24	2013/07/07 (188) 07:34:31.240	1.00000071525574
673450	1384413934.99	2013/11/14 (318) 07:25:34.990	0.439016073942184
673450	1390720700.31	2014/01/26 (026) 07:18:20.310	0.574684619903565
673450	1396846482.95	2014/04/07 (097) 04:54:42.950	0.50291645526886
673467	1373864199.89	2013/07/15 (196) 04:56:39.890	1.00000047683716
673467	1397542473.35	2014/04/15 (105) 06:14:33.350	0.69752049446106
673470	1373948235.27	2013/07/16 (197) 04:17:15.270	1.00000178813934
673470	1383725342.6	2013/11/06 (310) 08:09:02.600	0.55306339263916
673470	1391676866.92	2014/02/06 (037) 08:54:26.920	0.649919033050537
673482	1374989826.27	2013/07/28 (209) 05:37:06.270	1
673482	1387870659.98	2013/12/24 (358) 07:37:39.980	0.470462948083878
673482	1398670905.1	2014/04/28 (118) 07:41:45.100	0.49013677239418
673521	1377760164.54	2013/08/29 (241) 07:09:24.540	1.00000023841858
673521	1387870660.72	2013/12/24 (358) 07:37:40.720	0.574798882007599

673576 1378833829.29 2013/09/10 (253) 17:23:49.290 0.8559849858284
673576 1382580449.94 2013/10/24 (297) 02:07:29.940 1.00000011920929

673598 1385022086.29 2013/11/21 (325) 08:21:26.290 1.00000131130219
673598 1392797693.36 2014/02/19 (050) 08:14:53.360 0.454909533262253

673619 1373178899.72 2013/07/07 (188) 06:34:59.720 0.700773239135742
673619 1386492273.74 2013/12/08 (342) 08:44:33.740 0.999999284744263
673619 1386751245.11 2013/12/11 (345) 08:40:45.110 0.616145968437195
673619 1396170357.33 2014/03/30 (089) 09:05:57.330 0.540585160255432

673665 1386797718.6 2013/12/11 (345) 21:35:18.600 1.00000083446503
673665 1394740183.25 2014/03/13 (072) 19:49:43.250 0.799919128417969

674249 1390892540.76 2014/01/28 (028) 07:02:20.760 0.511285066604614
674249 1391067062.39 2014/01/30 (030) 07:31:02.390 1
674249 1398330287.71 2014/04/24 (114) 09:04:47.710 0.61169958114624

674427 1394961536.73 2014/03/16 (075) 09:18:56.730 1.00000011920929
674427 1396946339.72 2014/04/08 (098) 08:38:59.720 0.719720005989075

674549 1396939415.68 2014/04/08 (098) 06:43:35.680 0.565645813941956
674549 1398585948.65 2014/04/27 (117) 08:05:48.650 1.00000071525574
674549 1400392471.89 2014/05/18 (138) 05:54:31.890 0.658092558383942

RHT04

<u>DetectorEpoch</u>	<u>Time</u>	<u>Human readable time</u>	<u>detection statistic</u>
675783	1373178896.00	2013/07/07 (188) 06:34:56.000	1
675783	1386492270.00	2013/12/08 (342) 08:44:30.000	0.4669548869133
675784	1373182477.63	2013/07/07 (188) 07:34:37.627	1
675784	1390720706.67	2014/01/26 (026) 07:18:26.670	0.4863898754120
675784	1396846489.31	2014/04/07 (097) 04:54:49.310	0.4498935341835
675871	1373864205.37	2013/07/15 (196) 04:56:45.373	1
675871	1397542478.81	2014/04/15 (105) 06:14:38.810	0.4282422661781
676748	1376900674.11	2013/08/19 (231) 08:24:34.113	1
676748	1379410842.28	2013/09/17 (260) 09:40:42.280	0.4586229026318
679101	1386492269.05	2013/12/08 (342) 08:44:29.050	1
679101	1386751240.39	2013/12/11 (345) 08:40:40.390	0.6184936761856
680028	1390892536.86	2014/01/28 (028) 07:02:16.863	1
680028	1391067058.45	2014/01/30 (030) 07:30:58.450	0.4742188453674
680240	1393832981.37	2014/03/03 (062) 07:49:41.370	1
680240	1395906173.82	2014/03/27 (086) 07:42:53.820	0.5347999334335
680264	1396765271.66	2014/04/06 (096) 06:21:11.660	1
680264	1398062939.72	2014/04/21 (111) 06:48:59.720	0.4153373539448
680268	1396939421.33	2014/04/08 (098) 06:43:41.327	1
680268	1398585954.27	2014/04/27 (117) 08:05:54.270	0.4847251474857
680268	1400392477.51	2014/05/18 (138) 05:54:37.510	0.5975801348686

RHT14

<u>DetectorEpoch</u>	<u>Time</u>	<u>Human readable time</u>	<u>detection statistic</u>
678354	1372658119.22	2013/07/01 (182) 05:55:19.220	1.00000
678354	1376900666.58	2013/08/19 (231) 08:24:26.580	0.4151279032230
678354	1379410834.76	2013/09/17 (260) 09:40:34.760	0.4189143478870
678370	1373948234.55	2013/07/16 (197) 04:17:14.550	0.9999996423721
678370	1383725341.88	2013/11/06 (310) 08:09:01.880	0.4764178097248
679005	1394961545.21	2014/03/16 (075) 09:19:05.210	1.0000001192093
679005	1396946348.20	2014/04/08 (098) 08:39:08.200	0.5303349494934

RHT15

<u>DetectorEpoch</u>	<u>Time</u>	<u>Human readable time</u>	<u>detection statistic</u>
679458	1378709988.58	2013/09/09 (252) 06:59:48.580	0.4858857989311
679458	1378795184.56	2013/09/10 (253) 06:39:44.560	0.9999984502792
679632	1386492271.08	2013/12/08 (342) 08:44:31.080	1.0000019073486
679632	1386751242.49	2013/12/11 (345) 08:40:42.490	0.4898315072060
679717	1390720702.89	2014/01/26 (026) 07:18:22.890	1.0000010728836
679717	1396846485.47	2014/04/07 (097) 04:54:45.470	0.4454029202461
679923	1394961536.19	2014/03/16 (075) 09:18:56.190	1.0000011920929
679923	1396946339.18	2014/04/08 (098) 08:38:59.180	0.6409233808517
680068	1398585950.97	2014/04/27 (117) 08:05:50.970	1.0000022649765
680068	1400392474.27	2014/05/18 (138) 05:54:34.270	0.4550865590572